Sintering behaviour and properties of beta'-Si3Al3O3N5 ceramics

SINTERING BEHAVIOUR AND PROPERTIES

OF ß'-Si$_3$Al$_3$O$_3$N$_5$ CERAMICS

Esther Kokmeijer

SINTERING BEHAVIOUR AND PROPERTIES
OF ß'-$Si_3Al_3O_3N_5$ CERAMICS

SINTERING BEHAVIOUR AND PROPERTIES OF ß'-Si$_3$Al$_3$O$_3$N$_5$ CERAMICS

PROEFSCHRIFT

door

Esther Kokmeijer

geboren te Amsterdam

Dit proefschrift is goedgekeurd door de promotoren:
Prof. dr. R. Metselaar
Prof. dr. G. de With

Aan Tonnis

CONTENTS

SYMBOLS

a, c	unit cell dimensions	[m]
a_s	radius of the circle of support points	[m]
a	cracklength in SENB specimen (chapter 6)	[m]
b	radius of region of uniform loading	[m]
B	width of SENB specimen	[m]
d	thickness	[m]
d_p	pellet diameter	[m]
d_r	lattice spacing	[m]
D	diffusion coefficient	$[m^2 s^{-1}]$
E	Young's modulus	[Pa]
E_{act}	activation energy	$[J\ mol^{-1}]$
f_c	friction coefficient	[-]
F_n	normal force	[N]
G	grain size	[m]
h	reaction rate constant	[-]
HV2	Vickers hardness at 2 N load	[Pa]
I	intensity	[-]
k	Boltzmann's constant	$[J\ K^{-1}]$
k_m	mass transfer coefficient	$[m\ s^{-1}]$
k_s	surface reaction rate constant	$[m\ s^{-1}]$
K_{Ic}	fracture toughness	$[Pa\ m^{1/2}]$
L	length of SENB specimen	[m]
L_p	half thickness of a plate	[m]
m	mass	[kg]
m_w	Weibull modulus	[-]
P	load	[N]
P_f	probability of failure	[-]
P_i	power density of the ith harmonic	$[V^2]$
R	gas constant (8.314)	$[J\ mol^{-1}\ K^{-1}]$
R_d	radius of bending disc	[m]
S_v	specific surface area per volume	$[m^2\ m^{-3}]$
S_m	specific surface area per mass	$[m^2\ kg^{-1}]$
t	time	[s]
T	temperature	$[^{\circ}C]$
v	velocity	$[m\ s^{-1}]$
V	volume	$[m^3]$

W	heigth of SENB specimen	[m]
W_G	grain boundary width	[m]
x	displacement	[m]
X	transformed fraction	[-]
ε	strain	[-]
μ	dynamic viscosity	[kg m^{-3}]
ν	Poisson's ratio	[-]
ρ	density	[kg m^{-3}]
ρ_0	green density	[kg m^{-3}]
ρ_{th}	theoretical density	[kg m^{-3}]
ρ_{rel}	relative density	[%]
σ	stress	[Pa]
σ_{bi}	biaxial strength	[Pa]
$\hat{\delta}$	reaction modulus (eq. (2.24))	[-]
τ	total reaction time when chemical reaction is rate controlling (eq. (2.22))	[s]
Ω	volume of diffusing species	[m^3]

chapter 1

GENERAL INTRODUCTION
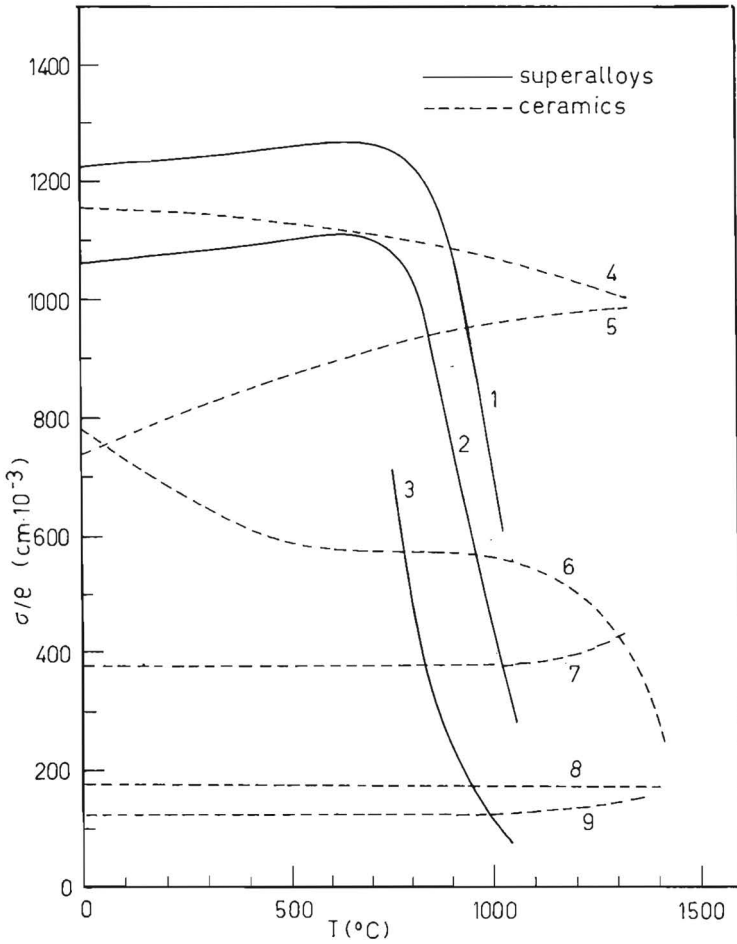
Fig. 1.1. The specific strength (σ/ρ) of several ceramics and superalloys (e.g. cast IN100 [2] as function of the temperature (T) [3-5].

1: superalloys ultimate strength
2: superalloys yield strength
3: superalloys 1 % creep at 1000 hours
4: hot-pressed Si_3N_4 98 % dense
5: silicon carbide hot-pressed 99 % dense
6: alumina hot-pressed 98 % dense
7: reaction bonded Si_3N_4 75 % dense
8: silicon carbide 79 % dense
9: graphite (ATJ)

1.1 Engineering ceramics

The earliest efforts in the development of engineering ceramics were made on reaction sintered or reaction bonded silicon nitride and self bonded silicon carbide (1950 - 1970). But even though some ceramics became commercially available, industry hesitated to apply these new materials. Both the non-reproducibility in the production and the brittleness stagnated the use of engineering ceramics. After 1970 the governments of several countries (notably USA, Japan and FRG) started to support large research projects on engineering ceramics. Because of the above mentioned problem the bulk of these funds went to the industry and not to the universities [1]. An important purpose was to show that in certain applications ceramics can compete with traditional materials e.g. cutting tools, high temperature components and parts demanding a high wear resistance.

An important application of ceramics is found in high temperature technology. In comparison with metals, properties of ceramics like strength and corrosion resistance remain constant up to much higher temperatures. Fig. 1.1 shows the specific strength of some superalloys and ceramics as function of the temperature. Above 800 °C the strength of superalloys decreases rapidly while the strength of certain ceramics can remain constant up to 1300 °C. Examples of high temperature applications are inlet guide vanes, rotor blades and other high temperature components for gas turbines. An increase in turbine inlet temperature without the need for blade cooling increases the specific power output and reduces the fuel consumption.

Another property of ceramics is the generally low thermal conductivity. The main advantange of ceramics in e.g. Diesel engines is the minimization of the heat losses on account of this low thermal conductivity. This leads to the conversion of a greater portion of thermal energy to mechanical energy.

For a long time silicon nitride and carbide remained the only non-oxide engineering ceramics. The favourable properties of silicon nitride are: high strength, good wear resistance, high decomposition temperature, good oxidation resistance, excellent thermal shock resistance, low coefficient of friction and good resistance to corrosive environments. Silicon nitride materials can be divided according to their sintering process: pressureless sintered silicon nitride (SSN), reaction bonded silicon nitride (RBSN), hot-pressed silicon nitride (HPSN), and hot-isostatically-pressed silicon nitride (HIPSN). The reaction bonded type has a high porosity (15 - 20 %) and consequently low strength
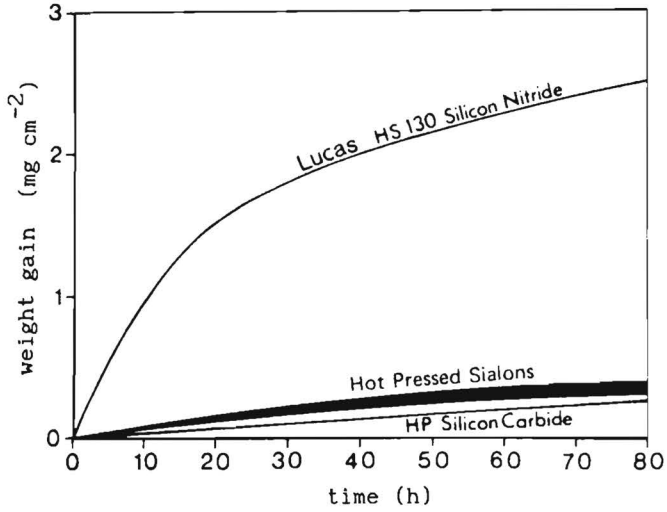
Fig. 1.2. The oxidation of hot-pressed silicon nitride, sialon and silicon carbide in flowing air at 1400 °C [11].
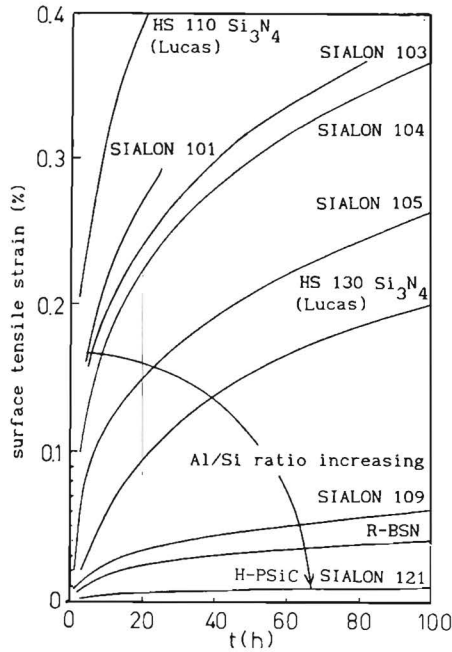
Fig. 1.3. Creep of various ceramic materials at 1225 °C and 77 MPa [11].

(150 - 300 MPa bending strength). The advantage of this material is the versatile production technology and possibility of near net shape sintering. On the other hand, the hot-pressed silicon nitride is a high density, high strength (600 - 850 MPa bending strength) material. The hot-press technique, however, restricts the product shape to simple ones e.g. cylinders or tablets.

Generally covalent bonded materials like silicon nitride have a very poor sinterability. Therefore the development of sintering additives to favour liquid phase sintering was of great importance. The use of sintering additives in pressureless sintered silicon nitride resulted in higher densities at lower temperatures and shorter sinter times. Metal oxides like Y_2O_3, MgO, CeO_2, CaO and Al_2O_3 can be used as additive. These sintering additives form an eutectic liquid with the SiO_2 layer which is always present on the silicon nitride powder particles. Densification starts at the onset of liquid formation. Usually remainders of the liquid phase form an amorphous intergranular phase. However, this amorphous phase can affect the intrinsically favourable properties strongly. For example, MgO as sintering additive decreases the high temperature strength above 1000 °C. Y_2O_3 on the other hand can improve the high temperature strength but lowers the creep resistance at about 1000 °C in an oxidative environment [6].

The discovery that silicon partially can be replaced by aluminium and nitrogen by oxygen led to a class of materials called 'sialons' [8-10]. Silicon nitride exists in two crystallographic modifications: α and β. Both structures consist of SiN_4 tetrahedra, joined in a three dimensional network by sharing corners. Some authors [7] believe that in the α phase about one in every thirty nitrogen atoms is replaced by oxygen. According to these two modifications of silicon nitride, two types of sialon can be formed: α'-sialon and β'-sialon. The α'-sialon and β'-sialon have crystal structures similar to α- and β-Si_3N_4 respectively. The unit cell dimensions of the sialons are somewhat larger than those of the silicon nitride types. The degree of enlargement depends on the degree of substitution of Si and N by Al and O respectively.

The general term 'sialon' is the acronym for phases in the Si-Al-O-N and related systems. The sialons combine the properties of silicon nitride with improved properties like chemical resistance and sinterability. E.g. fig. 1.2 shows the much higher oxidation resistance of hot-pressed sialons in comparison with silicon nitride. By varying the concentration of aluminium and oxygen in the sialon the properties of the product can be influenced. As an example the influence of the Al/Si ratio on the creep resistance is given in fig. 1.3. As can be seen, creep resistance of sialons can vary from rather low, similar to

silicon nitride (HS110), to very high like that of hot-pressed silicon carbide. This variation in properties results in a wide application area like cutting tools, welding and extrusion, parts for molten metal handling, bearing and wear parts [10,11].

A review of commercially available sialons and their properties is given by P. Ferguson [12]. The main producer of sialons is Lucas Cookson Syalon Limited. The sialons can be divided in engineering Syalon grades and refractory Syalon grades. The engineering grades are characterized by high mechanical strength at ambient and elevated temperatures, high specific strength and low coefficient of thermal expansion. The refractory grades are optimized with respect to thermal shock resistance and compatibility with molten metals.

1.2 Scope of this thesis

In this thesis β'-$Si_3Al_3O_3N_5$ is studied which results from the general formula β'-$Si_{6-z}Al_zO_zN_{8-z}$ by substitution of $z = 3$. The value of z indicates the degree of substitution of Si and N by Al and O. The purpose is to optimize different production processes for β'-$Si_3Al_3O_3N_5$ and to study the influence of several additives on the production process as wel as the mechanical properties.

The sialons can be produced by reaction sintering of a mixture of Si_3N_4, AlN and Al_2O_3 but also by carbothermal production from kaolinite ($2SiO_2.Al_2O_3.2H_2O$). The reaction sintering process starts with a green product of a mixture of Si_3N_4, Al_2O_3 and AlN. During the sintering process the product is densified and converted to sialon. During carbothermal production of sialon a mixture of kaolin and carbon is converted under a nitrogen flow into β'-$Si_3Al_3O_3N_5$, CO and H_2O. The process temperature varies from 1350 to 1550 ^{o}C. After the carbothermal production of sialon the powder has to be milled and shaped prior to the sintering process. An advantage of this method is the relatively low cost of the raw materials kaolin and carbon. Thus an engineering ceramic may be obtained at relatively low costs. A study on the carbothermal production of β'-$Si_3Al_3O_3N_5$ from kaolinite was done by Van Dijen [13]. Van Dijen showed that carbothermal production can result in a material with rather good properties. Impurities in the kaolin, however, can deteriorate the properties of the sintered product. To optimize the properties of the kaolin derived sialon it is necessary to study the influence of the several impurities on these properties. Therefore both production routes (carbothermal production and reaction sintering) are studied in

this thesis and the properties of the products are compared.

Chapter 2 reviews the production routes of sialon. Treated are reaction sintering, reaction hot-pressing and carbothermal production of sialon.

The reaction sintering behaviour of powder mixtures with and without additives is studied in chapter 3. The starting powder is a mixture of Si_3N_4, Al_2O_3 and AlN corresponding to $\beta'\text{-}Si_{6-z}Al_zO_zN_{8-z}$ with $z = 3$. As sintering additives CaO and CeO_2 are used. The CeO_2 additive is chosen because of the resemblance between the Ce-Si-O-N and Y-Si-O-N phase systems [7]. This suggests that the sintering behaviour and properties of the CeO_2 doped sialons will be similar to those doped with Y_2O_3. Y_2O_3 is known as a good but expensive sintering additive. CeO_2 is cheaper and therefore more suitable for application in kaolin derived sialons. Studies of the carbothermal production of sialon from kaolin showed that CaO has a 'catalytic' effect on the reaction and seems to stabilize the sialon structure [13]. Therefore CaO is chosen as sintering additive although it is known that CaO doped materials do not yield optimum high temperature strength. The influence of impurities on the sintering behaviour is studied on CaO doped sialon. The emphasis is put on impurities that can be present in kaolin: Fe_2O_3, TiO_2 and SiO_2.

Chapter 4 describes the reactive hot-pressing behaviour of similar mixtures. The purpose in both chapters (3 and 4) is to optimize the sintering respectively hot-pressing procedure of the samples. The procedures are optimized with respect to the density, conversion to β'-sialon, Vickers hardness and microstructure. For reaction sintering experiments, a 'two-step' sintering procedure is optimized.

Chapter 5 deals with the carbothermal production of sialon. Pellets of kaolin and carbon are reacted in a nitrogen flow. First, the influence of the process parameters (reaction time, temperature, nitrogen flow and pellet size) on the carbothermal reduction is studied. The reaction is followed by monitoring the CO-content. The products are characterized by X-ray diffraction and nitrogen content. Second, the sinterability of the powders thus obtained is investigated.

Mechanical properties of the different sialons are measured and compared in chapter 6. Measured are the Young's modulus (E), Poisson's ratio (υ), fracture toughness (K_{Ic}), biaxial strength (σ_{bi}) and wear resistance of some sialons. The strength is determined by a ball-on-ring set up. The wear is measured in a pin-on-plate apparatus with ceramic (ZrO_2) pins against sialon plates.

In chapter 7 the final conclusions of this study are summarized and recommendations for further investigations are given.

References

1. P. Popper, "Convention paper: Industrial ceramics-special, technical or engineering", Trans. J. Brit. Ceram. Soc. 83(1983)187-189.

2. D.W. Richerson, "Modern ceramic engineering", Marcel Dekker, New York 1982.

3. M.H. van de Voorde, C.A.M. Siskens and W. Beteridge, "Ceramics for high temperature energy applications", Sprechsaal 115(1982)1027-1034.

4. M.H. van de Voorde, C.A.M. Siskens and W. Beteridge, "Ceramics for high temperature energy applications, part II", Sprechsaal 115(1982)1108-1111.

5. M.H. van de Voorde, C.A.M. Siskens and W. Beteridge, "Ceramics for high temperature energy applications, part III", Sprechsaal 116(1983)178-184.

6. K.H. Jack, "The relationship of phase diagrams to research and development of sialons", Phase Diagrams 5(1978)241-285.

7. K.H. Jack, "Review: Sialons and related nitrogen ceramics", J. Mater. Sci. 11(1976)1135-1158.

8. Y. Oyama and O. Kamigaito, "Solid solubility of some oxides in Si_3N_4", Japan. J. Appl. Phys. 10(1971)1637-1638.

9. K.H. Jack and W.I. Wilson, "Ceramics based on the Si-Al-O-N and related systems", Nat. Phys. Sci. 238(1972)28-29.

10. K.H. Jack and W.I. Wilson, "Sialons: A study in materials development", Proc. Int. Conf. Non-oxide Tech. Eng. Ceram., 1985, ed. S. Hampshire, Elsevier, London (1986)1-30.

11. W.J. Arrol, "The sialons - properties and fabrication", Proc. Army Mater. Technol. Conf. 2nd, 1973, ed. Brook Hill Publ. Co., Mass., (1974)729-738.

12. P. Ferguson and A.W.J.M. Rae, "Sialon and Syalon powders: Production, properties and applications", Proc. Int. Conf. Non-oxide Tech. Eng. Ceram., 1985, ed. S. Hampshire, Elsevier, London (1986)97-104.

13. F.K. van Dijen, "The carbothermal production of $Si_3Al_3O_3N_5$ from kaolin, its sintering and its properties", Ph.D. Thesis, Eindhoven University of Technology, 1986.

chapter 2

PREPARATION TECHNIQUES FOR

SIALON CERAMICS
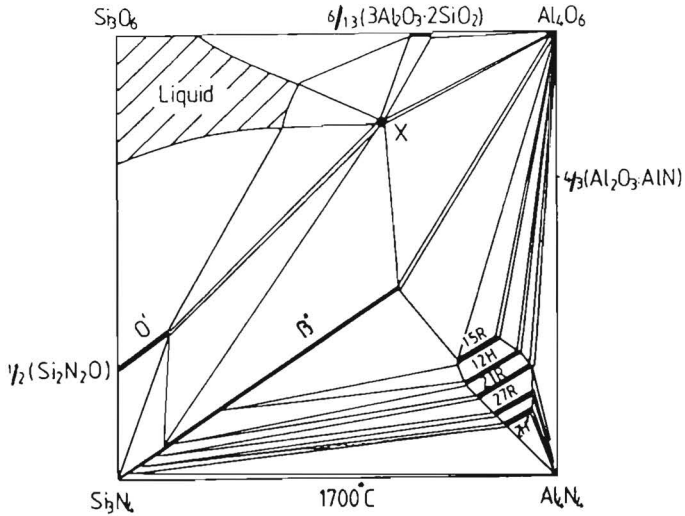
Fig. 2.1. The behaviour diagram of Si_3N_4-AlN-SiO_2-Al_2O_3 at 1700 °C [1].
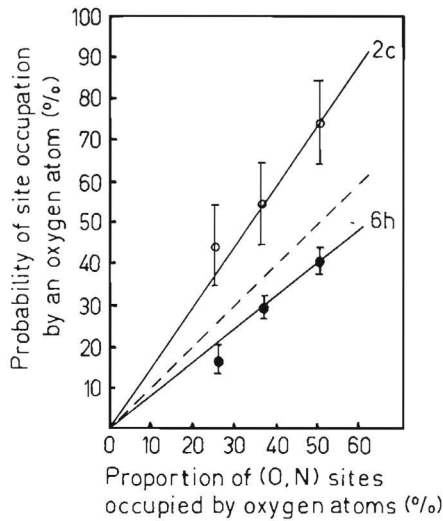
Fig. 2.2. The probability of occupation of the crystallographic 2c (o) and 6h
(•) sites by an oxygen atom plotted against the percentage of oxygen
atoms among the (O, N) atoms for $Si_{6-z}Al_zO_zN_{8-z}$. The broken line
indicates random distribution [2].

In a brief introduction (2.1) the chemical formula and structure of the sialons are presented. Subsequent sections give a literature review on three preparation techniques of sialon: reaction sintering (2.2), reaction hot-pressing (2.3) and carbothermal production (2.4).

2.1 Sialon materials

Sialon can be considered as silicon nitride in which part of the silicon is replaced by aluminium and part of the nitrogen by oxygen. The Si-Al-O-N system is commonly represented as in fig. 2.1. Since it is not certain that all lines in this figure represent a thermodynamic equilibrium it is called a behaviour diagram instead of a phase diagram. In this behaviour diagram from the left to the right side the silicon is replaced by aluminium and from the bottom to the top side the nitrogen is replaced by oxygen. The β'-compound can be represented by $Si_{6-z}Al_zO_zN_{8-z}$ with $0 \leq z \leq 4.2$.

The structure of β-Si_3N_4 can be described as a three-dimensional network of tetrahedral SiN_4 groups joined by sharing the N corners (see cover). Each nitrogen atom is common to three tetrahedra. The space group is $P6_3/m$. This space group contains two different occupied atom sites called the 6h and 2c position. The silicon atoms occupy 6h positions and the nitrogen atoms occupy both 6h and 2c positions. As a result of the structure there are three distinct Si-N nearest neighbour distances: 1.730, 1.740 and 1.746 Å [2]. The structure of β'-sialon is similar to that of β-Si_3N_4. Due to the replacement of silicon by aluminium and nitrogen by oxygen the original Si-N nearest neighbour distances are increased. The smaller oxygen atoms preferentially fill the 2c sites of the nitrogen atoms. The probability of an oxygen atom occupying a 2c or 6h site is given in fig. 2.2. The deviation from the random site occupation (indicated with the broken line in the figure) is not strong enough to result in a superlattice.

Ekström [3] investigated the relation between the cell dimensions and z. His data resulted in the following linear equations:

$$a = 7.603 + 0.0296\ z\ (\text{Å}) \tag{2.1}$$

$$c = 2.907 + 0.0255\ z\ (\text{Å}) \tag{2.2}$$
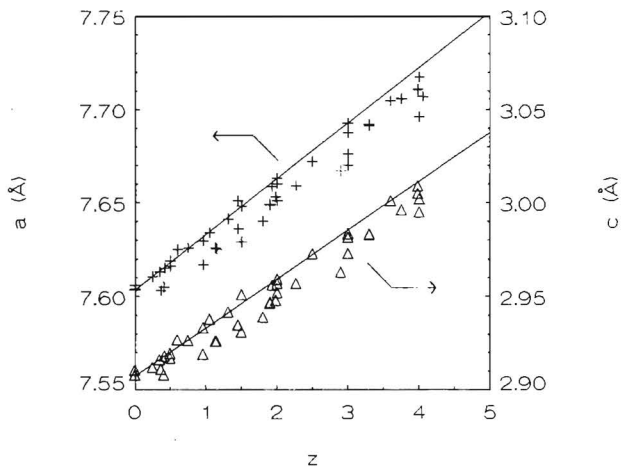
Fig. 2.3. The unit cell dimensions a (+) and c (Δ) of β'-Si$_{6-z}$Al$_z$O$_z$N$_{8-z}$ as function of z. Presented are data from [2-6]. The lines present the eqs. (2.1) and (2.2).

The above equations together with experimental data from other authors [2-6] are represented in fig. 2.3. Linear least-squares fitting on all data results in the following equations:

$$a = 7.599 + 0.0276 \; z \; (\text{Å}) \tag{2.1*}$$

$$c = 2.904 + 0.0244 \; z \; (\text{Å}) \tag{2.2*}$$

Some authors [3,4] report a difference between the aimed z-value and the actual resulting z-value. This might explain the difference between eqs. (2.1), (2.2) and (2.1*), (2.2*) respectively. The figure shows an overall accuracy in the z-value determination of $\pm$ 0.3.

$Si_{6-z}Al_zO_zN_{8-z}$ can be formed from Si_3N_4, Al_2O_3 and AlN according to:

$$(2 - \tfrac{z}{3}) \; Si_3N_4 + \tfrac{z}{3} \; (Al_2O_3 + AlN) \rightarrow Si_{6-z}Al_zO_zN_{8-z} \tag{2.3}$$
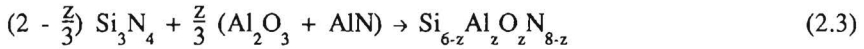
For each nitrogen atom replaced by one oxygen atom, one silicon atom is replaced by one aluminium atom. In earlier literature [7,8], production of β'-sialon from only Si_3N_4 and Al_2O_3 is described. The corresponding reaction equation is given by:

$$(2 - \tfrac{x}{3}) \; Si_3N_4 + \tfrac{x}{3} \; Al_2O_3 \rightarrow Si_{6-0.75x}Al_{0.67x}O_xN_{8-x} \tag{2.4}$$
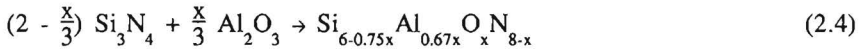
This method implies that for every nitrogen atom replaced by an oxygen atom, three quarters of a silicon atom are replaced by two thirds of an aluminium atom resulting in one twelfth vacancy on a metal atom site. The X-ray diffraction patterns of both sialons (z, x = 3) are very similar. Gillot et al. [2] report the presence of structural vacancies supporting eq. (2.4). Their starting composition was a mixture of Si_3N_4 and Al_2O_3 and a small number of weak peaks in the X-ray diagrams indicated the presence of some second phases. Van Dijen et al. [9] using the carbothermal conversion of kaolin to produce sialon did not find any indication for the presence of structural vacancies. This indicates that eq. (2.3) presents the correct formula of β'-sialon.

An important advantage of β'-sialon over silicon nitride is its easier densification by pressureless sintering as well as hot-pressing. The sinterability of covalently bonded materials like Si_3N_4 is poor. High density is obtained only if sintering aids are used to promote liquid phase sintering. Silicon nitride pow-

ders always contain some surface oxide. The surface oxide reacts with the sintering aids and forms a liquid phase. Therefore sintered products will never be single phased. Theoretically it should be possible to obtain a single phased sialon by transient liquid sintering. However, this is only rarely observed [10]. Most sialons are produced by liquid phase sintering with additives like Y_2O_3, CeO_2, MgO or CaO. Y_2O_3 has proved to be a very good sintering additive because it produces high density materials with a good room temperature strength and reasonable strength up to 1000 °C. Some phase equilibrium studies on Si-Al-O-N systems with different sintering additives were done by Sun and Yan [1] and Jack [6]. Use of sintering additives leads to a multi-phase product. Mostly an amorphous intergranular phase is present which severely influences the properties of the material. Especially the creep properties at high temperature are influenced in a negative way.

Careful processing of Y_2O_3 doped sialons, possibly with a post heat treatment, can lead to a completely crystalline product of β'-sialon and YAG ($3Y_2O_3.5Al_2O_3$) leading to improved creep behaviour [11].

2.2 Reaction sintering

Reaction sintering is a process where during sintering of a powder mixture a reaction (in this case sialon formation) takes place in the powder mixture. In this way it is possible to obtain sialons from mixtures of oxides and nitrides e.g. according to eq. (2.3) or

$$Si_3N_4 + SiO_2 + 6\ AlN \rightarrow 2\ Si_3Al_3O_3N_5 \qquad (2.5)$$
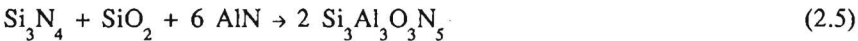
The reaction sintering process is strongly influenced by the properties of the powders (specific surface area, particle size, purity and presence of surface layers) and sintering conditions (time, temperature, gas pressure).

The densification of sialons is a liquid phase sintering process. Generally the kinetics of densification are described by Kingery's model of liquid-phase sintering [12]. This model distinguishes three stages:

  I. Particle rearrangement in the first formed liquid, depending on liquid volume, viscosity, particle size, etc.

  II. Solution-reprecipitation in which shrinkage ($\Delta V/V_0$) varies with time (t) according to:

$$\frac{\Delta V}{V_0} \propto t^{1/n} \qquad (2.6)$$

In this equation n equals 3 if the rate-controlling process is solution into or precipitation from the liquid and n equals 5 if diffusion through the liquid is rate-controlling.

III. Solid state diffusion to remove remaining closed porosity.

The three stages of the model shade off into one another and are difficult to distinguish. It is often not possible to determine a constant slope n as predicted by eq. (2.6) and therefore impossible to correlate the value of a constant slope directly to the rate controlling process. Requirements for complete densification are: a sufficient amount of liquid, appreciable solubility of the solid and complete wetting of the solid by the liquid.

During the first two stages the reaction to sialon might contribute to the densification. Hampshire and Jack [13] describe the kinetics of the reaction by the Avrami-Erofe'ev equation [14]:

$$X = 1 - e^{-h(t-t_0)^s} \qquad (2.7)$$

where X is the transformed fraction, t_0 a threshold time and h and s are constants at constant temperature (T). The activation energy for the reaction can be determined from Arrhenius plots of log(h) against $1/T$. A study on Y_2O_3 and MgO doped silicon nitride and sialons [13] resulted in the same activation energy for the sialons as well as the Si_3N_4 for both additives: 405 kJ mol^{-1}. This value is close to the dissociation energy of the Si-N bond (435 kJ mol^{-1}) indicating that the reaction mechanism probably requires the breaking of these bonds [13].

The slopes s are all close to unity which converts eq. (2.7) into the equation of a first-order reaction. First-order kinetics are strong evidence that the reaction is not a solid state reaction beween AlN, Al_2O_3 and Si_3N_4. Apparently the reaction to sialon takes place in the liquid and eq. (2.7) represents the precipitation of sialon from the liquid.

Papers on the reaction sintering process study the influence of:
- powder processing [15-20]
- composition of the powder mixture [21-26]
- additives [13,24]

25

Powder processing

Powder processing includes all steps from powders to green product i.e.: milling, mixing, pressing, binder removal.

Ceramic powders contain agglomerates: groups of particles which should be broken by milling. If the green product consists of different powders, thorough mixing should assure a homogeneous product. After pressing a green product is obtained. The product should have enough strength for handling and a homogeneous density. Inhomogeneous density causes inhomogeneous sintering. This can result in microstructural defects and loss of shape. Addition of a binder can promote homogeneous densification during pressing. The binder has to be burned out before sintering by a heating cycle. The binder removal rate must be sufficiently low to prevent cracking due to gas development.

The sinterability of a powder compact can be related to the distribution of pore coordination numbers, i.e. the number of touching particles surrounding and defining each void space [15]. Thermodynamic arguments suggest that pores disappear only when their coordination number is less than a critical value. Agglomerates and packing conditions cause the formation of pores with higher coordination number [15]. These pores can only disappear after reducton of their coordination numbers due to grain growth [16]. Evans [17] studied the consequences of inhomogeneous packing by analysing the transient and residual stresses that accompany sintering: non-uniform sintering rates create stresses which influence particle rearrangements and can result in the development or enlargement of void space.

Although the importance of powder processing is clear, papers on reaction sintering of sialon hardly pay attention to this subject. Generally the powder processing consists of wet milling in iso-propanol (0.5 to 300 h) with alumina balls, die-pressing and isostatic pressing.

Some authors [18,19] studied the influence of the milling time on the sinter behaviour of sialon and silicon nitride. Both studies conclude that longer milling resulted in an improved sinterability and structure. Wet sieving the powders with 20 and 10 μm aperture screens also increased the density obtained slightly [19].

The kind of silicon nitride powder used influences the sinterability. The use of a powder with a smaller particle size (4 μm versus 8 μm) increased the density of sialon samples from 2.93 to 3.02 g cm^{-3} [18]. It is difficult to study the influence of the individual parameters like oxygen content, particle size or production method because two powders often differ in more than one parameter.

26

After experiments with four different silicon nitride powders Mitomo et al. [20] defined the following requirements for a good sinterability: 1) high purity, 2) spherical particles, 3) narrow size distribution.

Composition of the powder mixture

The composition of the powder mixture can be varied in two ways: 1) along the β'-sialon existence region (different z-values) [21-23] and 2) across the β'-sialon existence region [24,25]. Apart from that, different powder mixtures (e.g. according to eqs. (2.3) or (2.5)) can be used to obtain the same sialon [21].

Generally the sinterability of $AlN/Al_2O_3/Si_3N_4$-mixtures increases with increasing z-value. Samples sintered at 1800 °C for 1.5 h, contained some amorphous intergranular phases and X-phase [23]. The sialon with z = 3 also contained some undissolved material at the grain boundaries indicating incomplete conversion. The average grain size was 2-5 μm; the grain size of the z = 3 sialon is somewhat larger than that of the sialons with z = 1.5 and z = 2. This phenomenon, an increasing grain size with increasing z, was also noticed by Ekström [24]. He observed a grain size varying from 1 μm at low z to 5 μm at high z-value. In this range the hardness decreased from 16.7 to 13.4 GPa (HV98) and fracture toughness from 3.0 to 2.4 MPa m$^{1/2}$ (fig. 2.4 [24]).

The strength of sialon with z = 2 was reported to be higher (440 MPa) than that of sialon with z = 1.5 (315 MPa) or z = 3 (370 MPa) and constant up to about 1200 °C [23]. The high temperature strength degradation is related to grain boundary sliding due to softening of the intergranular phase. Thus high temperature strength can be expected to be increased by decreasing the intergranular phase. Cracks were initiated at large pores, particles and surface flaws.

Mitomo et al. [25] studied the sinterability of a sialon with z = 2 as function of the degree of deviation of Al_2O_3 content. The samples were sintered for 1.5 h at 1800 °C. The density of the samples increased with increasing amount of Al_2O_3 excess. The minimum amount of excess Al_2O_3 to obtain high density (> 93 % of the theoretical density of 3.11 g cm^{-3}) was 1.5 wt%. The sialon containing 2.4 wt% excess Al_2O_3 had a grain size of 2 μm, a density of 2.99 g cm^{-3} (96.1 % of the theoretical value) and a strength of 490 MPa at room temperature and 480 MPa at 1200 °C.

Rahaman et al. [26] studied compositions in the region of z = 0.75. These experiments confirm that an oxygen excess increases the sinterability: the den-
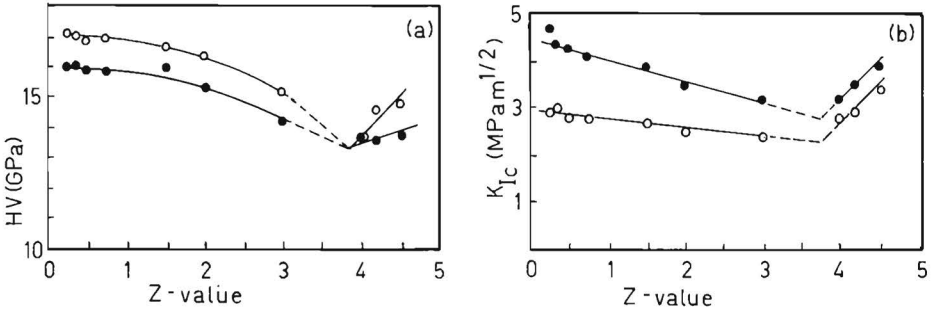
Fig. 2.4. The Vickers hardness HV98 (a) and the fracture toughness K_{Ic} (b) as a function of the z-value for single phase β-sialon ceramics, with (•) and without (o) 1 % Y_2O_3 addition [24].

o: Si_3N_4 + AlN + Al_2O_3
+: SiO_2 + AlN
x: $Si_2Al_4O_4N_4$
•: Si_3N_4
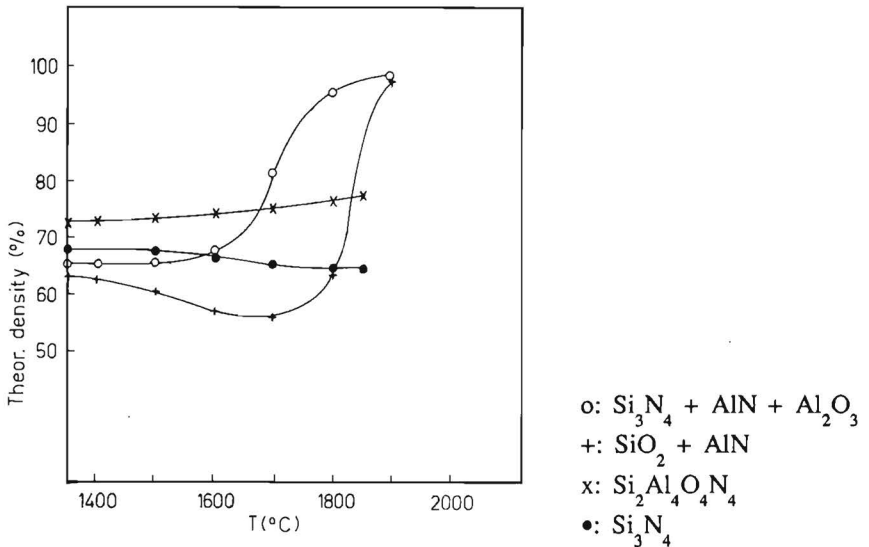
Fig. 2.5. Densification during (reaction) sintering of $Si_2Al_4O_4N_4$ from different starting powder mixtures in comparison with the densification with silicon nitride [21].

28

sification rate decreases with decreasing second phase content. The densification behaviour could not be analysed by Kingery's model for liquid phase sintering. The data fitted to eq. (2.6) did not result in a constant n value. The conversion rate was not influenced by the oxygen excess.

The influence of different starting powder mixtures on the sintering behaviour of sialon with z = 4 was studied by Petzow et al. [21], who compared mixtures of $Si_3N_4/Al_2O_3/AlN$ and SiO_2/AlN with prereacted $Si_2Al_4O_4N_4$ and Si_3N_4. The relative density of samples with these compositions is given in fig. 2.5 as function of the sintering temperature (sintering time 1.0 h). Both powder mixtures can result in a high density sialon. Densification of the $Si_3N_4/Al_2O_3/AlN$-mixture starts at a lower temperature than the SiO_2/AlN-mixture. The sinterability of the prereacted sialon is very poor, comparable to that of Si_3N_4. This may be caused by insufficient powder processing (no data on particle size are given) but also can indicate that the reaction promotes the densification.

Additives

Additives are used to improve the sinterability of a powder mixture. Silicon nitride powder always contains some silica and/or silicon oxynitride. Oxide additives react with these oxides and some of the nitride to give an oxynitride liquid at high temperature. The liquid formation temperature is an important indication for the minimum sintering temperature: usually the shrinkage starts at the onset of the liquid formation. Table 2.1 [13] shows that, for a silicon nitride powder with 5 wt% metal oxide, the liquid formation temperature is lower than the lowest solidus temperature of the SiO_2-oxide system. This difference can be caused by impurities in the silicon nitride powder or by the fact that an oxynitride liquid is formed due to the presence of Si_3N_4.

TABLE 2.1
Liquid formation temperature for silicon nitride powder with 5 wt% addition of metal oxide [13].

oxide	Li_2O	MgO	Y_2O_3	CeO_2	ZrO_2	Al_2O_3
liquid formation [°C]	1050	1390	1440	1470	1590	1470
oxide-SiO_2 solidus [°C]	1030	1543	1660	1560	1640	1595

29

The sintering behaviour of silicon nitride and sialons with MgO and Y_2O_3 was analysed by Hampshire and Jack [13] according to Kingery's model for liquid phase sintering. It appeared that the rate controlling process in the second step, solution-precipitation, is solution into or precipitation from the liquid (n = 3) for MgO doped Si_3N_4 and diffusion through the liquid (n = 5) for Y_2O_3 doped Si_3N_4. In case of the sialons the rate controlling process is for both additives solution into or precipitation from the liquid (n = 3). Apparently the amount of liquid is larger and/or the viscosity lower for Y_2O_3 doped sialon in comparison with Y_2O_3 doped Si_3N_4. As mentioned before, the activation energy of the α-β silicon nitride transformation is equal to that of the β'-sialon formation for both additives.

The influence of Y_2O_3 on the hardness and fracture toughness of sialon has been studied by Ekström [24]. The Y_2O_3 addition resulted in more elongated grains, some grain growth and increase of the amount of intergranular glassy phase. Addition of 1 wt% Y_2O_3 decreased the hardness and increased the fracture toughness (fig. 2.4).

2.3 Reaction hot-pressing

Reaction hot-pressing is reaction sintering under uniaxial pressure. The shape of the specimens is restricted to rather simple forms like cylinders or balls. The hot-press procedure can be done with a die filled with loose powder or with prepressed specimens. On account of the resemblance with reaction sintering the broad outline described in the previous paragraph can be applied to reaction hot-pressing. First-order kinetics as suggested for the sialon formation in reaction sintering have also been demonstrated for reaction hot-pressing [27,28]. Generally the applied pressure results in a lower processing temperature and/or shorter processing time as compared with pressureless sintering.

Again the densification process can be described by the three stages of Kingery's model for liquid phase sintering: I) particle rearrangement, II) solution in and precipitation from the liquid and III) solid state diffusion. Several authors have tried to model the influence of the applied pressure on the second stage densification. Some authors (e.g. [29]) have described the densification with the relation for Nabarro-Herring creep:

$$\dot{\epsilon} = 13.33 \; \frac{D_L \Omega \sigma}{G^2 k T} \qquad\qquad (2.8)$$

where $\dot{\epsilon}$ = strain rate,

D_L = lattice diffusion coefficient,

σ = applied stress,

G = grain size,

Ω = volume of the diffusing species.

k = Boltzmann's constant

Other authors [27,29] used a model for grain boundary diffusion controlled or Coble creep:

$$\dot{\epsilon} = \frac{47.5 D_b W_G \Omega \sigma}{G^3 k T} \qquad\qquad (2.9)$$

where W_G is the grain boundary width and D_b the grain boundary diffusion coefficient.

Both equations are derived for materials of theoretical density. The above equations therefore do not apply. Even when applied, a further problem is that the effective stress which motivates material transport is not precisely known in relation to the applied pressure and porosity. It is therefore not possible to predict the time dependence of the densification with these equations. To overcome this problem Vieira et al. [30] developed a model to predict the effective stress. At a measured density and grain size the densification rate might be approximated by eqs. (2.8) and (2.9).

Another description of the influence of stress on the densification is given by Rahaman et al. [31]. They assumed the following relation:

$$\left(\frac{d\rho}{dt}\right) \propto (\sigma - \sigma_0)^n \qquad\qquad (2.10)$$

where σ_0 is a threshold stress and ρ the density. The exponent n should indicate the densification mechanism by comparing the experimentally determined stress exponents n with those predicted by theoretical models. E.g. $n = 1$ can indicate Nabarro-Herring or Coble creep and $n = 2$ grain boundary sliding. Several processes can take place at the same time, such that each process will contribute to the exponent n. It may therefore not be possible to connect n with a particular densification mechanism. Generally the theoretical models discussed are

31

based on only one mechanism and often demand unavailable information. Though in certain cases application of these models seems useful and results in reasonable fitting with experimental data, the models often fail.

Mechanical properties of reaction hot-pressed specimens can be compared with those of dense reaction sintered specimens. Mitomo et al. [32] obtained a 3-point bending strength of 430 and 470 MPa for two different hot-pressed sialons with z = 2. A decreasing strength with increasing z-value is noticed by Tani et al. [33]. The strength decreased from 490 to 370 MPa with z increasing from 1 to 4. At the same time the Vickers hardness decreased from 21 to 13 GPa. The Young's modulus and fracture toughness both decreased up to z = 3 and remained constant between z = 3 and z = 4. The Young's modulus decreased from 285 to 230 GPa and the fracture toughness from 3.6 to 2.4 MPa m$^{1/2}$. The influence of additives (5 wt%) on the bending strength was studied by Nakamura et al. [33]. MgO and Y_2O_3 increased the room temperature strength but strongly decreased the strength at 1200 °C. TiO_2, ZrO_2, ZrN, ZrC and HfC had a similar effect though the changes were smaller. SiC, WbC, TiC and TiN increased the strength at room temperature and at 1400 °C. BN and TaN introduced defects and lowered the strength.

2.4 Carbothermal production from kaolin

Production of sintered sialon from kaolinite consists of two main steps:
− the carbothermal production of sialon powder from kaolinite,
− sintering of the sialon powder.
Between these steps generally a milling procedure is necessary.

The production of β'-$Si_3Al_3O_3N_5$ from kaolinite and carbon is given by the overall reaction:

$$3(2SiO_2.Al_2O_3.2H_2O) + 15C + 5N_2 \rightarrow 2Si_3Al_3O_3N_5 + 15CO + 6H_2O \qquad (2.11)$$
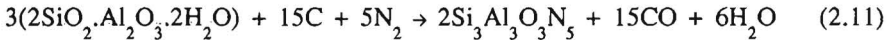
The overall reaction (2.11) can be separated into several stages. During the first stage the crystal water will be removed from the kaolinite at about 560 °C resulting in meta-kaolinite which, at about 960 °C, dissociates into mullite and SiO_2 according to:

$$3(2SiO_2.Al_2O_3) \rightarrow 3Al_2O_3.2SiO_2 + 4SiO_2 \qquad (2.12)$$
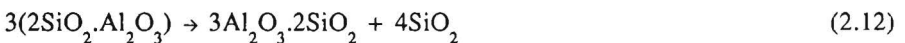
A possible further reaction mechanism is given by Higgens and Hendry [35]. This mechanism comprises the formation of SiC from the SiO_2 and finally the formation of β'-$Si_3Al_3O_3N_5$ from the mullite and SiC:

$$SiO_2 + 3C \rightarrow SiC + 2CO \tag{2.13}$$

$$3Al_2O_3.2SiO_2 + 4SiC + 3C + 5N_2 \rightarrow 2Si_3Al_3O_3N_5 + 7CO \tag{2.14}$$
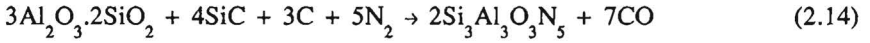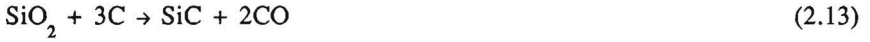
In most cases sialon production is performed in a packed bed reactor. The quality of the β'-sialon is strongly affected by the exact composition of the raw materials and reaction parameters like temperature, time, nitrogen flow and pellet size [35,36]. Main impurities that are present in the kaolinite are CaO, TiO_2, Fe_2O_3, MgO and SiO_2. Reaction times vary from 3 to 40 h at a temperature varying from 1350 to 1550 °C depending on the other process parameters.

In case mass transfer (film diffusion) is rate determining, Van Dijen [36] suggested that the reaction rate in the packed bed is dependent on the Reynolds number:

$$Re = \frac{\rho_g v_g d_p}{\mu} \tag{2.15}$$

with ρ_g the gas density, v_g the superficial gas velocity, d_p the effective pellet diameter and μ the dynamic viscosity of the gas. The reaction rate for low Reynolds numbers (< 0.05) can be expressed in height of transfer units (HTU). One HTU is defined as the reactor length in which the driving force is reduced by a factor e = 2.718.

$$HTU = \frac{v_g}{k_m S_v} \tag{2.16}$$

with S_v the specific area of the reactor (0.36 d_p^{-1} [m^{-1}] for a packed bed with a porosity of 40 %) and k_m the mass transfer coefficient. With D_g as the diffusion coefficient of the gas, eq. (2.16) can be rewritten in the dimensionless numbers of Sherwood (Sh = $k_m d_p D_g^{-1}$), Schmidt (Sc = $\mu D_g^{-1} \rho_g^{-1}$) and Reynolds. For low Reynolds numbers Van Dijen derived [36]:

$$Sh = 0.03\ Re^{4/3} \tag{2.17}$$

Under the given conditions Van Dijen [36] assumed, without reasoning, Sc = 0.68 resulting in:

$$HTU = 6.2 \ d_p \ Re^{-1/3} \qquad\qquad (2.18)$$

Eq. (2.18) indicates that the reaction rate is proportional to $d_p^{-2/3} v_g^{1/3}$. According to Van Dijen [36] at a Reynolds number above 0.05 the chemical reaction becomes rate controlling.

Van Dijen et al. [37] also observed that the reaction product varies not only with the carbon content but also with the Reynolds number. At high Reynolds numbers a mixture of silicon nitride, aluminium nitride and aluminium oxide was obtained instead of β'-sialon. An excess of carbon under these conditions leads to the formation of a mixture of silicon nitride and aluminium nitride. At low Reynolds number and appropriate carbon content only β'-$Si_3Al_3O_3N_5$ is formed. An excess of carbon results in the formation of 15R phase and a shortage of carbon leads to the presence of α-Al_2O_3.

Higgens and Hendry [35], on the other hand did not find any influence of the pellet size and stated that the gas flow rate is the dominant factor in the reactor. At low flow rates the reaction rate is determined by the equilibrium CO pressure. At high flow rates the reaction rate is controlled by the reactivity of the powders.

Van Neerven [38,39] used Szekely's grain model to describe the carbothermal production of β'-sialon. This grain model combines the model for catalysed reactions on porous solids and the shrinking unreacted core model. The conversion according to the grain model is the sum of three terms:

$$\frac{t}{\tau} \propto f_g(X) + \hat{\sigma}^2(f_p(X) + \frac{2X}{Sh}*) \qquad\qquad (2.19)$$

with τ = total reaction time when the chemical reaction is rate controlling. The three terms are described in the following paragraphs.

The first term, $f_g(X)$, describes the conversion according to the shrinking unreacted core model in case the chemical reaction is rate controlling. The shrinking unreacted core model describes a chemical gas-solid reaction at the grains from which the pellets are made up:

$$A_{(g)} + bB_{(s)} \rightarrow cC_{(g)} + dD_{(s)} \qquad\qquad (2.20)$$

In our case spherical pellets are composed of kaolinite plates with relatively small carbon particles (d_{50}(kaolin) = 2 μm, d_{50}(carbon) = 0.06 μm). The carbon makes up only 20 % of the mixture. Van Dijen et al. [37] found no influence of the type of carbon black on the reaction. Therefore the core model is applied to the kaolinite plates with half thickness L_p. The following conversion-time function $f_g(X)$ can be derived in case the chemical reaction is rate controlling [38]:

$$f_g(X) = \frac{t}{\tau} = X \qquad (2.21)$$

with

$$\tau = \frac{\rho_B L_P}{b k_s f(c_A, c_C)} \qquad (2.22)$$

where k_s = surface reaction rate constant

$\quad f(c_A, c_C)$ = function of the concentrations of A and C

$\quad \rho_B$ = molar density of B (mol m^{-3})

The kaolinite plates are actually not monosized but have a certain size distribution. According to the theory, the conversion function of the grains $f_g(X)$ will be strongly influenced by this distribution (see fig. 2.6).

The model for catalysed reactions on porous solids describes simultaneous pore diffusion and chemical reaction in porous pellets. The second term of eq. (2.19) is a conversion function determined by pore diffusion in the porous pellets. For spherical pellets the geometrical part of this function, $f_p(X)$, is given by:

$$f_p(X) = 1 - 3(1 - X)^{2/3} + 2(1 - X) \qquad (2.23)$$

The reaction modulus $\hat{\sigma}$ is comparable to the Thiele modulus and given by:

$$\hat{\sigma}^2 = \frac{d_p^2 \, k_s \, S_v}{24 L_P D_e} \left(1 + \frac{1}{K}\right) \qquad (2.24)$$

with K an equilibrium constant.

With the third term of eq. (2.19) the influence of film diffusion is incorporated in the model using a modified Sherwood number Sh*:

35
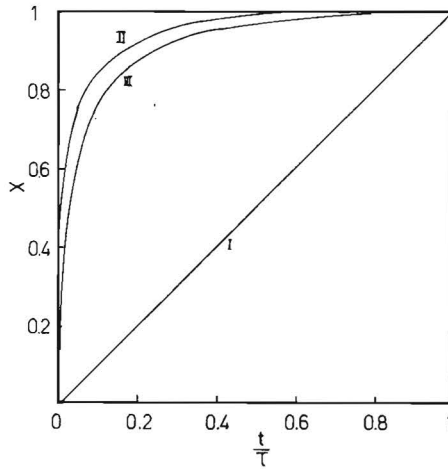
Fig. 2.6. Conversion curves, calculated from various grain size distributions on Monarch kaolinite. Given is the degree of conversion (X) as function of the dimensionless time (t/τ) [38].

I = uniform grain size
II = according to sedimentation analysis distribution
III = according to dry state laser diffraction analysis distribution
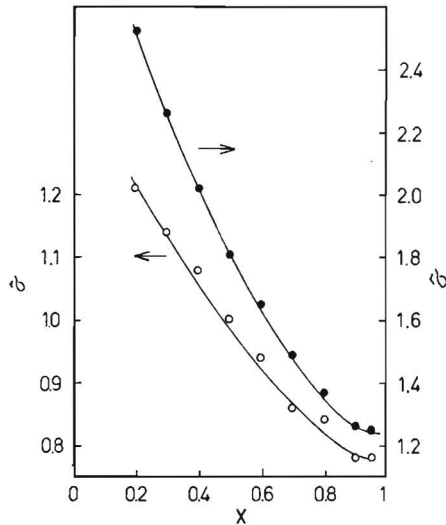
Fig. 2.7. The reaction modulus $\hat{\sigma}$ as function of the conversion X for two pellet diameters 3.5 mm (o) and 6.5 mm (•).

$$Sh^* = Sh \frac{D_g}{D_e} \tag{2.25}$$

with D_e the effective diffusion coefficient of the gas through the product layer which is strongly influenced by the microstructure of this layer.

Szekely's grain model applies to one pellet. Therefore experiments should be performed under differential conditions which means that the reaction conditions may not be influenced by the reaction itself. In case of carbothermal production of sialon the reaction product CO may not influence the reaction. This indicates the limitation of the model, because in a packed bed this condition will never be fulfilled.

Experiments [38] showed that the reactor content should be less than 0.3 g. Van Neerven [38] mixed 0.25 g of pellets with fused corundum grains ranging from 1 to 2 mm. It was therefore not possible to verify the formation of β'-$Si_3Al_3O_3N_5$ in the reaction product. At a flow of 9 l/h N_2, film diffusion could be neglected. Under these conditions, at 1400 °C, pore diffusion could be neglected for a pellet diameter below 1 mm. Calculations of $\hat{\sigma}$ for a pellet diameter of 3.5 and 6.5 mm as function of the conversion show an increasing reaction modulus at decreasing conversion (fig. 2.7). Theoretically the modulus should be independent of the conversion. This can be explained by the size distribution of the kaolinite plates. If monosized kaolinite plates are assumed, L is a constant and S will remain constant during the whole reaction time. If the kaolinite (and consequently L) has a certain size distribution, small plates will react completely before the total conversion is reached. Thus S will decrease during the reaction time. The reaction modulus has to be calculated on those plates that contribute to S. Therefore the average thickness of the reacting plates L will increase during the reaction time. Both effects, increasing L and decreasing S, will cause a decrease of $\hat{\sigma}$ at increasing X.

The sinterability of sialon derived from kaolinite is strongly influenced by the addition of sintering aids, the particle size of the powder and the purity of the sialon, which is directly dependent on the purity of the kaolinite used. This explains the differences between results from several authors. Sintering temperatures varied from 1600 to 1800 °C [40-43] at times from 1 to 20 h.

The resulting strength for sialon without additives varies from 110 MPa to 250 MPa 3- and 4-point bending strength [40-43]. A very low strength can be caused by unconverted carbon particles [41]. Lee [42] obtained a 4-point bending strength of 310 MPa for a YAG ($3Y_2O_3.5Al_2O_3$) doped sialon sintered for 1 h at

1800 °C. Using a diametral compression test, Van Dijen [36] found a relatively high strength of 550 MPa for a Y_2O_3 doped sialon sintered for 20 h at 1675 °C. The grain size was rather large and varied strongly. Needle shaped grains with an aspect ratio of 5 and length up to 20 μm were observed.

The sinterability of the β'-sialon powder depends strongly on the milling behaviour of the powders [44]. After carbothermal production the powders consist of agglomerates of varying strength. The strength of these agglomerates is influenced by the purity of the raw materials and process conditions. If, due to impurities or high temperature, liquid formation occurred during carbothermal production, the strength of the agglomerates will be higher. Insufficient milling of the agglomerates can result in a microstructure consisting of clusters of sialon grains (the original agglomerates) surrounded by regions richer in second phase material. Such a structure will have inferior mechanical properties.

2.5 Summary

In a brief introduction (2.1) the chemical formula and structure of the sialons are presented. Subsequent sections give a review of the literature three preparation techniques for sialon: reaction sintering (2.2), reaction hot-pressing (2.3) and carbothermal production (2.4).

Important process parameters are stated and some frequently used models are mentioned. The models have only a limited value: often they describe the process under restricted conditions or they incorporate model parameters which are unknown or change during the process.

Mechanical properties of reaction sintered and reaction hot-pressed sialons are similar. They are strongly influenced by the exact composition of the powder mixture and presence of impurities and additives. A 3-point bending strength up to 490 MPa is found [25]. The 4-point bending strength of sialons derived from kaolinite is much lower: up to 310 MPa. This low strength can be caused by impurities in the kaolin as well as by insufficient milling of the sialon powder prior to the sintering process.

References

1. W.Y. Sun and D.S. Yan, "Phase equilibria studies on nitride systems and their role for material compositional optimization", Rev. Solid State Sci. 1(1988)493-504.

2. L. Gillot, N. Cowlam and G.E. Bacon, "A neutron diffraction investigation of some β'-sialons", J. Mater. Sci. 16(1981)2263-2268.

3. T. Ekström, "Dense single-phase β-sialon ceramics by glass-encapsulated hot isostatic pressing", J. Mater. Sci. 24(1989)1853-1861.

4. M. Haviar and O. Johannesen, "Unit-cell dimensions of β'-sialons", Adv. Ceram. Mater. 3(1988)405-407.

5. S. Wild, H. Elliott and D.P. Thompson, "Combined infra-red and X-ray studies of β-silicon nitride and β'-sialons", J. Mater. Sci. 13(1978)1769-1775.

6. K.H. Jack, "Review: Sialons and related nitrogen ceramics", J. Mat. Sci. 11(1976)1135-1158.

7. K.H. Jack, "The relationship of phase diagrams to research and development of sialons", Phase Diagrams 5(1978)241-285.

8. Y. Oyama and O. Kamigaito, "Solid solubility of some oxides in Si_3N_4", Japan. J. Appl. Phys. 10(1971)1637-1638.

9. F.K. van Dijen, R. Metselaar, R.B. Helmholdt, "Neutron diffraction study of β'-sialon", J. Mater. Sci. Lett. 6(1987)1101-1102.

10. M. Mitomo, N. Kuramoto and H. Suzuky, "The formation of single phase β-sialon", Proc. of Int. Symp. on Factors in Densification and Sintering of Oxide and Non-oxide Ceramics, 1978, eds. S. Somiya and S. Saito, Gakujutsu biunken Fukyu-Kai, Tokyo, (1979)463-367.

11. M.H. Lewis, S. Mason and A. Zweda, "Syalon ceramics for application at high temperature and stress", Proc. Int. Conf. Non-oxide Tech. Eng. Ceram., 1985, ed. S. Hampshire, Elsevier Appl. Sci., London (1986) 175-190.

12. W.D. Kingery, "Densification during sintering in the presence of a liquid phase. I. Theory ", J. Appl. Phys. 30(1959)301-306.

13. S. Hampshire and K.H. Jack, "The kinetics of densification and phase transformation of nitrogen ceramics", Special Ceramics 7, eds. D. Taylor and P. Popper, British Ceramic Research Association, Stoke on Trent, (1981)37-49.

14. "Comprehensive chemical kinetics",vol. 22, "Reactions in the solid state", ed. C.H. Bamford and C.F.H. Tipper, Elsevier Scientific Publishing Company, 1980.

15. F.F. Lange, "Sinterability of agglomerated powders", J. Am. Cer. Soc. 67 (1984)83-89.

16. F.F. Lange, "Thermodynamics of densification: II Grain growth in porous compacts and relation to densification", J. Am. Ceram. Soc. 72(1989) 735-741.

17. A.G. Evans, "Considerations of inhomogeneity effects in sintering", J. Am. Cer. Soc. 65(1982)407-501.

18. R.R. Wills, R.W. Stewart and J.M. Wimmer, "Fabrication of reaction-sintered sialon", J. Am. Ceram. Soc. 60(1977)64-67.

19. W.A. Sanders and G.Y. Baaklini, "Correlation of processing variables with the strength and radiography of silicon nitride", Adv. Ceram. Mater. 3(1988)88-94.

20. M. Mitomo, N. Yang, Y. Kishi and Y. Bando, "Influence of powder characteristics on gas pressure sintering of Si_3N_4", J. Mater. Sci. 23(1988)3413-3419.

21. G. Petzow, L.J. Gauckler, T.Y. Tien and S. Boskovic, "β-Si_3N_4 solid solution formation by reaction sintering", Proc. of Int. Symp. on Factors in Densification and Sintering of Oxide and Non-oxide Ceramics, 1978, eds. S. Somiya and S. Saito, Gakujutsu biunken Fukyu-Kai, Tokyo, (1979)28-39.

22. S. Bandyopadhyay and J. Mukerji, "Sintering and properties of sialons without externally added liquid phase", J. Am. Ceram. Soc. 70(1987) C273-C277.

23. M. Mitomo, N. Kuramoto, Y. Inomata and M. Tsutsumi, "The strength of reaction sintered β-sialon", Yogyo-Kyokai-Shi 88(1980)489-496.

24. M. Mitomo, N. Kuramoto and Y. Inomata, "Fabrication of high strength β-sialon by reaction sintering", J. Mater. Sci. 14(1979)2309-2316.

25. M.N. Rahaman, F.L. Riley and R.J. Brook, "Reaction sintering and the α-Si_3N_4/β'-sialon transformation for compositions in the system Si-Al-O-N", J. Mater. Sci. 16(1981)660-668.

26. T. Ekström, "Fabrication and properties of yttrium sialon ceramics", Ceramic Developments, Mater. Sci. Forum 34-36(1988)605-610.

27. M. Kuwabara, M. Benn, F.L. Riley and R.J. Brook, "Reactive hot-pressing of $Si_{6-z}Al_zO_zN_{8-z}$ (β'-sialon) phases", Proc. of Int. Symp. on factors in densification and sintering of oxide and non-oxide ceramics, 1978, eds. S. Somiya and S. Saito, Gakujutsu biunken Fukyu-Kai, Tokyo, (1979) 527-537.

28. M. Benn, M. Kuwabara and F.L. Riley, "Reactive hot-pressing of phases in the system $Si_{6-z}Al_zO_zN_{8-z}$ (β'-sialon)", Sci. Cer. 9(1977)119-126.

29. R.L. Coble, "Diffusion models for hot pressing with surface energy and pressure effects as driving forces", J. Appl. Phys. 41(1970)4798-4807.

30. J.M. Vieira and R.J. Brook, "Kinetics of hot-pressing: the semi-logarithmic law", J. Am. Ceram. Soc. 67(1984)245-249.

31. M.N. Rahaman, F.L. Riley and R.J. Brook, "Mechanism of densification during reaction hot-pressing in the system Si-Al-O-N", J. Am. Ceram. Soc. 63(1980) 648-653.

32. M. Mitomo, Y. Hasegawa, Y. Bando, A. Watanabe and H. Suzuki, "The strength of hot-pressed β-sialon", Yogyo-Kyokai-Shi 88(1980)298-304.

33. E. Tani, S. Umebayashi, K. Okuzono, K. Kishi and K. Kobayashi, "Effect of composition on mechanical properties of β-sialon", Yogyo-Kyokai-Shi 93(1985)370-375.

34. H. Nakamura, S. Umebayashi, K. Kishi, E. Tani and K. Kobayashi, "The effects of additives on bending strength of hot-pressed β-sialon with z = 1", Yogyo-Kyokai-Shi 93(1985)175-181.

35. I. Higgens and A. Hendry, "Production of β'-sialon by carbothermal reduction of kaolinite", Brit. Ceram. Trans. J. 85(1986)161-166.

36. F.K. van Dijen, "The carbothermal production of $Si_3Al_3O_3N_5$ from kaolin, its sintering and its properties", Ph.D. Thesis, Eindhoven University of Technology, 1986.

37. F.K. van Dijen, R. Metselaar and C.A.M. Siskens, "Reaction-rate-limiting steps in carbothermal reduction processes", J. Am. Ceram. Soc. 68(1985) 16-19.

38. A.M. van Neerven, "Reaction engineering aspects of the carbothermal production of β'-sialon from kaolin", M.Sc. Thesis, Centre for Technical Ceramics, Eindhoven University of Technology (1988).

39. A.M. van Neerven, F. Blömer and R. Metselaar, "Reaction engineering parameters of the carbothermal production of β'-sialon from kaolin", Euro-Ceramics vol.I, eds. G. de With, R.A. Terpstra and R. Metselaar, Elsevier, London, (1989)572-576.

40. K. Mitchell and A. Hendry, "Sintering of non-oxide ceramics", Mater. Sci. Monogr. 38A(12987)901-910.

41. S. Bandyobadhyay and J. Mukerji, "Sintering and properties of sialons derived from kaolin", Adv. Ceram. Mater. 3(1988)328-331.

42. H.L. Lee, H.J. Lim, S. Kim and H.B. Lee, "Thermomechanical properties of β-sialon synthesized from kaolin", J. Am. Ceram. Soc. 72(1989)1458-1461.

43. C.J. Spacie, "Preparation of sialon ceramics from low cost raw materials", Proc. Int. Conf. Non-oxide technical and engineering ceramics, 1985, ed. S. Hampshire, Elsevier Appl. Sci., London, (1986) 133-147.

44. H. Mostaghaci, F.L. Riley and J.P. Torre, "The milling and densification behaviour of β'-sialon powders prepared from alumino-silicate minerals", Int. J. High Tech. Ceram. 4(1988)51-71.

41

chapter 3

REACTION SINTERING OF Si$_3$Al$_3$O$_3$N$_5$

3.1 Introduction

In this chapter the reaction sintering behaviour of mixtures of Si_3N_4, Al_2O_3 and AlN is studied. After a description of the experimental details, (3.2) the methods used for the characterization of the products are given in 3.3. Section 3.4 summarizes some preliminary experiments to optimize the powder processing.

The influence of CeO_2 and CaO on the sintering behaviour of β'-$Si_3Al_3O_3N_5$ is studied in 3.5 and 3.6. In both cases a two-step sintering process is optimized for mixtures with 1, 3 and 5 wt% additive. In the last section, 3.7, the influence of SiO_2, TiO_2 and Fe_2O_3 is studied on mixtures with 1 wt% CaO as sintering aid. These oxides are commonly present in kaolin and are expected to influence the sinterability and properties of sialon derived from kaolin. By preparing sialon samples with a defined concentration of one of these impurities, the influence of that impurity on the properties can be studied.

3.2 Experimental details

Raw materials

For reaction sintering as well as reaction hot-pressing tablets were made of a mixture of Si_3N_4, AlN and Al_2O_3. The silicon nitride (LC12) and aluminium nitride (grade C) were purchased from HC Starck and the aluminium oxide (AKP30) from Sumitomo Chemical Company. In the first experiments a different Al_2O_3 powder was used: CT3000 from Alcoa Chemicals. This powder was also used in the bed powder in reaction sintering experiments. Chemical composition and physical properties of the powders as given by the supplier are summarized in table 3.1.

Powder processing

$Si_{6-z}Al_zO_zN_{8-z}$ with z = 3 can be prepared from AlN, Al_2O_3 and Si_3N_4 according to:

$$Si_3N_4 + Al_2O_3 + AlN \rightarrow Si_3Al_3O_3N_5 \qquad (3.1)$$

In order to calculate the mixture composition the following assumptions were made:

- The oxygen content of the AlN powder is caused by surface Al_2O_3 on the particles: an oxygen content of 1.7 wt% corresponds to an Al_2O_3 content of 3.61 wt%.

TABLE 3.1

Chemical composition and physical properties of the materials used.

	Si_3N_4 (LC12)	AlN (grade C)	Al_2O_3 (CT3000)	Al_2O_3 (AKP30)
Al (wt%)		balance	52.7	
Si (wt%)			0.014	0.0018
N (wt%)	38.43	33.5		
C (wt%)	0.17	0.07		
O (wt%)	1.96	1.7		
Fe (wt%)	0.006	0.01	0.021	0.0004
Ca (wt%)	0.008		0.014	
Mg (wt%)			0.001	0.0003
Na (wt%)			0.085	0.0004
d_{50} (μm)	0.50	1.2	0.5	0.41
BET$^+$ (m^2/g)	20.2	3.7	3.5	6.5
LOI* (wt%)			< 0.5	
α-Si_3N_4 (wt%)	> 90			
purity (wt%)			> 99.6	> 99.99

$^+$BET = specific surface as determined by standard N_2 adsorption according to Brunauer, Emmett and Teller

*LOI = loss on ignition

– The oxygen content of the Si_3N_4 powder (1.96 wt%) is caused by an SiO_2 layer on the particles. This means an SiO_2 content of 3.68 wt%. This assumption is not completely correct since part of the oxygen can be present as silicon oxynitride. With a specific surface of 20.2 m^2/g and a density of SiO_2 of 2.3 g cm^{-3} the thickness of this oxide layer can be calculated: 0.8 nm.

– The SiO_2 reacts to $Si_3Al_3O_3N_5$ according to:

$$Si_3N_4 + 6\ AlN + 3\ SiO_2 \rightarrow 2\ Si_3Al_3O_3N_5 \tag{3.2}$$
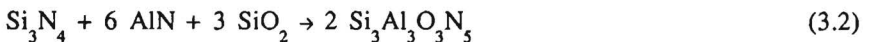
These assumptions result in the following mixing weight ratio:

$$Si_3N_4 : Al_2O_3 : AlN = 49.91 : 33.31 : 16.77 \tag{3.3}$$

45
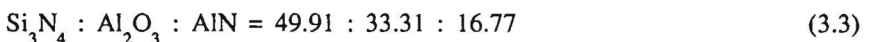
Fig. 3.1. Weight loss as function of time during heating up to 550 °C to remove the pressing aid.

The powders (together with the sintering additives) were mixed in batches of 100 g with 250 ml propanol-2 and 200 g Si_3N_4 grinding balls in a polyethylene bottle. Polyethyleneglycol, PEG, (2.5 - 5.0 wt%) was added as a pressing aid. The mixing time was 4 hours in a turbula mixer (type T2C, W.A. Bachofen AG Maschinenfabrik). This resulted in an average weight loss of the grinding balls of 0.2 g.

After evaporation of the isopropanol in a rotavapor (type RE 111, Büchi) and drying at 100 °C, the powder was passed through a 63 μm aperture sieve. For reaction sintering experiments tablets of 1.5 (∅ 13 mm) and 7.0 g (∅ 22 mm) were uniaxially pressed at 15 MPa. For hot-pressing experiments tablets of 20 g (∅ 32 mm) were pressed at 3 MPa. Afterwards the tablets were isostatically repressed at 250 MPa. Finally they were slowly heated up to 500 °C in air to remove the pressing aid. If the pressing aid is evaporated too fast the green products may crack. A typical curve for binder removal is given in fig. 3.1. This powder processing results in a green density of approximately 2.1 g cm^{-3}.

Sintering experiments

The reaction sintering experiments were done in a gas pressure sintering furnace (type FPW 100/150-2200-100 DIL, KCE Sondermaschinen GmbH). The furnace had graphite h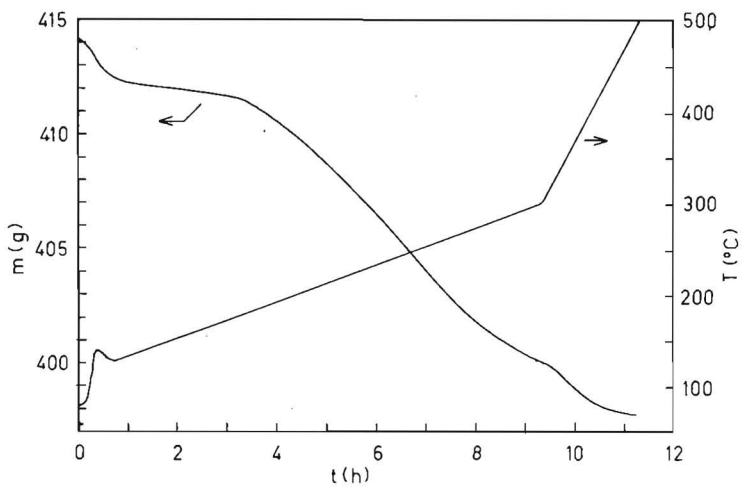eating elements and a maximum temperature of 2200 °C. The maximum gas pressure (N_2 or Ar) is 10 MPa. The useful volume had a diameter of 80 mm and a height of 100 mm (temperature controlled within ± 10 °C at 2200 °C). The temperature was measured by a pyrometer placed on top of the furnace. The minimum measurable temperature for the pyrometer was 1100 °C.

The experiments were done with a large boron nitride crucible (∅ 80 mm, h 90 mm) with a lid. In experiments with small samples (1.5 g) the samples are placed in a small boron nitride crucible (∅ 52 mm, h 43 mm) within the large crucible. In experiments with large samples (7.0 g) the samples are put directly in the large crucible.

In all experiments the samples are embedded in a powder mixture. This bed powder contained 25 wt% BN and 75 wt% of a mixture with a composition equal to that of the samples.

The sinter experiments can be divided in single step and two step procedures. In a single step procedure the samples were heated to a certain temperature and held at this temperature under a pressure of 0.5 MPa. In a two step procedure after this, an N_2-pressure of 10 MPa was applied and in most cases the temperature was increased at the same time. The samples were held for a second period

47

under these conditions.

The heating procedure was as follows. Within 1.8 h the furnace was heated to 1200 °C. This part of the heating procedure was power controlled. From 1200 °C the process was temperature controlled. The tempeature was held at 1200 °C for 0.25 h and then raised to the desired value at a rate of 600 °C/h.

The heating procedure was started in a vacuum of 0.5 Pa. After 1.40 h a pressure of 0.5 MPa was applied. If the experiment was a two step sintering procedure a pressure of 10 MPa was applied within 0.17 h after the first sintering step. In most cases the temperature was increased during the application of the gas pressure.

3.3 Characterization methods

X-ray diffraction

The composition of the products was determined by X-ray diffraction. Thus only the composition of the crystalline part was analysed. Cu $K\alpha$ radiation is used. The 2ϑ range from 10 to 60° was scanned. A quantitative analysis was performed from the measured intensities. This analysis is based on the adiabatic principle of auto-flushing [1-3]. The method assumes that the intensity-concentration relationship between each and every pair of components in a multi-component system is not perturbed by the presence or absence of other components.

For each compound N of a mixture a reference peak with intensity I_{rN} is chosen. These peaks have relatively high intensities and have no overlap with other peaks. The measured intensities of the reference peaks (I^m_{rN}) are converted to the 100 % intensity peak by dividing by I_{rN}/I_{oN} and correlated to the intensity of corundum by dividing by I_{oN}/I_{cor}. I_{oN} is the intensity of the 100 % peak of compound N and I_{cor} is the intensity of the 100 % corundum peak. Thus the concentration of compound N is given by:

$$[N] = \frac{I^*_N}{\sum\limits_N I^*_N} \tag{3.4}$$

with:

48

$$I_N^* = I_{rN}^m \; \frac{I_{oN}}{I_{rN}} \frac{I_{cor}}{I_{oN}}$$
(3.5)

Table 3.2 lists the reference peaks used with their relative intensities and correction factors I_{oN}/I_{cor}. The correction factors I_{oN}/I_{cor} were calculated by Visser [4] according to the method described in [5,6].

X-ray analysis on a mixture according to eq. (3.3) by the method described above resulted in 43.7 % α-Si_3N_4, 2.7 % β-Si_3N_4, 38.3 % Al_2O_3 and 15.3 % AlN which is in good agreement with (3.3). Some other analyses on mixtures of the compounds of table 3.2 showed that the relative accuracy of this method is about 15 %.

TABLE 3.2

The reference peaks indicated by their lattice spacing (d_r), their relative intensity I_{rN}/I_{oN} and correction factor I_{oN}/I_{cor} of the most frequently occurring compounds.

compound	JCPDS (no.)	d_r (Å)	I_{rN}/I_{oN} (%)	I_{oN}/I_{cor} (%)
β'-$Si_3Al_3O_3N_5$	36-1333	2.72	100	1.142
β-Si_3N_4	33-1160	3.30	100	1.170
α-Si_3N_4	9-250	2.90	85	0.796
α-Al_2O_3	10-173	1.60	80	1.000
AlN	25-1133	1.56	40	1.600
$SiAl_4O_2N_4$	32-26	2.78	100	0.963
Si_2N_2O	18-1171	4.44	89	1.492
$2SiO_2 \cdot 3Al_2O_3$	15-776	3.39	100	0.705
α-SiO_2	11-695	4.05	100	5.021
β-SiC	1-1119	1.54	40	3.562

Density

The density of green products was determined by dividing the sample weight by the calculated volume. The volume was calculated from the sample dimensions. The density of sintered products was determined by the Archimedes technique. In this method the sample volume is calculated from the difference in weight between the

sample weighed in air (m_a) and weighed in water (m_w). Thus the density is given by:

$$\rho = \frac{m_a}{m_a - m_w} \rho_w \tag{3.6}$$

where ρ_w is the density of water at the measuring temperature. It will be clear that this method only gives reliable results if the sample does not contain open porosity. The masses m_a and m_w were determined several times after each other. If m_a remained constant the sample was assumed not to suck water.

Vickers hardness

Micro hardness measurements were done with a Durimet 1C from Leitz. The hardness was measured with a Vickers indenter and load of 2N. The hardness is calculated from the diagonal (d_v) of the indentation according to:

$$HV = \frac{2P \sin(136/2)}{d_v^2} = 1.85 \frac{P}{d_v^2} \text{ [Pa]} \tag{3.7}$$

where P is the applied load.

Microstructure

The residual porosity was studied with optical microscopy on polished samples. Grain size and second phases were studied with optical microscopy as well as scanning electron microscopy (SEM) on etched samples.

Several etching procedures were tested. The etching temperature for thermal etching was between 1325 °C and 1375 °C. The etching temperature and time appeared to be very dependent on the production process and sintering additives. To prevent oxidation the etching had to be done in nitrogen. Therefore thermal etching was very laborious. Etching with molten KOH removed the second phase completely before the β'-$Si_3Al_3O_3N_5$ grain boundaries were etched. Two agents gave a reasonable result:

I) a solution of NH_4FHF in H_2O at about 80 °C and a weight ratio $NH_4FHF : H_2O$
    = 3 : 8
II) a mixture of HF (40%), H_2O_2 (30 %) and HNO_3 (65 %) at room temperature and
    a volume ratio HF : H_2O_2 : HNO_3 = 6 : 5 : 1.

The average etching time for both methods was a few minutes. Both agents gave a similar image. Because the second agent can be used at room temperature this method was preferred.

3.4 Influence of powder processing on the sintering behaviour of $Si_3Al_3O_3N_5$ without additives

In order to develop the powder processing route described above some experiments were done with a powder mixture without additives. Studied were the influence of the Al_2O_3 powder source, milling time, milling apparatus and pressing aid on the sinter behaviour. Compared were the turbula mixer, planetary ball mill and roller bench.

The resulting densities of the samples in these experiments are given in table 3.3. The sinterability of all mixtures appeared to be very poor due to the absence of sintering aids. Sintering at 1850 °C for 2 h did not result in closed porosity. Increasing the temperature resulted in decomposition of the sialon into 15R and SiO and weight loss up to 20 %.

The sinterability of the mixture with AKP30 Al_2O_3 was somewhat better than that of the mixture with CT3000 Al_2O_3: The density increased from 2.00 to 2.24 g cm^{-3}. CT3000 Al_2O_3 is a strongly agglomerated powder. Probably these agglomerates were not completely broken during milling, resulting in this low sinterability.

TABLE 3.3

Reaction sintering experiments without additive as function of the process conditions. The varied process conditions are the milling time (t), milling apparatus (MA), use of pressing aid (PEG) and type of Al_2O_3. All samples are sintered for 2 h at 1850 °C and 0.5 MPa. Given are the resulting density after sintering in a graphite (ρ_C) and boron nitride (ρ_{BN}) crucible.

t (h)	MA*	PEG	Al_2O_3	ρ_C (g/cm^3)	ρ_{BN} (g/cm^3)
4	t	+	CT3000	2.00	
4	t	+	AKP30	2.24	2.41
4	p	+	AKP30	2.07	
94	r	+	AKP30	2.17	2.24
94	r	-	AKP30	2.08	2.12
21	t	+	AKP30	2.40	2.54

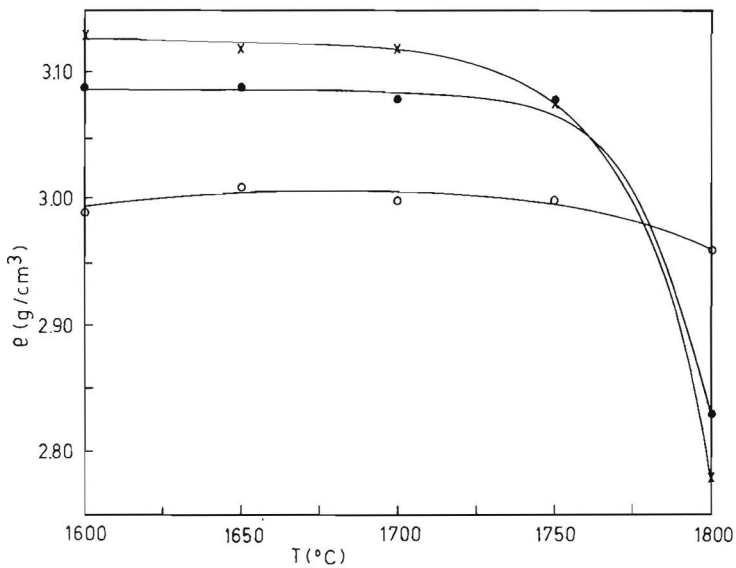* t = turbula mixer, p = planetary ball mill and r = roller bench

Fig. 3.2. The density of samples with 1 (o), 3 (•) and 5 (x) wt% CeO_2 as function of the sintering temperature (T). The sintering time is 1 h and nitrogen pressure 0.5 MPa.

Milling for 94 h at the roller bench gave a density of 2.17 g cm^{-3}. A milling time of 4 h in the planetary ball mill and turbula mixer resulted in densities of 2.07 and 2.24 g cm^{-3} respectively. Mixing with the turbula mixer seemed to be the most effective. However, it should be noted that the resulting densities are low and the milling processes were not optimized with respect to e.g. milling media weight, ball sizes, liquid volume. An increase of the milling time in the turbula mixer to 21 h resulted in an increase of the density from 2.24 to 2.40 g cm^{-3}.

The use of a pressing aid (2.5 wt% polyethylene glycol (PEG)) increased the density from 2.08 to 2.17 g cm^{-3}.

The first sintering experiments were done in a graphite crucible. The average weight loss during sintering was 3 wt%. XRD analysis showed that all samples consisted of β'-Si$_3$Al$_3$O$_3$N$_5$ with 15 - 20 wt% 15R. A last experiment was done in a boron nitride crucible: this resulted in a higher density with a weight loss of less than 1 %. The samples consisted of β'-Si$_3$Al$_3$O$_3$N$_5$ with only traces of 15R.

Thus the best results are obtained with a mixture with AKP30 Al$_2$O$_3$ and pressing aid, milled for 21 h in the turbula mixer (2.55 g cm^{-3}) and a similar mixture with a milling time of 4 h (2.41 g cm^{-3}). Since the much longer milling time results in a larger ball wear, the procedure with a milling time of 4 h is chosen in spite of the somewhat lower density. Finally the material of the crucible is very important. The use of a boron nitride crucible instead of a graphite crucible results in a higher density, lower weight loss and less second phase (15R).

3.5 Sintering of CeO$_2$ doped Si$_3$Al$_3$O$_3$N$_5$

A two step sintering process for mixtures of Si$_3$N$_4$, Al$_2$O$_3$ and AlN according to eq. (3.3) with 1, 3 and 5 wt% CeO$_2$ was optimized. For the optimization tablets of 1.5 g and green density of about 2.1 g cm^{-3} were sintered under various conditions. In order to optimize the first sintering step experiments were done at 0.5 MPa N$_2$-pressure, a sintering time of 1 h and temperature between 1600 °C and 1800 °C. The resulting densities are given in fig. 3.2. A temperature of 1800 °C appeared to be too high. These samples showed swelling and in fig. 3.2 it can be seen that the density decreased strongly at this temperature. This decrease of density was stronger at higher CeO$_2$ content. The weight loss was 0.5 - 0.8 % regardless of the sintering temperature. Thus swelling is not
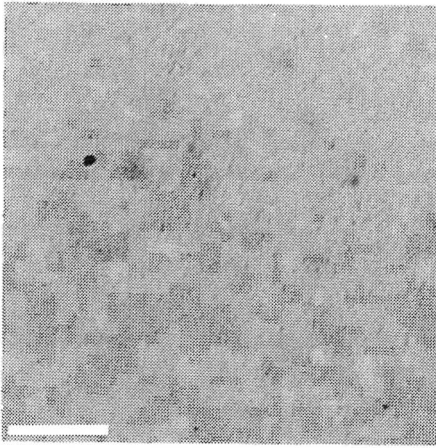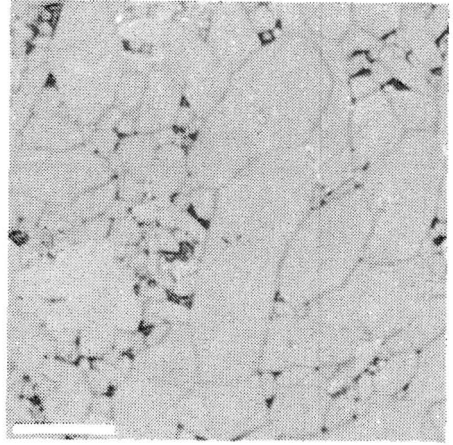
(a)   (b)
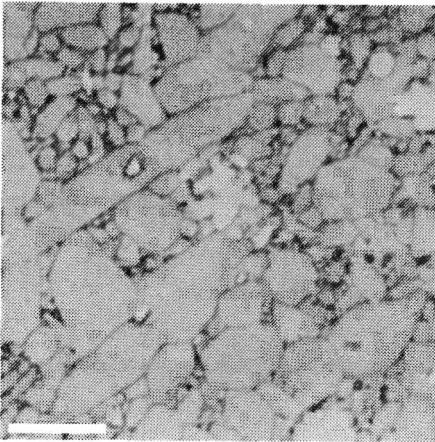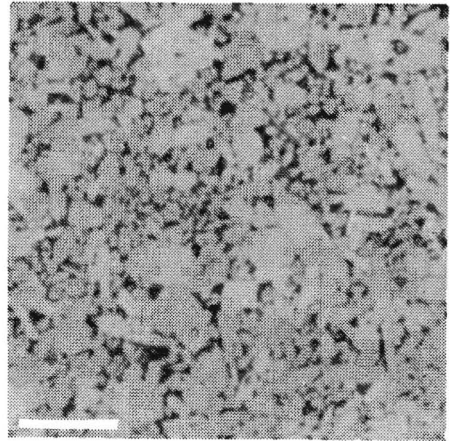
(c)   (d)

Fig. 3.3. Microstructure of samples with CeO$_2$ sintered 0.5 h at 1600 $^\circ$C, 0.5 MPa
followed by:

a) 0.5 h at 1650 $^\circ$C, 10 MPa, 3 wt% (unetched, bar = 50 μm)
b) 1.0 h at 1700 $^\circ$C, 10 MPa, 1 wt% (bar = 10 μm)
c) 0.5 h at 1650 $^\circ$C, 10 MPa, 1 wt% (bar = 10 μm)
d) 0.5 h at 1650 $^\circ$C, 10 MPa, 5 wt% (bar = 10 μm)

related to severe decomposition and evaporation of the samples. For all three compositions closed porosity was obtained at a sintering temperature of 1600 °C and sintering time of 1 h.

The density obtained increased with the CeO_2 content. If the product contains only β'-$Si_3Al_3O_3N_5$ ($\rho = 3.08$ g cm^{-3}) and CeO_2 (7.132 g cm^{-3} [8]) the theoretical density is 3.10, 3.13 and 3.17 g cm^{-3} for 1, 3 and 5 wt% CeO_2 respectively. The CeO_2 is present in the amorphous intergranular phase and often some second phase (15R) is present. Therefore relative densities calculated with these theoretical densities will not be completely correct. The relative densities after sintering at 1600 °C were 96.5, 98.7 and 98.7 % for 1, 3 and 5 wt% CeO_2 respectively. A reduction of the sintering time to 0.5 h resulted in closed porosity and relative densities of 95.1, 98.1 and 97.8 % for 1, 3 and 5 wt% CeO_2.

The composition of all samples is β'-$Si_3Al_3O_3N_5$ with 4 - 12 % 15R. The concentration 15R increases slightly with the CeO_2 content. The CeO_2 forms a liquid with the SiO_2. An increasing CeO_2 content will result in a larger amount of liquid phase. Consequently more SiO_2 will be used for the formation of the liquid phase and less SiO_2 can be used for the formation of β'-$Si_3Al_3O_3N_5$ according to eq.(3.2). A decreasing SiO_2 content in the crystalline phase will promote the formation of 15R which contains less Si than β'-$Si_3Al_3O_3N_5$.

With 1600 °C and 0.5 h as conditions for the first sintering step three experiments were done to optimize the second step. The conditions for the second sintering step under 10 MPa N_2 pressure were: I) 1 h, 1700 °C, II) 1 h, 1650 °C and III) 0.5 h, 1650 °C. In all cases the density was within the accuracy of the measurement equal to the theoretical density. The weight loss was 0.5 - 0.8 %. The products contained β'-$Si_3Al_3O_3N_5$ with 6 - 12 % 15R.

The microstructures are shown in fig. 3.3. Fig. 3.3a shows the unetched sample with 3 wt% CeO_2 sintered under condition II. The sample still contains some porosity. The pore size is up to 15 μm. The porosity decreases with increasing CeO_2 content and increasing sintering temperature and time. Higher temperature and longer time, however, cause grain growth as is visible in figs. 3.3b and c. Both pictures show a sample with 1 wt% CeO_2. The sample in fig. 3.3b is sintered under condition I and the sample in fig. 3.3c under condition III.

It is clear that the higher temperature and longer sintering time during the second sintering step result in a much coarser structure. The needle-shaped grains have a length up to 30 μm and an aspect ratio of about 3 (fig. 3.3b). A decrease of 50 °C of the sintering temperature in the second sintering step and halving of the time results in needles up to 20 μm with an aspect ratio of about
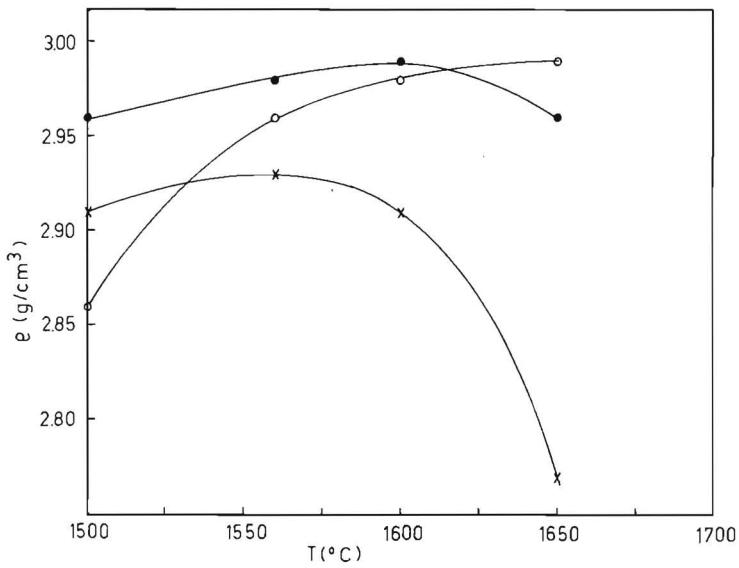
Fig. 3.4. The density of samples with 1 (o), 3 (•) and 5 (x) wt% CaO as function of the sintering temperature (T). The sintering time is 0.5 h and nitrogen pressure 0.5 MPa.

4 (fig. 3.3c). An increasing CeO_2 content also causes a finer structure. Fig. 3.3d shows a sample sintered under condition III but with 5 wt% CeO_2. The needles in this sample have a length up to 15 μm and an aspect ratio of about 4. Comparison of the figs. 3.3c and 3.3d shows the strong increase of the amount of intergranular phase as the CeO_2 content is increased from 1 to 5 wt%. Remarkable is further the strong bimodal grain size distribution. All the pictures show relatively large needles with areas in between that are filled with much smaller needles. The average grain size of microstructures given in the literature [9-11] varied from sub-micron to 4 μm. All these structures also showed an inhomogeneous grain size. Even without the use of sinter additives Mitomo et al. [11] found a large amount of intergranular phase in a β'-$Si_{6-z}Al_zO_zN_{8-z}$ with z = 3. They attributed the inhomogeneous structure to the high z-value.

A second phase, recognizable by the light colour, is present in clusters and also has a structure of needle shaped grains. Analysis with the microprobe showed that these regions contain relatively more Al and less Si confirming that these regions consist of 15R. The amount of 15R increases with the additive content. Wills et al. [12] observed similar light coloured regions in their sialons. They assumed that these were caused by elemental Si, but no regions with high Si content could be found in the sialons prepared in this chapter. Most of the 15R is present as clusters in the structure. This is probably caused by insufficient mixing.

The hardness of the samples sintered in a two step sintering process is 16.4 ± 0.7 GPa. The hardness in the literature [7,9,13] varied from 14 to 17 GPa. There is no correlation between the hardness and the three different sintering conditions or between the hardness and the CeO_2 content.

3.6 Sintering of CaO doped $Si_3Al_3O_3N_5$

For the optimization of a two step sintering process the same procedure was followed as in 3.5. The samples contained 1, 3 and 5 wt% CaO added to the powder mixture as $CaCO_3$. The theoretical densities of β'-$Si_3Al_3O_3N_5$ with 1, 3 and 5 wt% CaO (ρ_{th} = 3.32 g cm^{-3} [8]) are 3.08, 3.09 and 3.09 g cm^{-3} respectively.

The first sintering step was optimized in a series of experiments at 0.5 MPa N_2-pressure, 0.5 h and a sintering temperature varying from 1500 °C to 1650 °C. The resulting densities of these experiments are given in fig. 3.4. Again swelling was observed above a certain temperature resulting in a decrease in
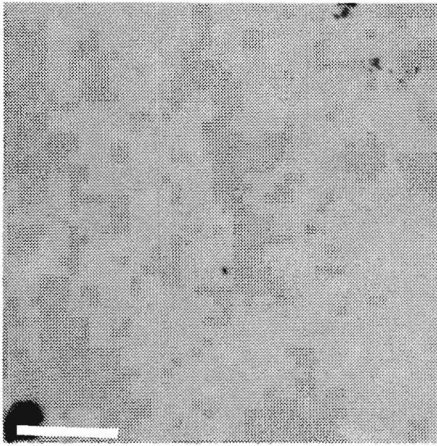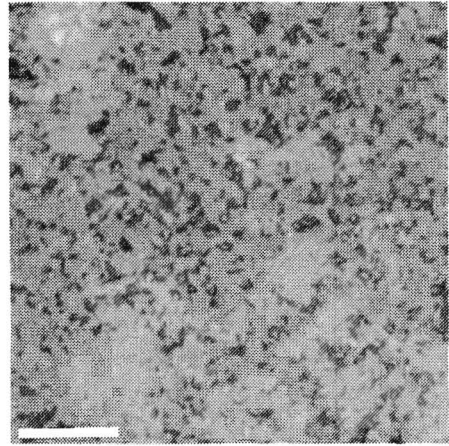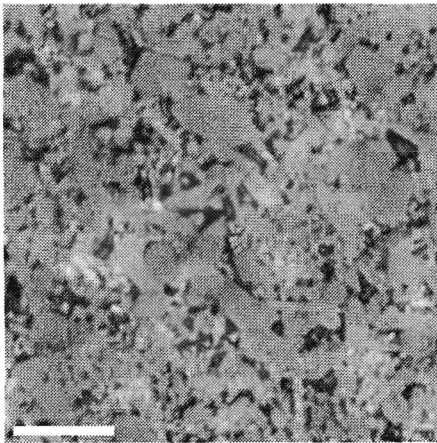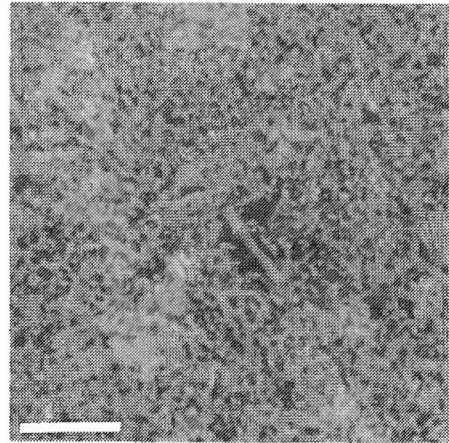
Fig. 3.5. Microstructure of samples with CaO. Sintering conditions are 0.5 h
at 0.5 MPa and 0.5 h at 10 MPa at the following temperatures:

a) 1550 °C and 1600 °C, 3 wt% CaO (unetched, bar = 50 μm)
b) 1500 °C and 1550 °C, 1 wt% CaO (bar = 10 μm)
c) 1600 °C and 1650 °C, 1 wt% CaO (bar = 10 μm)
d) 1500 °C and 1550 °C, 5 wt% CaO (bar = 10 μm)

density. For CaO concentrations of 3 and 5 wt% a decreasing density was observed above 1600 °C and 1550 °C respectively. The samples with 1 wt% CaO did not swell within the studied temperature range. The swelling behaviour was similar to that of CeO$_2$ doped sialons. The tendency to swell increases with the additive concentration. The temperature above which swelling occurs decreases with increasing additive concentration.

An increase of the sintering time at 1500 °C to 1 h resulted in an increase of the density from 2.86, 2.96 and 2.91 g cm^{-3} to 2.93, 2.99 and 2.97 g cm^{-3} for 1, 3 and 5 wt% CaO respectively. These densities are nearly the same as those obtained after sintering for 0.5 h at 1550 °C: 2.96, 2.98 and 2.93 g cm^{-3}.

The effect that the (relative) density at a similar sintering procedure increases with the additive concentration like with the CeO$_2$ doped samples was not observed with CaO doped samples. Within the entire temperature range studied, samples with 3 wt% CaO had a higher density than samples with 5 wt% CaO. Samples with 1 wt% CaO had the lowest density at 1500 °C. Apparently the densification rate at this temperature is lower on account of the smaller amount of liquid phase. At higher sintering temperatures, however, the highest density was obtained for the composition with 1 wt% CaO. The density of samples with 3 wt% and 5 wt% CaO did not increase at these higher temperatures due to swelling.

The weight loss of the samples was about 1.2, 2.5 and 3.8 wt% for 1, 3 and 5 wt% CaO respectively. A part of the weight loss is caused by decomposition of the CaCO$_3$ into CaO and CO$_2$. Taking this into account the weight losses were 0.7, 1.0 and 1.3 wt% for 1, 3 and 5 wt% CaO respectively. Thus the weight loss increased with increasing CaO content. The weight loss was not influenced by the sintering temperature.

The composition of the samples was β'-Si$_3$Al$_3$O$_3$N$_5$ with 15R. Identical to the CeO$_2$ doped samples the 15R content increased with increasing additive content: 7, 17 and 28 wt% for 1, 3 and 5 wt% CaO respectively. The effect of additive concentration on the composition is much stronger for CaO than for CeO$_2$.

The optimum sintering conditions for the first sintering step are 0.5 h at 1500 °C for 3 and 5 wt% CaO and 0.5 h at 1550 °C for 1 wt% CaO. In order to optimize a two step sintering process some experiments were done under conditions given in table 3.4. The experiment R64 was done with 1 wt% CaO samples only. The weight loss and composition of the products are comparable with the results after the first sintering step. Some of the measured densities are higher than the theoretical density (see table 3.4) although the samples still contain some porosity. This is possible because the theoretical density is only

an estimate as explained in 3.5.

Optical microscopy of unetched samples did not show significant influence of the sintering conditions on the porosity. Only the 1 wt% CaO samples of experiment R31 had significantly more porosity than those obtained under other conditions. The porosity is partly present in large pores (see fig. 3.5). This is very similar to the porosity distribution in CeO_2 doped samples. Probably these large pores are caused by insufficient powder processing. The large pores were present probably as large defects in the green product. As is shown by Lange [14] pores can only be closed if their coordination number is below a critical value (see 2.2). Pores with a coordination number above this critical value can only be closed if their coordination number is reduced as a result of grain growth.

TABLE 3.4
Conditions of two step sintering experiments. Given are the sintering time (t_1, t_2) and temperature (T_1, T_2) during the first (0.5 MPa) and second (10 MPa) sintering step and the resulting densities of samples with 1 (ρ_1), 3 (ρ_3) and 5 (ρ_5) wt% CaO.

code	t_1 (h)	T_1 (°C)	t_2 (h)	T_2 (°C)	ρ_1 (g/cm³)	ρ_3 (g/cm³)	ρ_5 (g/cm³)
R31	0.50	1500	0.50	1550	3.07	3.10	3.11
R52	0.75	1500	0.75	1550	3.08	3.10	3.11
R29	0.50	1550	0.50	1600	3.08	3.09	3.10
R64	0.50	1600	0.50	1650	3.08		

The microstructure of some samples is shown in fig. 3.5b,c,d. The grain size is smaller ($\leq$ 10 μm for the coarse structure) than that of the CeO_2 doped sialons. The influence of sintering conditions or additive concentration on the grain size is similar as in the CeO_2 doped samples. Again the grain size distribution is bimodal. This is most clear for the coarse structure in fig. 3.5c. The amount of intergranular phase is rather large and increases with CaO content (fig. 3.5c,d). This confirms the suggestion that the increasing amount of 15R at increasing CaO content is related to the amount of liquid phase. Again part of the 15R is present in clusters, visible as light regions in the structure. The

lower sintering temperature of the CaO doped samples will be caused by this larger amount of liquid phase.

The Vickers hardness (2 N load) of the CaO doped samples is about 13 GPa for 3 and 5 wt% CaO and 14 GPa for 1 wt%, though this difference is not significant. This hardness is rather low in comparison with values given in the literature, i.e. 14 - 17 GPa [7,9,13].

A strange phenomenon is observed in the sintering of large tablets with CaO for the measurement of mechanical properties. Under sintering conditions that resulted in high density and certainly no swelling for small samples (1 g) these large tablets (7 g) with 3 and 5 wt% CaO showed severe swelling. Initially this was thought to be due to the evaporation of CO_2 from the $CaCO_3$. Therefore the tablets were first slowly heated under nitrogen up to 850 °C. Measured weight loss indicated that all the $CaCO_3$ was decomposed into CaO and CO_2. Sintering under the same conditions as in R29 still resulted in swelling of the 3 and 5 wt% CaO samples. Sintering under conditions like in R31 resulted in swelling of the 5 wt% CaO tablets only. The swelling is caused by large holes, cracks that are blown up (fig. 3.6). This observation indicates gas formation. On the other hand swelling is not accompanied by a larger weight loss. This suggests that swelling starts after (nearly) closed porosity is reached. In that situation a small amount of gas can cause swelling.

Gas is formed due to decomposition of some phase. Because swelling is more severe at higher concentrations of additive it is likely that gas is formed from (an additive in) the liquid phase. At higher temperature more gas will be formed. Thus the tendency to swell will increase with increasing temperature. Under similar conditions with larger tablets the gas can cause swelling at a higher degree of porosity than in smaller tablets. The production of gas is related to the mass of the tablet or the volume of the tablet if tablets of similar densities are considered. The removal of gas is related to the surface of the tablets. The surface volume ratio for tablets with a height h and radius r is equal to $(h^{-1} + 2r^{-1})$ which decreases at increasing sample size. Thus larger tablets will be more sensitive to swelling as is observed.

61
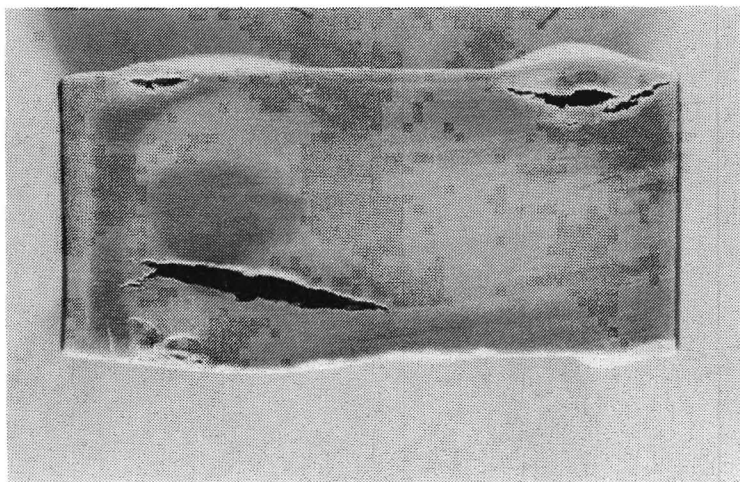
(a)
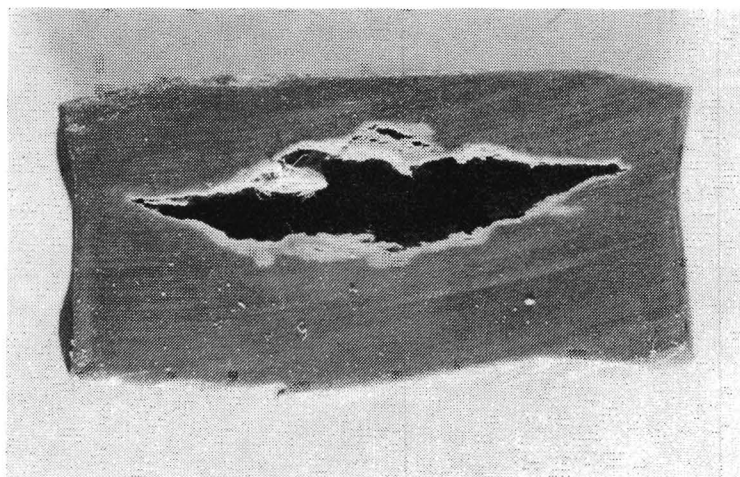
(b)

Fig. 3.6. The cross section of two swollen tablets. Sample (a) contains 5 wt% CaO and sample (b) 1 wt% CaO and 0.5 wt% Fe_2O_3.

3.7 Influence of impurities on the sintering behaviour of CaO doped $Si_3Al_3O_3N_5$

Kaolin contains impurities that can influence the properties of sialon derived from kaolin. SiO_2, TiO_2 and Fe_2O_3 are some of the most common impurities of kaolin. To study the influence of these oxides on the properties, powder mixtures with 0.5 wt% of these oxides were reaction sintered. The samples also contained 1 wt% CaO as sintering additive. As starting point for the sintering conditions the conditions of experiment R29 (see table 3.4) were chosen. The sintering conditions as well as the resulting densities are given in table 3.5.

TABLE 3.5
Sintering conditions and resulting densities of samples with 0.5 wt% SiO_2, TiO_2 and Fe_2O_3 (ρ_{SiO_2}, ρ_{TiO_2} and $\rho_{Fe_2O_3}$). Given are the temperatures T_1 and T_2 during the first (0.5 MPa) and second (10 MPa) sintering step. The sintering time is 0.5 h at both sintering steps.

code	T_1 (°C)	T_2 (°C)	ρ_{SiO_2} (g cm^{-3})	ρ_{TiO_2} (g cm^{-3})	$\rho_{Fe_2O_3}$ (g cm^{-3})
R49	1550	1600	3.06	3.08	3.09
R50	1600	1650	3.07	3.10	3.09
R51	1650	1700	3.08	3.09	3.09

As can be seen in the table the density could be slightly increased by increasing the temperature with 50 °C in both sintering steps. The density of samples with SiO_2 is somewhat lower than that of samples with Fe_2O_3 and TiO_2. The colour of the samples was strongly influenced by the kind of additive. The colour varied from light grey (SiO_2) to dark grey (TiO_2). All samples had a weight loss of 1.4 wt% including the CO_2 evaporation of the $CaCO_3$ and contained about 5 wt% 15R. Traces of Fe_3Si originating from the Fe_2O_3 are recognizable as white spots on the polished cross section (fig. 3.7a). The spots were analysed by the microprobe. TiO_2 will react to TiN during the sintering process. However, the TiN content was too low to be detected.

The microstructure of the samples is illustrated in the figs. 3.7 and 3.8. Figs. 3.8 a and b show the influence of increasing sintering temperature of
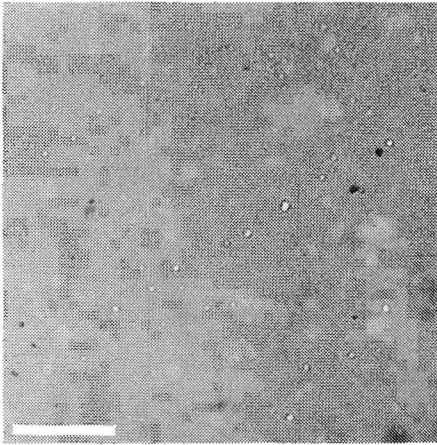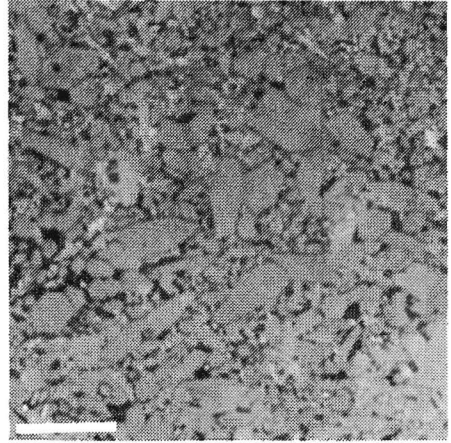
(a) bar = 50 μm   (b) bar = 10 μm

Fig. 3.7. Residual porosity (a) and microstructure (b) of a sample with 1 wt% CaO and 0.5 wt% Fe_2O_3 sintered 0.5 h at 1600 °C, 0.5 MPa and 0.5 h at 1650 °C, 10 MPa.
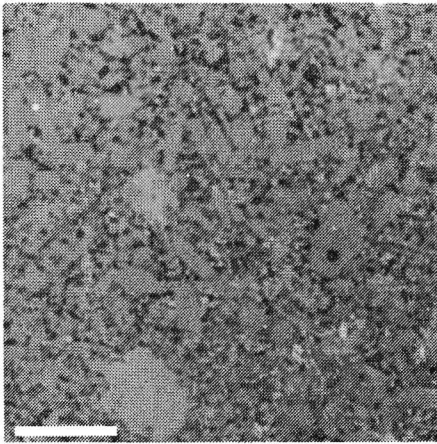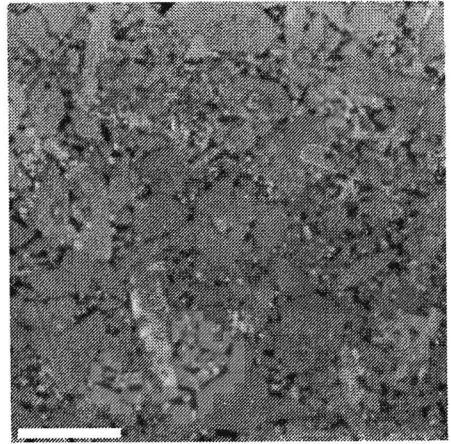
a) T_1 = 1550 °C, T_2 = 1600 °C   b) T_1 = 1650 °C, T_2 = 1700 °C

Fig. 3.8. Microstructure of samples with 1 wt% CaO and 0.5 wt% SiO_2. The sintering time at both steps was 0.5 h (bar = 10 μm).

samples with SiO_2. The grain size increases with increasing temperature. The grain size is approximately the same for all three additives. Fig. 3.7b shows the microstructure of samples R50 with Fe_2O_3. Comparison with fig. 3.4c indicates that the microstructure is not influenced by these three additives.

The Vickers hardness of the samples is 14 GPa (2 N load) regardless of the sintering conditions or additive. This is the same hardness as in samples with only 1 wt% CaO. As expected, the hardness is not influenced by these small amounts of impurities.

Large tablets (7 g), sintered according to the conditions of R50, also showed swelling. This time only the tablets in the centre of the crucible were swollen, regardless of the type of additive (see fig. 3.6). The powder bed shrinks during the sintering process resulting in an empty space between the powder bed and the wall of the crucible. Gas can easily be removed through this space. For tablets in the centre of the crucible the removal of gas will be the most difficult. Therefore these tablets will show the greatest tendency to swell.

3.8 Conclusions

Mixtures of Si_3N_4, Al_2O_3 and AlN without sintering aid show a low sinterability. It was not possible to sinter this mixture to high density. However, the results may be improved by further optimization of the powder processing.

With CeO_2 and CaO as sinter additive a high density can be obtained. In both cases, an additive content of 1 wt% is enough to obtain high density. An increasing additive content results in an increasing amount of intergranular phase. In CeO_2 doped samples, the grain size decreased with increasing amount of CeO_2. The grain size of CeO_2 doped samples is much larger than that of CaO doped samples. The tendency to swell increased with increasing additive content and increasing temperature. This made it difficult to sinter the samples with 5 wt% CaO to high density.

The Vickers hardness is rather insensitive to the additive content. The hardness of CeO_2 doped samples is 16.4 GPa and for CaO doped samples with 3 or 5 wt% CaO 13 GPa. Samples with 1 wt% CaO and samples with 1 wt% CaO and 0.5 wt% SiO_2, TiO_2 or Fe_2O_3 have a hardness of 14 GPa.

65

References

1. F.H. Chung, "Quantitative interpretation of X-ray diffraction patterns of mixtures. I. Matrix-flushing method for quantitative multicomponent analysis", J. Appl. Cryst. 7(1974)519-525.

2. F.H. Chung, "Quantitative interpretation of X-ray diffraction patterns of mixtures. II. Adiabatic principle of X-ray diffraction analysis of mixtures", J. Appl. Cryst. 7(1974)526-531.

3. F.H. Chung, "Quantitative interpretation of X-ray diffraction patterns of mixtures. III. Simultaneous determination of a set of reference intensities", J. Appl. Cryst. 8(1974)17-19.

4. J.W. Visser, personal communication, 1987.

5. C.R. Hubbard, E.H. Evans and D.K. Smith, "The reference intensity ratio, I/I_c, for computer simulated powder patterns", J. Appl. Cryst. 9(1976)169-174.

6. D.K. Smith, M.C. Nichols and M.E. Zolensky, "A fortran IV program for calculating X-ray powder diffraction patterns - version 10", internal report of the college of earth and mineral science, the Pennsylvania State University, 1983.

7. F.K. van Dijen, "The carbothermal production of $Si_3Al_3O_3N_5$ from kaolin, its sintering and its properties, Ph.D. Thesis, Eindhoven University of Technology, 1986.

8. "Handbook of chemistry and physics", 64th edition, eds. R.C. Weast, M.J. Astle, W.H. Beyer, CRC Press, Inc. Boca Raton, USA, (1984).

9. T. Ekström, "Fabrication and properties of yttrium sialon ceramics", Ceram. Developments, eds. C.C. Sorrell and B. Ben-Nissan, Mater. Sci. Forum Vol. 34-36 (1988)605-610.

10. S.S. Campbell and S. Dutta, "Effects of heating rate on density, microstructure, and strength of Si_3N_4-6 wt% Y_2O_3 and a β'-Sialon", Ceram. Bull. 61(1982)854-856.

11. M. Mitomo, N. Kuramoo, Y. Inomata and M. Tsutsumi, "The strength of reaction sintered β-sialon", Yogyo-Kyokai-Shi 88(1980)489-96.

12. R.R. Wills, R.W. Stewart and J.M. Wimmer, "Fabrication of reaction-sintered sialon", J. Am. Ceram. Soc. 60(1977)64-67.

13. M.B. Trigg and E.Tani, "Effect of fabrication routes and heat treatments on the microstructure of silicon nitride based materials", Ceram. Developments, eds. C.C. Sorrell and B. Ben-Nissan, Mater. Sci. Forum Vol. 34-36 (1988)593-597.

14. F.F. Lange, "Sinterability of agglomerated powders", J. Am. Cer. Soc. 67(1984)83-89.

chapter 4

REACTION HOT-PRESSING OF $Si_3Al_3O_3N_5$
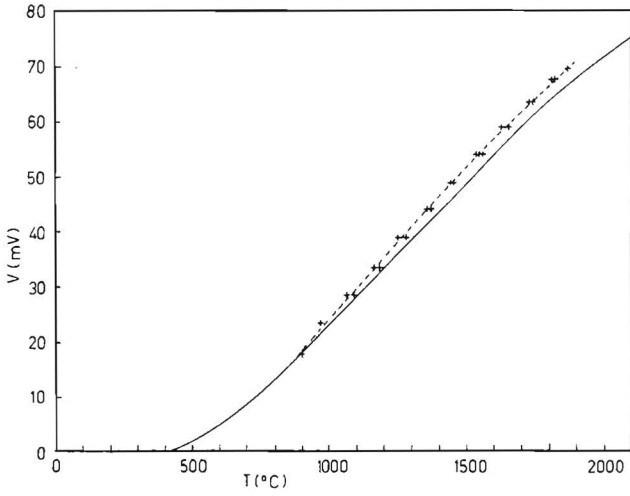
Fig. 4.1. Calibration curve for a BGT-2 thermocouple. Given are the used curve (——) and the curve measured by a pyrometer (---).
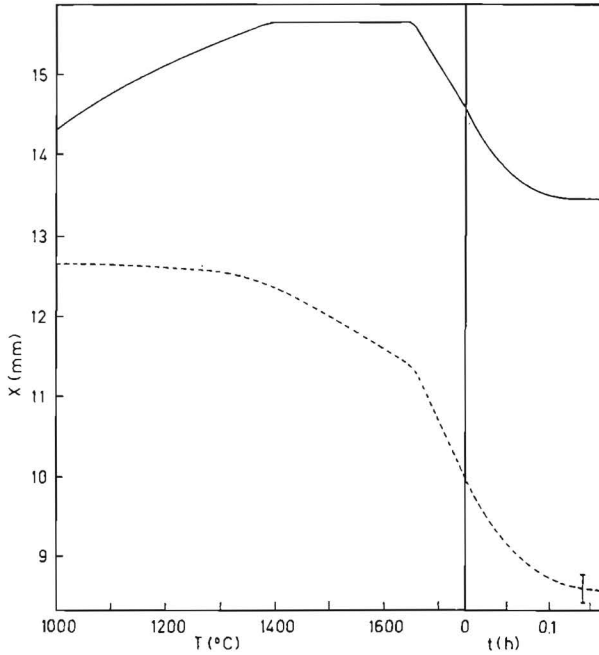
Fig. 4.2. An original displacement curve (——) and the corrected hot-pressing curve (----). Given are the displacements against the temperature (T) and time (t) at 1750 °C.

4.1 Introduction

In this chapter the reaction hot-pressing behaviour of mixtures of Si_3N_4, Al_2O_3 and AlN is studied. Reaction hot-pressing is reaction sintering under uniaxial pressure. The raw materials and powder processing were similar for both methods and described in 3.2. The methods used for characterizing the products are given in 3.3. Experimental details on the hot-pressing setup are given in 4.2.

The hot-pressing behaviour of samples without sintering aid is studied in 4.3. Attention is paid to the influence of the applied pressure. In 4.4 and 4.5, where the hot-pressing behaviour of CeO_2 and CaO doped β'-$Si_3Al_3O_3N_5$ is described, the emphasis is put on the influence of the additive content.

4.2 Experimental details

The hot-pressing experiments were done in a hot-press model HP20 of Thermal Technology Ind., using an Astro furnace model 100-4560-FP provided with graphite heating elements. The maximum temperature is 2000 °C. The temperature is measured by a BGT-2 (graphite versus boron graphite) thermocouple. The temperature given by the thermocouple was checked with a pyrometer before and after the experiments (see fig. 4.1). During this period the temperature measured with the pyrometer decreased about 20 °C with respect to the calibration curve. This decrease can be caused by aging of the thermocouple as well as pollution of the furnace window. During all experiments the calibration curve was used for setting the temperature.

The punch and die set is made of graphite. Only the lower punch of the load frame moves. The displacement of this punch is measured at the foot of the load frame. This means that the measured displacement is an addition of:
- change in sample thickness
- thermal expansion of the graphite punches
- elasticity of the punches

Since only the first effect is of interest, some blank displacement curves were monitored at different loads. Subtracting the proper blank curve from an experimental curve leads to the desired densification curve of the sample.

Coating of the punch and die set with boron nitride was not sufficient to prevent the tablet from sticking to the die. Therefore the hot-pressing

procedure was changed: the die was filled with a tablet instead of loose powder. This tablet (20 g) was first pressed in the hot-press punch and die set at 3 MPa. After isostatically pressing, the diameter of the tablet was smaller than the inner diameter of the die, $\varnothing$ 29 mm and $\varnothing$ 33.7 mm respectively. The tablet was packed in graphite paper which was coated with boron nitride and placed in the die. This construction guaranteed easy unloading after hot-pressing. However, when the pressure was applied too early, the strength of the tablet was not high enough and the tablet cracked.

The hot-pressing procedure was as follows. The furnace was heated to 500 °C in approximately 0.25 h (power controlled) and further heated at a rate of about 1500 °C/h to a maximum temperature at which the sample was held for a certain time. This temperature is called the hot-pressing temperature. In the first experiments the load was applied at the onset of the heating procedure. Later the load was applied at higher temperatures (1400 - 1500 °C) to prevent cracking of the sample. During the experiment the furnace was purged with N_2.

An example of an original displacement curve and the corresponding corrected curve is given in fig. 4.2. The slope at the onset of the original curve is caused by the thermal expansion of the graphite punches. After correction it is clear that up to about 1400 °C no dimensional changes take place in the sample. The changes in sample thickness appear to be in the same order as the blank. The reproducibility of the measurements is indicated with an error mark in fig. 4.2. A disadvantage of the use of tablets instead of powder is that the diameter of the tablet changes during the hot-pressing procedure. Thus the decrease in sample thickness is caused by the increase of the density and the deformation of the tablet. Therefore it is not possible to do any quantitative analysis (as suggested in 2.3) on the hot-pressing curves.

4.3 Hot-pressing of $Si_3Al_3O_3N_5$ without additives

Influence of the applied pressure

To study the influence of the pressure 4 experiments were done at 10.9, 21.8, 32.7 and 43.6 MPa respectively. The pressure in these experiments was applied at room temperature. All samples were hot-pressed 0.5 h at 1750 °C. Three of the hot-pressing curves are given in fig. 4.3. The density and hardness of the products are given in table 4.1.

As expected, the densification rate increases with the applied pressure. At

1750 °C and 10.9 MPa it was not possible to obtain full density. By increasing the hot-pressing time from 0.5 to 1.0 h the density increased from 2.90 to 2.96 g cm^{-3} which shows the low densification rate under these conditions. Increasing the pressure to 21.8 MPa improved the densification behaviour considerably (see fig. 4.3). A further increase of the pressure increased the densification rate only slightly. For further experiments a pressure of 21.8 MPa is used.

The hardness is measured at 156 N and at 2 N. The macro-hardness increased with the density whereas the micro-hardness was rather insensitive to the amount of porosity. Only at high porosity the micro-hardness decreased.

TABLE 4.1

The density (ρ) and hardness (HV2 and HV156) of samples hot-pressed for 0.5 h at 1750 °C at the given pressure (σ).

σ (MPa)	ρ (g/cm^3)	HV156 (GPa)	HV2 (GPa)
10.9	2.90	8.8	12.3
21.8	3.08	10.3	14.9
32.7	3.10	12.9	13.7
43.6	3.11	12.3	14.6

As mentioned in 4.2, the pressure may not be applied too early to prevent cracking of the specimen. Therefore some experiments were done to study the influence of the moment of application of the pressure. As can be seen in fig. 4.3 the onset of the densification is at about 1400 °C. Apparently at this temperature some liquid phase is formed. It appeared that cracking could be avoided if pressure was applied above 1450 °C. If pressure was applied at the hot-pressing temperature the resulting density was lower than in case the pressure was applied at 1450 °C. For a hot-pressing time of 0.5 h at 1800 °C and 21.8 MPa the first method resulted in a density of 2.90 and the second method in a density of 3.08 g cm^{-3}. Even at a longer hot-pressing time the first method never led to the same density as the second method. The reaction to β'-Si$_3$Al$_3$O$_3$N$_5$ starts at 1400 - 1450 °C. During the reaction some transient liquid will be present which disappears after the reaction is complete [1].
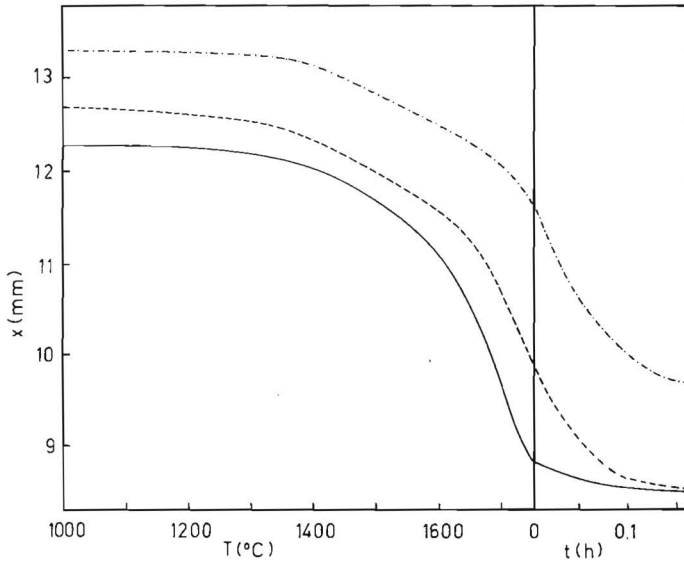
Fig. 4.3. Hot-pressing curves at different pressures. Given is the corrected displacement of the punch as function of the temperature T during heating up and the time t at 1750 °C.
(-·--- = 10.9 MPa, ---- = 21.8 MPa, ———— = 43.6 MPa)
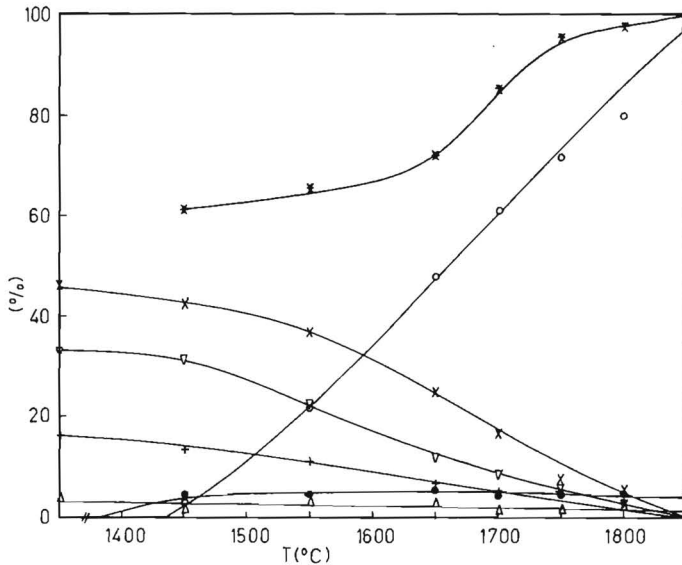
Fig. 4.4. The composition and relative density of samples hot-pressed for 0.08 h at 21.8 MPa as function of the hot-pressing temperature. (x: α-Si$_3$N$_4$, o: β'-Si$_3$Al$_3$O$_3$N$_5$, ∇: Al$_2$O$_3$, +: AlN, Δ: β-Si$_3$N$_4$, •: 15R, *: ρ_{rel})

Apparently the amount of transient liquid can result in densification only if enough pressure is applied.

Influence of the hot-pressing temperature and time

A series of experiments was done at a pressure of 21.8 MPa, hot-pressing time of 0.08 h and varying temperatures. The composition of the product as function of the temperature is given in fig. 4.4. The theoretical density of a mixture can be calculated according to:

$$\rho_{th} = \left[\sum_i \frac{x_i}{\rho_i} \right]^{-1} \tag{4.1}$$

where x_i is the weight fraction of component i with density ρ_i. With a theoretical density of Si_3N_4, Al_2O_3 and AlN of 3.18, 3.97 and 3.26 g cm^{-3} [2], the theoretical density of the starting mixture is 3.44 g cm^{-3}. Assuming that the samples are composed of β'-$Si_3Al_3O_3N_5$ and a mixture of Si_3N_4, Al_2O_3 and AlN according to the starting composition, the theoretical density can be calculated with eq. (4.1). The relative density calculated with this theoretical density is given in fig. 4.4. The figure shows that the reaction to β'-$Si_3Al_3O_3N_5$ starts at about 1430 °C. The densification rate increases strongly at 1650 °C, probably due to the formation of a large quantity of liquid phase. Nearly 50 % of the conversion is completed at the onset of the densification.

Fig. 4.5 gives the displacement as function of the hot-pressing time at several temperatures. The densification rate increases with the hot-pressing temperature. Above 1800 °C full density is obtained within a few minutes. Although the initial densification rate at 1700 °C and 1750 °C is rather high, full densification was not reached. At temperatures below 1800 °C the conversion is completed before full density is reached. Completion of the reaction will change the composition and properties of the liquid phase. Apparently this results in a decrease of the densification rate which explains the fact that full densification is not reached below 1800 °C.

The microstructure of a sample hot-pressed for 0.75 h at 1800 °C is given in fig. 4.6. The grain size is 1 - 2 μm. The grains are not needle shaped as in the reaction sintered samples, but equi-axed. Although no sintering aid was added, rather a large amount of intergranular phase is present. A high amount of inter-granular phase at high z values is also observed by Mitomo et al. in reaction sintered specimens [3]. The structure is inhomogeneous and contains large
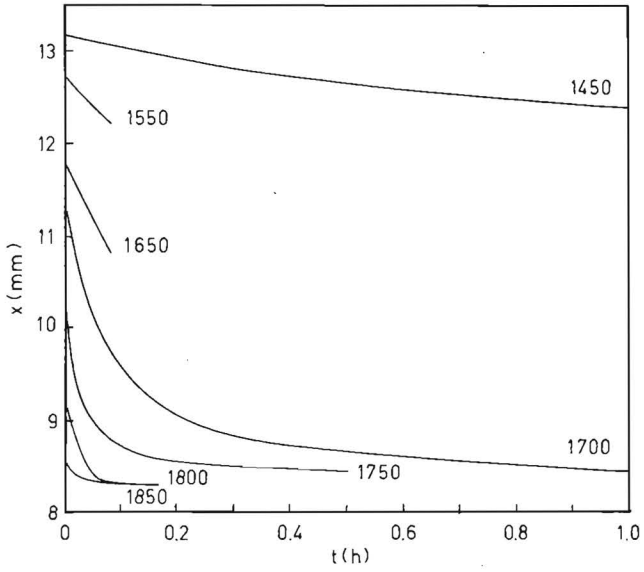
Fig. 4.5. The densification during hot-pressing as function of the time at the indicated temperatures (°C).

(bar = 10 μm)
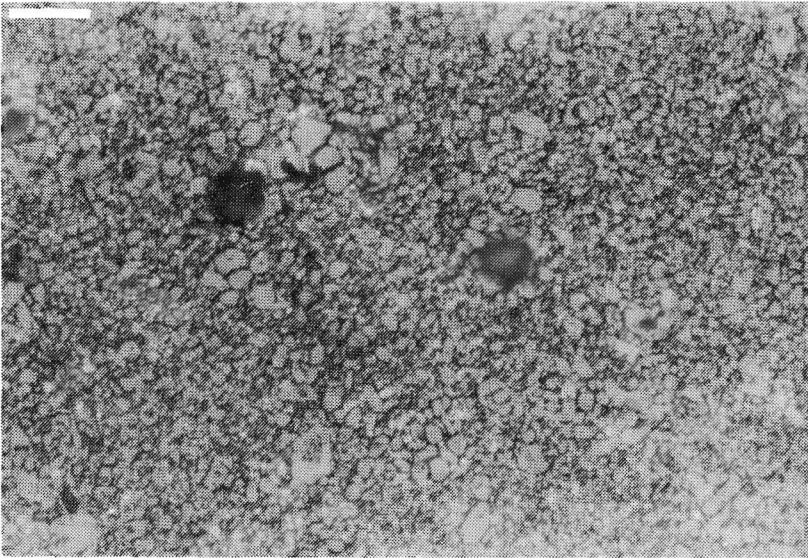
Fig. 4.6. Microstructure of a sample hot-pressed for 0.75 h at 1800 °C.

clusters of second phase (15R). The inhomogeneity impedes a proper etching: the etching time required in different parts of the structure varies strongly. The sample shown in fig. 4.6 was etched in molten KOH which removed the 15R phase completely (see the large 'pores' in fig. 4.6).

The size of the clusters of second phase is comparable to that found in reaction sintered specimens (see chapter 3). This confirms the suspicion that these clusters are caused by insufficient powder processing. Analysis of the X-ray diffraction pattern results in β'-$Si_3Al_3O_3N_5$ with 2 % 15R. Nearly all hot-pressed samples contain traces of β-Si_3N_4. Probably the reactivity of β-Si_3N_4, originating from the silicon nitride powder, is lower than that of α-Si_3N_4.

4.4 Hot-pressing of CeO_2 doped $Si_3Al_3O_3N_5$

The hot-pressing conditions for mixtures with 0.5, 1.0 and 3 wt% CeO_2 were optimized by a series of experiments with different hot-pressing temperatures and times. The pressure, 21.8 MPa, was applied at 1450 °C. Hot-pressing curves for these mixtures and a mixture without additive are given in fig. 4.7. The hot-pressing temperature decreases strongly with the amount of additive. The hot-pressing temperatures to obtain full density within 0.25 h for mixtures with 0, 0.5, 1 and 3 wt% CeO_3 are 1800, 1700, 1650 and 1600 °C respectively.

The conversion to β'-sialon is not much influenced by the addition of CeO_2. Fig. 4.8 shows the percentage β'-$Si_3Al_3O_3N_5$ as function of the hot-pressing temperature at a hot-pressing time of 0.08 h. The addition of CeO_2 accelerates the reaction slightly but above 0.5 % an increasing amount of CeO_2 does not increase the reaction rate any further. Because the densification rate is much more increased than the reaction rate it is possible to obtain full density with incomplete conversion to β'-$Si_3Al_3O_3N_5$. After complete conversion the crystalline phase consists of β'-$Si_3Al_3O_3N_5$ with in most cases traces of β-Si_3N_4. Some samples contain traces of 15R and/or α-Si_3N_4. The amount of α-Si_3N_4 increases slightly with the CeO_2 content. An example of an XRD-pattern is given in fig. 4.9.

The microstructure of a sample is given in fig. 4.10. The grain size is very small (< 1 µm) and decreases with increasing CeO_2 content. Again, large clusters (Ø 10 µm) of second phase are present. Fig. 4.10b shows an Al and Si scan, performed with a microprobe (Jeol Superprobe 733), across the cluster of second phase indicated in fig. 4.10a. The increasing Al-content and decreasing Si-
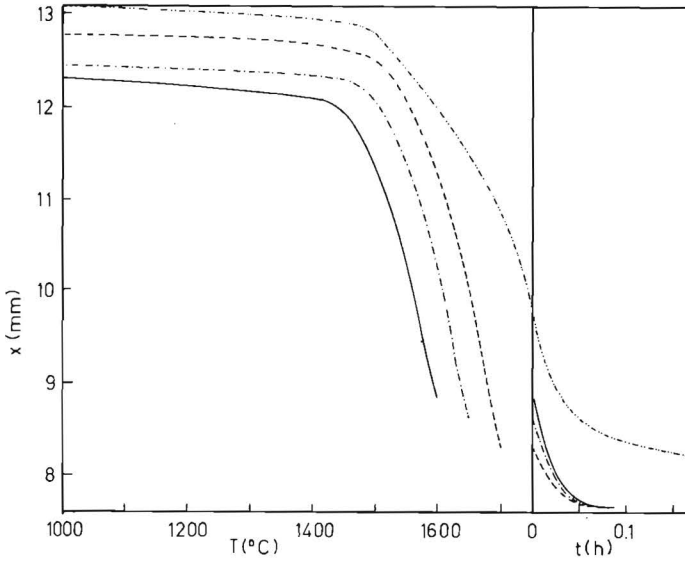
Fig. 4.7. Hot-pressing curves of mixtures with different CeO_2 content. The hot-pressing temperatures are 1750 °C for 0 wt% (–··–··–), 1700 °C for 0.5 wt% (–––), 1650 °C for 1.0 wt% (–·–·–) and 1600 °C for 3 wt% (——).
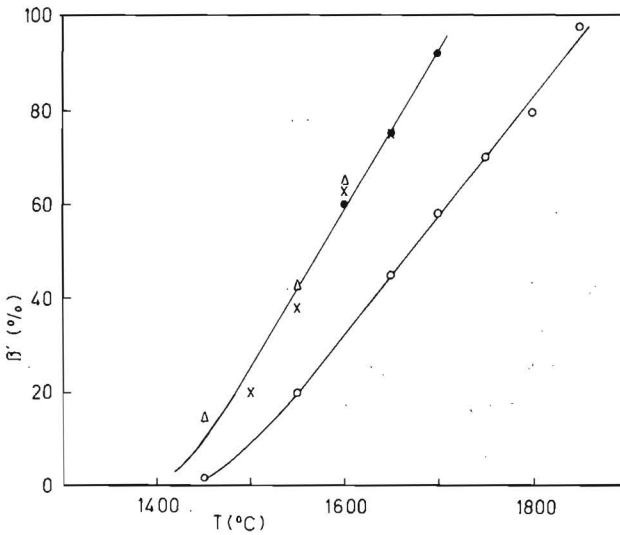
Fig. 4.8. The β'-$Si_3Al_3O_3N_5$ content as function of the hot-pressing temperature at a hot-pressing time of 0.08 h and different CeO_2 contents. (o = 0 wt%, • = 0.5 wt%, x = 1.0 wt%, Δ = 3wt%)

76

content confirm that the second phase is 15R.

Of each additive concentration three samples were hot-pressed at 0.08, 0.25 and 0.5 h. The hot-pressing temperatures were 1600 °C (3 wt%), 1650 °C (1 wt%) and 1700 °C (0.5 wt% CeO_2). For each of these 9 samples the β'-$Si_3Al_3O_3N_5$ content was determined (table 4.2).

TABLE 4.2
The transformed fraction (equal to the β'-$Si_3Al_3O_3N_5$ content) at different hot-pressing times (X_t) as function of the hot-pressing temperature (°C). t_0^* is the time at which the temperature is 1400 °C.

T (°C)	t_0^* (h)	$X_{0.08}$ (-)	$X_{0.25}$ (-)	$X_{0.50}$ (-)
1600	-0.13	0.66	0.82	0.90
1650	-0.17	0.74	0.86	0.97
1700	-0.20	0.88	0.95	0.99

With these values and eq. (2.7) the activation energy E_{act}, can be estimated. The reaction rate constant h is calculated with s = 1. The threshold time t_0 in eq. (2.7) is approximated as follows. The reaction starts at 1400 °C (see fig. 4.8) and the heating rate is 1500 °C/h. This implies that for an experiment with a hot-pressing temperature of 1700 °C the reaction started at $t_0^* = -(300/1500)$ h before reaching the hot-pressing temperature. In a first approximation the threshold time t_0 is taken -(300/1500) h. With this t_0 and the data from table 4.2, an activation energy of 180 kJ mol^{-1} is calculated. A subsequent estimate of t_0 is made by calculating the conversion X_0 at t = 0 taking into account the heating rate from the onset of the reaction according to:

$$h = h_0 \exp - \frac{E_{act}}{RT} \qquad (4.2)$$

$$T = 1673 + \frac{5}{12} (t - t_0^*) \qquad (4.3)$$

$$X_0 = \int_0^{-t_0^*} h_0 \exp\left[- \frac{E_{act}/R}{1673 + \frac{5}{12} t} - t h_0 \exp\left[- \frac{E_{act}/R}{1673 + \frac{5}{12} t} \right] \right] dt \qquad (4.4)$$

77
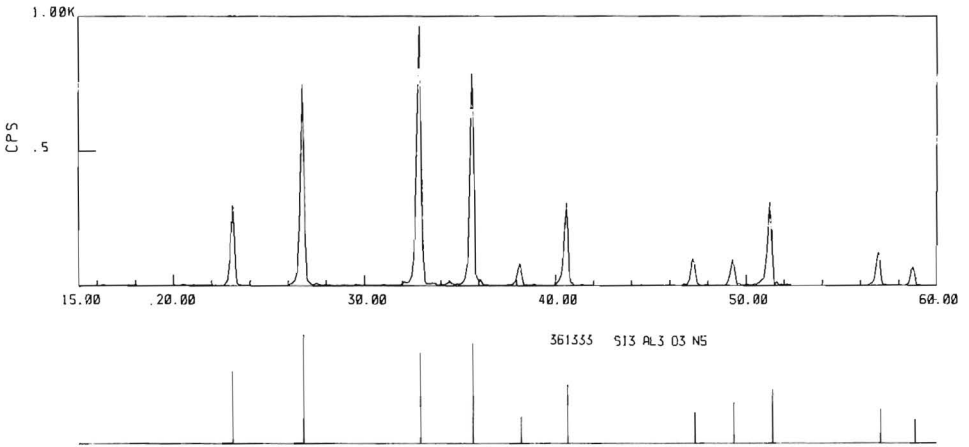
Fig. 4.9. The XRD-pattern of a sample with 0.5 wt% CeO_2 hot-pressed for 0.5 h at 1700 °C and XRD-pattern of β'-$Si_3Al_3O_3N_5$ (JCPDS no. 36-1333).

(a)   (b)
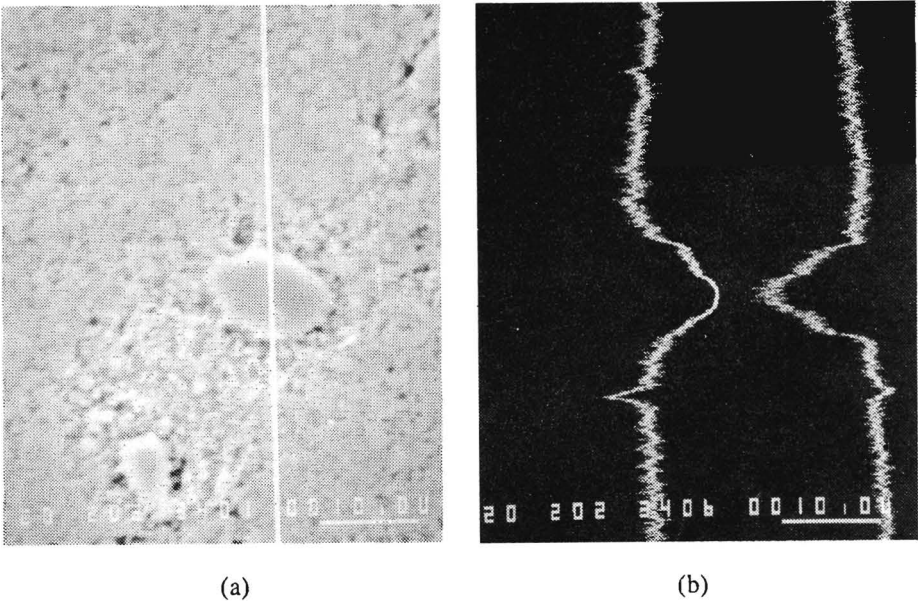
Fig. 4.10. Microstructure of a sample with 0.5 wt% CeO_2 as sintering aid, hot-pressed for 0.75 h at 1700 °C (a) and an Si (left) and Al (right) scan across the marked line (b).

78

Substitution in the isothermal equation (2.7) results in:

$$t_0 = \frac{1}{h} \ln(1 - X_0) \tag{4.5}$$

After two iterations the activation energy converges to 199 kJ mol^{-1}, which is only half the value calculated by Hampshire et al. [3] (405 kJ mol^{-1}). The error in the reaction rate constant as indicated in the Arrhenius plot is calculated by [5]:

$$S = S_y \left[\frac{N}{N \sum X_i^2 - (\sum X_i)^2} \right]^{1/2} \tag{4.6}$$

with

$$S_y = \left[\frac{\sum (\Delta Y_i)^2}{N - 2} \right]^{1/2} \tag{4.7}$$

where N is the number of points (X_i, Y_i) and ΔY the difference between the measured value Y_i and the value Y_i from the calculated line. Because of the limited amount of data the error in the activation energy is large but this cannot explain the large difference with the value given by Hampshire et al. [3].

The hardness of the nine samples mentioned above is 16.9 ± 0.6 GPa. No relation is found between the hardness and the hot-pressing time or additive concentration.

4.5 Hot-pressing of CaO doped $Si_3Al_3O_3N_5$

The procedure to optimize the hot-pressing of mixtures with 0.5, 1 and 3 wt% CaO was similar to that of mixtures with CeO_2. Hot-pressing curves for mixtures with CaO are given in fig. 4.12. Again the hot-pressing temperature decreases with increasing additive content. The increases of the CaO content from 0.5 to 1.0 and 3.0 wt% decrease the hot-pressing temperature with about 25 °C and 50 °C.

CaO addition influences the conversion to β'-$Si_3Al_3O_3N_5$ in the same way as CeO_2. Addition of 0.5 wt% increases the conversion rate but a further increase of the additive content has no effect. The sintering process increases the
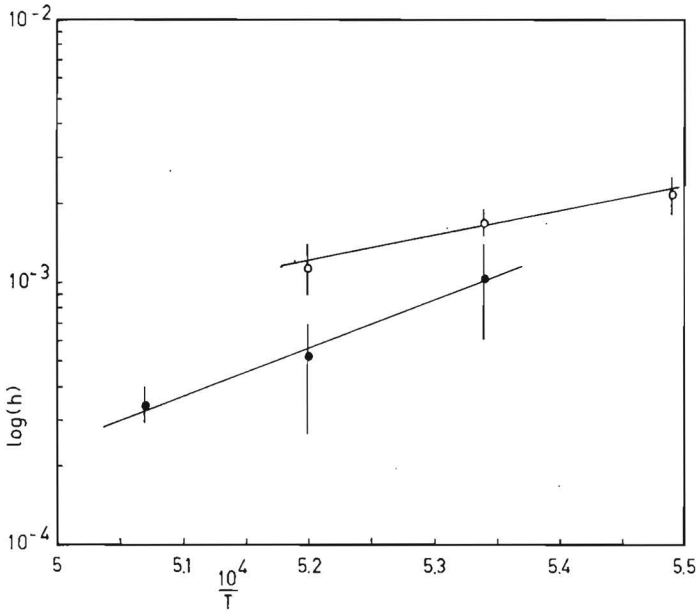
Fig. 4.11. Arrhenius plot of the reaction rate constant log(h) against 1/T for CeO$_2$ doped (o) and CaO doped (•) sialons.
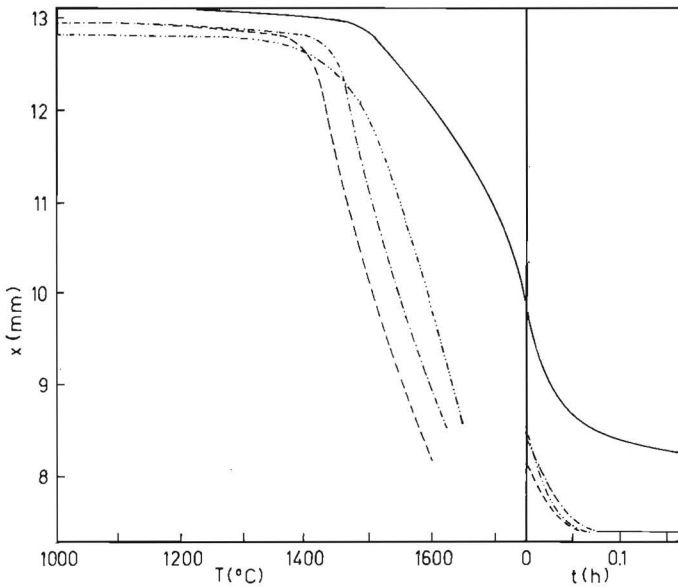
Fig. 4.12. Hot-pressing curves of mixtures with different CaO content. The hot-pressing temperatures are 1750 °C for 0 wt% (——), 1650 °C for 0.5 wt% (-··-), 1625 °C for 1.0 wt% (-·-) and 1600 °C for 3 wt% (---).

density while the conversion to β'-$Si_3Al_3O_3N_5$ decreases the density. This results in a maximum in the density as function of the hot-pressing temperature at a hot-pressing time of 0.08 h (fig. 4.13). The densification proceeds at lower temperature as the CaO content increases, thus the maximum moves to lower temperature at increasing CaO content. At low temperature the densification rate increases with the CaO content but at higher temperatures the densification rate decreases with the CaO content. This is comparable to the effect of CaO in the reaction sintering experiments (see also fig. 3.7) and limits the hot-pressing temperature.

Experiments done at hot-pressing times of 0.08 h and 0.5 h and hot-pressing temperatures of 1550 °C, 1600 °C and 1650 °C result in an estimated value of the activation energy of 330 kJ mol^{-1}. The energy is calculated in the same way as for CeO_2 doped sialons. Since less data were available than in the calculation of the activation energy for CeO_2 doped sialon, the accuracy of this value is very low (see fig. 4.11). An explanation for the difference between the activation energies for CaO and CeO_2 doped sialons is not found. The activation energy obtained by Hampshire et al. [3] was independent of the kind of additive. They suggested that the reaction mechanism requires the breaking of the Si-N bonds because their activation energy was close to the dissociation energy of these bonds (435 kJ mol^{-1}). A much lower activation energy for CeO_2 doped sialons or different energies for different additives contradicts this suggestion. However, more data are neccesary for a more reliable determination of the activation energy.

After complete conversion, the crystalline phase consists of β'-$Si_3Al_3O_3N_5$ with traces of β-Si_3N_4, α-Si_3N_4 and 15R. The 15R content increases slightly with increasing CaO content up to about 5 wt% 15R at 5 wt% CaO. This effect is negligible in comparison with the increase detected in reaction sintered specimens (see 3.6). More pronounced is the increase of α-Si_3N_4 with the amount of CaO. The α-Si_3N_4 content increases to about 15 wt% at 3 wt% CaO. The presence of α-Si_3N_4 in nearly all hot-pressed specimens is hard to explain. It could indicate an improper composition of the starting mixture. However, the powder processing for reaction sintering and hot-pressing is identical. None of the reaction sintered specimens contained α-Si_3N_4. It may be possible that decomposition of α-Si_3N_4 is stronger during reaction sintering than during hot-pressing. This should indicate that the mechanical pressure during hot-pressing prevents decomposition more effectively than the powder bed and gas pressure during reaction sintering.
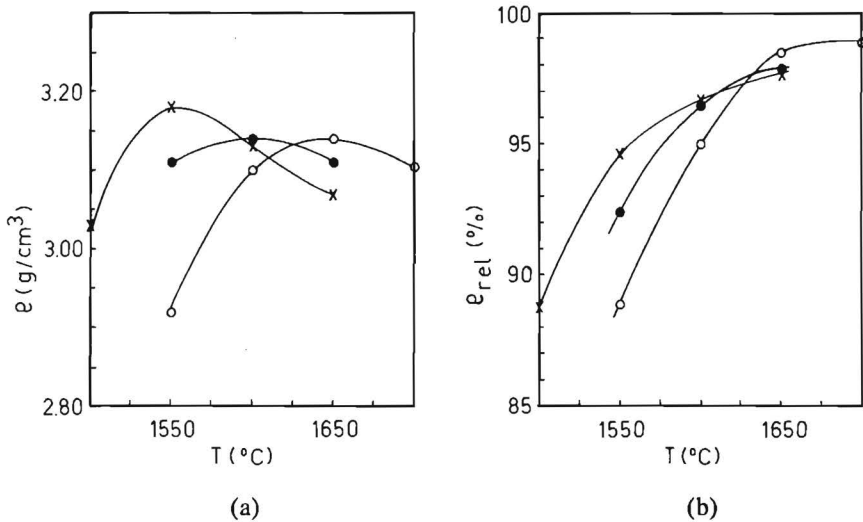
Fig. 4.13. The absolute (a) and relative (b) densities of samples with CaO, hot-pressed for 0.08 h at the given temperature.

(o = 0.5 wt%, • = 1.0 wt% and x = 3 wt% CaO)

The hardness (HV2) of the hot-pressed samples with CaO is about 15 GPa. The polished samples do not have a homogeneous colour. This effect is described by Clarke [6] and attributed to elemental silicon, but no elemental Si could be demonstrated in the samples here described. The microstructure of the samples is similar to that of the CeO_2 doped hot-pressed samples: small equi-axed grains (< 1 μm) with relative large areas of 15R phase.

4.6 Conclusions

Mixtures of Si_3N_4, Al_2O_3 and AlN without sintering aid can be hot-pressed to high density at a temperature of 1800 °C and a pressure of 21.8 MPa. An increase of this pressure does not increase the densification rate much. It is important to apply the pressure before the hot-pressing temperature is reached: at about 1450 °C.

The hot-pressing temperature decreases with the additive concentration. CeO_2 addition decreased the temperature to 1700 °C, 1650 °C and 1600 °C for 0.5, 1.0 and 3.0 wt% CeO_2 respectively. CaO addition decreased the temperature to 1675 °C, 1650 °C and 1625 °C for 0.5, 1.0 and 3.0 wt% respectively.

The conversion to β'-$Si_3Al_3O_3N_5$ is slightly accelerated by the additions, but above 0.5 wt% the conversion rate is not increased by an increasing additive content. Nearly all samples contain some α-Si_3N_4. The α-Si_3N_4 content increases with the CaO content.

The hardness of the CeO_2 doped sialons is 16.9 GPa and that of the CaO doped sialons 15.0 GPa. The hardness is not influenced by the concentration of the additive. The microstructure is very inhomogeneous. Large clusters of second phase are present, indicating an insufficient powder processing. The grain size is 1 - 2 μm for samples without additive and decreases at increasing additive concentration.

References

1. R.M. German, "Liquid phase sintering", Plenum Press, New York, 1985.

2. "Handbook of chemistry and physics", 64th edition, eds. R.C. Weast, M.J. Beyer, CRC Press, Inc. Boca Raton, USA, 1984.

3. M. Mitomo, N. Kuramoto, Y. Inomata and M. Tsutsumi, " The strength of reaction sintered β-sialon", Yogyo-Kyokai-Shi 88(1980)489-496.

4. S. Hampshire and K.H. Jack, "The kinetics of densification and phase transformation of nitrogen ceramics", Special Ceramics 7, ed. F. Taylor and P. Popper, British Ceramic Research Association , Stoke on Trent, (1981)83-49.

5. B. Th. Berendts, H.J.A. Blaauw, B.J.M. Harmsen, J.C. Smit and S.H. Tijs, "Foutenleer en statistiek", Agon Elsevier, Amsterdam, 1973.

6. D.R. Clarke, "A large scale processing inhomogeneity in silicon nitride ceramics and its effect on oxidation", Mater. Sci. Forum 47(1989)110-118.

chapter 5

CARBOTHERMAL PRODUCTION OF $Si_3Al_3O_3N_5$

5.1 Introduction

In this chapter some research on the carbothermal production of sialon [1] is presented in the sections 5.2 and 5.3. The main objective of these experiments is to obtain a better understanding of the reaction mechanism and influence of clay type, additives and process parameters like N_2-flow, pellet size and temperature. Special attention is paid to the determination of the reaction rate controlling step. For this purpose the reaction is studied on basis of the CO content in the exhaust gas. Szekely's grain model is applied to the carbothermal reaction of pelletized mixtures of kaolin and carbon [2].

In section 5.4 the sinterability of the sialon powder is studied. The sintering conditions, temperature and time, are optimized in a single step sintering process. Since it is known that the powder processing and the particle size of the powder in particular are important, the influence of an extra milling procedure on the sintering behaviour is studied. The properties (density, hardness and microstructure) of the product with and without extra milling are compared.

5.2 Experimental details

One part of the experiments was performed with spherical pellets of kaolin (M) and carbon (Elftex 125, Cabot). The carbon had a purity of > 98 % (< 1 wt% LOI, < 0.1 wt% ash and < 0.5 wt% sulphur) and a specific surface of 27 m^2 g^{-1}. Detailed information on the minerals used is given in table 5.1. The pellets were produced by mixing the kaolin and carbon with water in an Eirich mixer (Labor mixer R02). To accelerate the carbothermal reaction, $CaCO_3$ was added [1]. Pellets of the desired diameter fraction were obtained by sieving. After drying, the composition of the pellets was: 79.5 wt% kaolin M, 19.1 wt% carbon and 1.4 wt% $CaCO_3$. The $CaCO_3$ will decompose at about 800 °C into CaO and CO_2. Thus 1.4 wt% $CaCO_3$ results in 1.0 wt% CaO with respect to the kaolinite.

The other part of the experiments was carried out with slipcasted tablets. The powders were mixed with water in a polyethylene bottle on a roller bench. The tablets (∅ 13 mm, height 4 mm) were slipcasted in plastic rings on a gypsum plate. The composition of these tablets varied in ratio as well as in kind of raw materials (see table 5.1 for specifications of the raw materials; the Al_2O_3 used, CT3000, is specified in table 3.1)

All experiments were done in a horizontal tube furnace. The pellets were

placed in an alumina tube ($\varnothing$ 25 mm) in a packed bed. Unless specified otherwise, the packed bed contained 42 g pellets and had a length of approximately 80 mm. The tablets were put on an Al_2O_3 boat and then placed in the furnace tube. During the entire experiment nitrogen gas (with 6000 ppm O_2) was led through the tube with a controlled flow rate (3 - 24 l/h, normal temperature and pressure). The reaction is followed by monitoring the concentration of the carbon monoxide in the exhaust gas (Defor gas analyzer, Maihak).

The composition of the reaction products at different stages of reaction was examined by X-ray diffraction. The residual carbon content was determined by the weight loss after firing at 650 °C in air.

TABLE 5.1

Composition of the minerals used.

		NZ	P	M	SiO_2	mul.
Al_2O_3	(wt%)	34.78	33.47	40.35	.045	72.9
SiO_2	(wt%)	47.36	44.96	43.1	99.8	24.9
Fe_2O_3	(wt%)	.3	1.86	.33	.008	.7
MgO	(wt%)	.005	.22	.01	}.01	.2
CaO	(wt%)	.008	.62	.03		.2
Na_2O	(wt%)	.05	.04	.03	}.01	.3
K_2O	(wt%)	.007	.15	.06		.7
MnO	(wt%)	.001	.003	.001		
P_2O_5	(wt%)	.09	.18	.09		
TiO_2	(wt%)	.08	2.14	1.67	.02	.1
LOI	(wt%)	15.2	15.2	13.9	.05	
d_{50}	(μm)	.5	--	2	2.5	--
BET	(m^2/g)	20	45.2	6.7	--	--

LOI = loss on ignition

-- = not determined

NZ = New Zealand Halloysite, China Clays Ltd.

P = Provins kaolin, Denain Anzin

M = Monarch kaolin, Cyprus Industrial Minerals Company

SiO_2 = milled sand, Sibelco Mam 1 special

mul. = K-REF sintered mullite, Sphinx
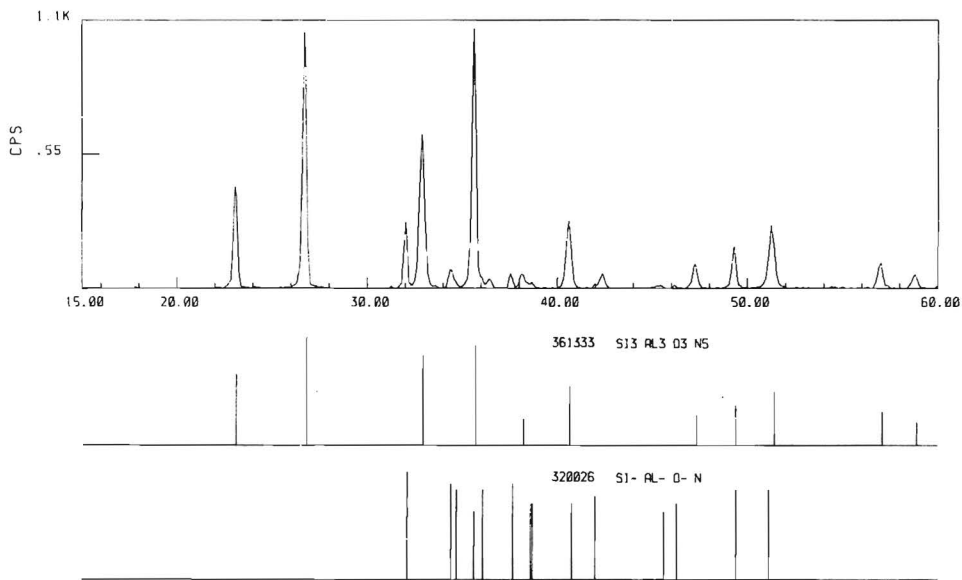
Fig. 5.1. X-ray diffraction pattern of sialon powder derived from kaolinite. Given are the intensity as function of the angle 2ϑ for the sialon powder, β'-$Si_3Al_3O_3N_5$ (JCPDS no. 36-1333) and 15R (JCPDS no. 32-0026).

For a study on the sinterability of the kaolin derived sialon, 500 g pellets (diameter fraction 2 - 4 mm) were reacted in a large horizontal tube furnace (Ø 50 mm). The pellets were reacted at 1500 °C, 48 l/h N_2-flow. After 40 h the CO content in the exhaust gas was below 0.3 % and the heating was switched off. The pellets were milled in the turbula mixer for 38 h in a polyethylene bottle with 200 g Si_3N_4 balls, 600 ml isopropanol and 7 g polyethylene glycol. XRD analysis of the powder showed conversion into β'-$Si_3Al_3O_3N_5$ with approximately 10 wt% 15R phase and traces of TiN (see fig. 5.1 for the diffraction pattern). The specific surface of the milled powder was 2.5 m^2 g^{-1} (BET) and the median agglomerate size, d_{50}, was 3.8 µm (Sedigraph 5100 V1.02). The green density of pressed tablets was 1.7 g cm^{-3}. The powder processing was performed similar to that described in 3.2 for reaction sintering.

A batch of 100 g powder was milled again for another 83 h on a roller bench. This milling procedure was done in a Si_3N_4 jar with 350 g Si_3N_4 balls and 150 ml H_2O. After this the median agglomerate size, d_{50}, was reduced to 1.3 µm. The green density of the tablets was 1.7 g cm^{-3}.

The sintering experiments were done in the gas pressure sintering furnace described in 3.2, under 0.5 MPa N_2. The powder bed consisted of 25 wt% BN and 75 wt% of a mixture of α-Si_3N_4, Al_2O_3, AlN and $CaCO_3$ corresponding to the β'-$Si_3Al_3O_3N_5$ with 3 wt% $CaCO_3$.

5.3 Influence of the process parameters on the conversion

Influence of time and temperature

The influence of time and temperature on the reaction is determined with experiments where the reaction time varied from 0 to 16 hours. These experiments were carried out with pellets (2 - 4 mm diameter) at 1400 °C and at 1500 °C. The heating time for the experiment at 1400 °C was 5.5 h and for the experiment at 1500 °C 4.5 h. The compositions of the reaction products are given in figs. 5.2 and 5.3. Note that the amount of residual carbon plus the crystalline content is set to 100 %, as the amount of amorphous phase is neglected.

The reaction intermediates at 1400 °C and 1500 °C were the same, though as expected, the reaction is faster at 1500 °C. In both cases the maximum β'-sialon content was about 80 wt%. The other compounds in the end product are 15R-phase, β-SiC and Al_2O_3. The presence of 15R-phase indicates an excess of carbon [3,4]. Another explanation for the presence of 15R is given by Higgens and Hendry [5].
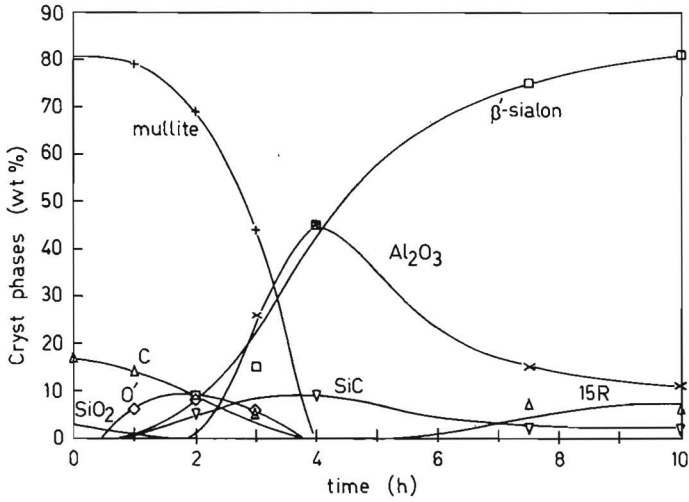
Fig. 5.2. Composition of the reaction product as function of the reaction time at 1400 °C (heating time is 5.5 h).
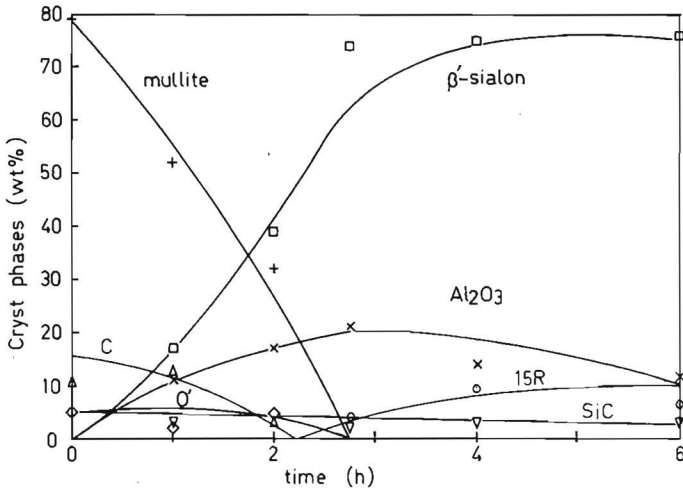
Fig. 5.3. Composition of the reaction product as function of the reaction time at 1500 °C (heating time is 4.5 h).

They state that calcium and magnesium impurities result in overnitriding and the formation of 15R on prolonged heating. The stoichiometric starting mixture of kaolin M and carbon black should be 18.8 wt% carbon and 81.2 wt% kaolin. A surplus of 0.3 wt% carbon was added to account for the reduction of impurities in the kaolin, oxygen in the nitrogen gas and the $CaCO_3$ additive, but is evidently too much. Lee and Cutler [3] report the formation of SiC above a reaction temperature of 1450 °C. Carbothermal production of β'-sialon was successful only below this temperature. Van Dijen et al. [6] also report the formation of SiC above 1450 °C, if sufficient carbon is present to remove all the oxygen. In the experiments described in this chapter the sialon formation at 1500 °C was similar to that at 1400 °C. There was no evidence of a process with mainly SiC formation at a reaction temperature of 1500 °C.

At the beginning of the reaction (see figs. 5.2 and 5.3) some O'-phase (Si_2N_2O) is formed which disappears at the same time as mullite and carbon. At this reaction time the Al_2O_3 content reaches a maximum. Possible reactions responsible for the presence of O', 15R and Al_2O_3 are:

$$2SiO_2 + 3C + N_2 \rightarrow Si_2N_2O + 3CO \tag{5.1}$$

$$2N_2 + 3Si_2N_2O + 3Al_2O_3 + 6C \rightarrow 2Si_3Al_3O_3N_5 + 6CO \tag{5.2}$$

$$2SiO_2.3Al_2O_3 + 6C \rightarrow 2SiC + 3Al_2O_3 + 4CO \tag{5.3}$$

$$7SiC + 5Al_2O_3 + 7N_2 \rightarrow SiAl_4O_2N_4 + 2Si_3Al_3O_3N_5 + 7CO \tag{5.4}$$

$$3(2SiO_2.3Al_2O_3) + 15C + 5N_2 \rightarrow Si_3Al_3O_3N_5 + 6Al_2O_3 + 15CO \tag{5.5}$$
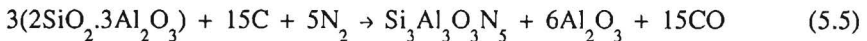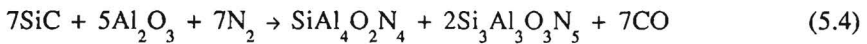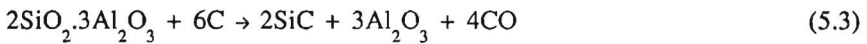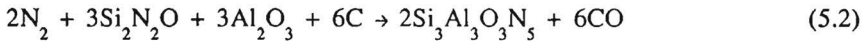
Reaction equations for the formation of SiC, SiO_2 and β'-$Si_3Al_3O_3N_5$ are given in eqs. (2.12), (2.13) and (2.14). Recalling:

$$3(2SiO_2.Al_2O_3) \rightarrow 3Al_2O_3.2SiO_2 + 4SiO_2 \tag{2.12}$$

$$SiO_2 + 3C \rightarrow SiC + 2CO \tag{2.13}$$

$$3Al_2O_3.2SiO_2 + 4SiC + 3C + 5N_2 \rightarrow 2Si_3Al_3O_3N_5 + 7CO \tag{2.14}$$
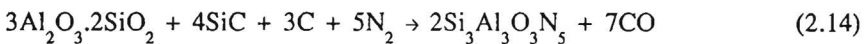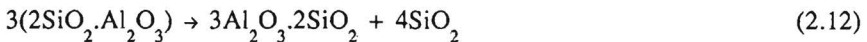
The reactions (5.3), (5.4), (5.5) and (2.14) have been studied separately.

91

Experiments with the slipcasted tablets of the compositions given in table 5.2 were performed at 1400 °C. The furnace was switched off at a CO content < 0.5 %. The starting composition and reaction products are given in table 5.2.

TABLE 5.2

Starting composition (s.c. in mol%) and reaction products (in mol%) of some slipcasted tablets reacted at 1400 °C with a nitrogen flow of 12 l/h.

s.c.	sialon	Al_2O_3	15R	mull.	SiC
39 % SiC, 61 % Al_2O_3	7	88	5	-	-
41 % mull., 59 % SiC	15	47	-	38	-
12 % mull., 50 % SiC, 38 % C	25	47	-	1	27
20 % mull., 80 % C	11	87	-	2	-

sialon = β'-$Si_3Al_3O_3N_5$	mull. = $2SiO_2.3Al_2O_3$	15R = $SiAl_4O_2N_4$

As expected β'-$Si_3Al_3O_3N_5$ is formed in all four cases. The SiC/Al_2O_3 tablet also contained 15R as a reaction product. The sialon/15R mole ratio of 1.4 is in reasonable agreement with the ratio of 2, expected according to eq. (5.4). The large amount of residual Al_2O_3 in combination with the total absence of residual SiC is not fully understood. Possible explanations are the low reactivity of the Al_2O_3 and the evaporation of SiO. A low reactivity of the mixture is confirmed by a long reaction time of 20 h and the low CO content (< 1 %) during the reaction. SiO evaporation may be possible by the oxidation of SiC by the oxygen impurity in the nitrogen flow. Higgens and Hendry [5] nitrided a mixture of SiC and Al_2O_3 at 1400 °C resulting in a mixture of β-Si_3N_4, Al_2O_3 and AlN. An explanation for this difference is not available at this juncture.

Analysis of the experiment with the mullite/SiC tablet gave a β'-$Si_3Al_3O_3N_5$ to Al_2O_3 mole ratio of 1 : 3.1. With the original tablet composition of 41 mole percent mullite and 59 mole percent SiC the results can be explained by assuming the following reaction:

$$9(2SiO_2.3Al_2O_3) + 18SiC + 10N_2 \rightarrow 4Si_3Al_3O_3N_5 + 21Al_2O_3 + 24SiO + 18CO$$

$$(5.6)$$
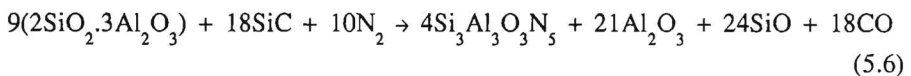
This reaction implies the formation of a large amount of volatile SiO. Analyses of the condensation products in the cold zone proved the presence of SiO, however, it was not possible to make an appropriate estimate of the degree of evaporation. The amount of SiO loss is further determined by the N_2-flow rate and the reaction temperature.

The mullite/SiC/C tablets, used to check eq. (2.14), also contained a large amount of Al_2O_3 and SiC after the reaction. This is probably due to reaction (5.3).

The fourth experiment with tablets of mullite and carbon resulted in a mixture of sialon and Al_2O_3, as expected from eq. (5.5), with some residual mullite. Taking some SiO loss into account the sialon/15R ratio of 0.35 is in good agreement with the value of 0.47 predicted by eq. (5.5).

Generally the observed reaction mechanism for the formation of β'-$Si_3Al_3O_3N_5$ from kaolinite is in good agreement with Higgens and Hendry [5]. One important difference is the large contribution of reactions (5.3) and (5.4). The ratio of β'-$Si_3Al_3O_3N_5$/Al_2O_3 at the moment the mullite content becomes zero indicates the relative contributions of eqs. (2.14) and (5.5). Calculations on the results in figs. 5.2 and 5.3 show that at 1400 °C nearly two thirds of the mullite react according to eq. (5.5), at 1500 °C this is about one third. Thus the contribution of the reaction mechanism given by (5.3) and (5.4) becomes larger at lower temperature.

During two experiments with pellets the CO content was measured. The recordings are given in fig. 5.4. Note that in the figures of CO curves t = 0 denotes the time when the furnace is switched on: the maximum temperature is reached after about 2.5 h for the experiment at 1400 °C and after 5 h for the experiment at 1500 °C. Fig. 5.4 shows the first release of CO at about 800 °C. This is due to the decomposition of $CaCO_3$ according to:

$$CaCO_3 + C \rightarrow CaO + 2CO \tag{5.7}$$

The CO release between 1000 °C and 1100 °C is probably due to the formation of SiC according to eqs. (2.9) and (2.10). The maximum CO release rate is recorded on reaching the reaction temperature. At 1400 °C the CO content of the gas stream is constant after a small drop. This steady state situation might be related to the movement of the reaction zone through the bed. The presence of a reaction zone was found from a clear distinction of zones with reacted and unreacted pellets in a bed. On the other hand at 1500 °C such a period of steady
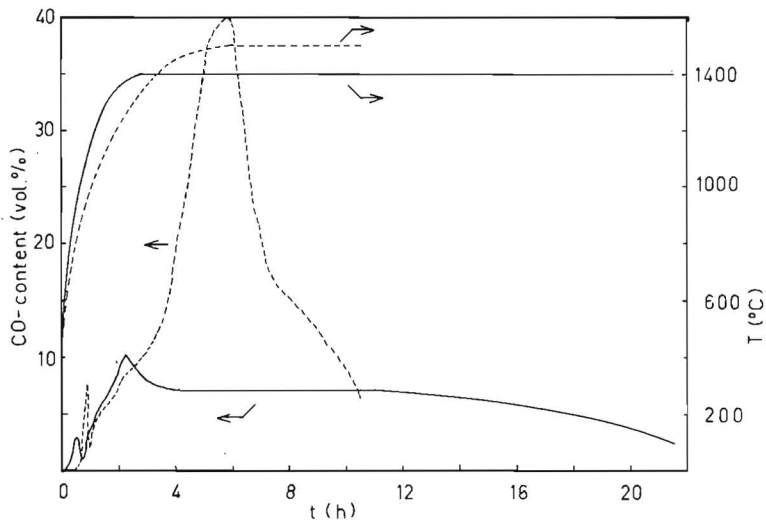
Fig. 5.4. The CO content in volume % of the exhaust gas stream during carbo-
thermal reduction at 1400 °C (——) and 1500 °C (----). For both
reactions the heating curves are indicated.

CO flow is absent though the presence of a reaction zone is clearly observed. Another explanation for the presence of a period with constant CO flow will be given in the next section.

In the figs. 5.2 and 5.3 it can be seen that the free carbon has disappeared after reaction times of 4 and 3 h at 1400 °C and 1500 °C respectively. Taking the heating time into account, this means that in fig. 5.4 the CO output after 6.5 and 8.5 h must be due to reactions in which no free carbon is involved (for example eq. (5.4)).

As mentioned above, SiO loss was proven by analysis of condensated products in the furnace tube. For the experiments with reacting pellets of kaolinite and carbon, SiO loss is most likely to be due to:

$$SiO_2 + C \rightarrow SiO + CO \qquad (5.8)$$

This reaction must be in equilibrium with eq. (2.13). The changes in Gibbs energy for eqs. (2.13) and (5.8) are [7]:

$$\Delta G(2.13) = 604823 - 339.4 \ T \ [J \ mol^{-1}] \qquad (5.9)$$

$$\Delta G(5.8) \ = 688025 - 343.8 \ T \ [J \ mol^{-1}] \qquad (5.10)$$

If the reaction rate constant for eq. (2.13) is equated with $k = [CO]^2$, the equilibrium CO content for reaction (2.13) can be calculated with eq. (5.9). For the reaction temperatures of 1400 °C and 1500 °C this results in an equilibrium CO content of 26 % and 90 % respectively. Fig. 5.4 shows that these contents are not reached indicating that the reaction step of SiC formation will not be rate determining. A reaction front, as is observed, is caused by a rate determining chemical reaction. Because the reaction bed beyond the reaction front still contained carbon, this front reaction must involve carbon. Thus it is most likely that eq. (2.14) is reaction rate determining at the reaction front.

Taking into account the observed CO content, the SiO content at equilibrium can be calculated by $k = [CO][SiO]$. At 1400 °C and a partial pressure $p[CO] \cong 7.5$ % of the total pressure of 10^5 Pa the equilibrium SiO content is 0.4 %. At 1500 °C and $p[CO] \cong 25$ % the equilibrium SiO content is 1.9 %. Even though the gas flow will cause a continuous removal of the SiO formed, the SiO loss due to (5.8) must be strongly limited at both temperatures.

95
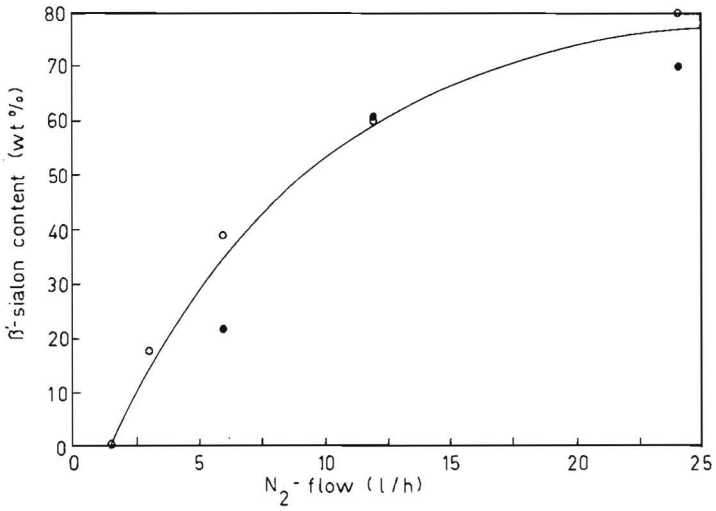
Fig. 5.5. The β'-$Si_3Al_3O_3N_5$ content of the reaction products after a reaction time of 2 hours at 1500 °C as function of the nitrogen flow for pellet size fractions of 0.8 - 2 mm (o) and 2 - 4 mm (•).
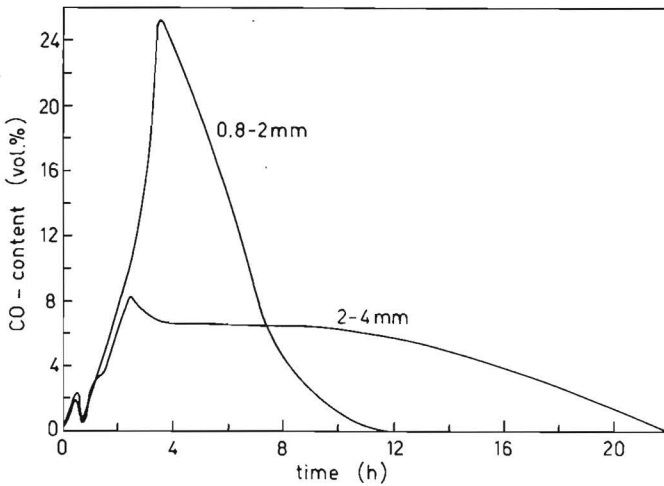
Fig. 5.6. The CO content in volume % of the exhaust gas during carbothermal reduction at 1400 °C for two indicated pellet size fractions.

Influence of N_2 flow and pellet size

The influence of flow and pellet size is studied by two series of experiments at 1500 °C; one with pellets of 2 - 4 mm and one with pellets of 0.8 - 2 mm. Each series consisted of a number of experiments performed at different flow rates with a reaction time of two hours. The crystalline phase content of the reaction products was analysed by XRD. The results are given in fig. 5.5. This figure shows that there is no significant difference between the experiments with the pellets of 0.8 - 2 mm and those of 2 - 4 mm. Apparently, under the given process circumstances, this variation of pellet size does not influence the reaction rate.

The influence of the pellet size is also measured with two experiments at 1400 °C. The CO curves of these experiments are given in fig. 5.6. In this case the small pellets show a much higher reaction rate than the large pellets. The CO curve of the small pellets does not show a period of steady CO flow anymore.

These experiments are in agreement with the results reported in the literature by Higgens en Hendry [5] and van Dijen [8]. Higgens and Hendry measured the CO flow during the reaction at a nitrogen flow of 24 l/h and 1450 °C and did not notice any difference between pellets of 1.5 or 3.5 mm. On the other hand Van Dijen claimed an influence of the pellet size on the reaction rate at 1400 °C. The difference between results in the figs. 5.5 and 5.6 can be explained by the reaction temperature. At a high reaction temperature (1500 °C) a decrease of the pellet size below 4 mm has no influence on the reaction rate. At a lower reaction temperature (1400 °C) a decrease of the pellet size from 2 - 4 mm to 0.8 - 2 mm does increase the reaction rate. Apparently at each reaction temperature a critical pellet diameter can be determined: below this diameter the reaction rate is determined by the chemical kinetics and above the critical diameter, pore diffusion in the pellet is rate controlling. This is described well by the Szekely grain model [2, 9] (see 2.4). This model combines the model for catalysed reactions on porous solids and the shrinking unreacted core model. As discussed in chapter 2 the reaction rate is the sum of three terms, determined by the chemical reaction rate, the pore diffusion rate and the film diffusion rate. Application of the shrinking unreacted core model to pellet shows that the driving force for pore diffusion is the difference in CO concentration over the product layer. It is important to note that an increase of temperature causes an increase of the gas velocity. A higher gas velocity will increase the removal of CO and thus increase the CO concentration difference over the product layer.
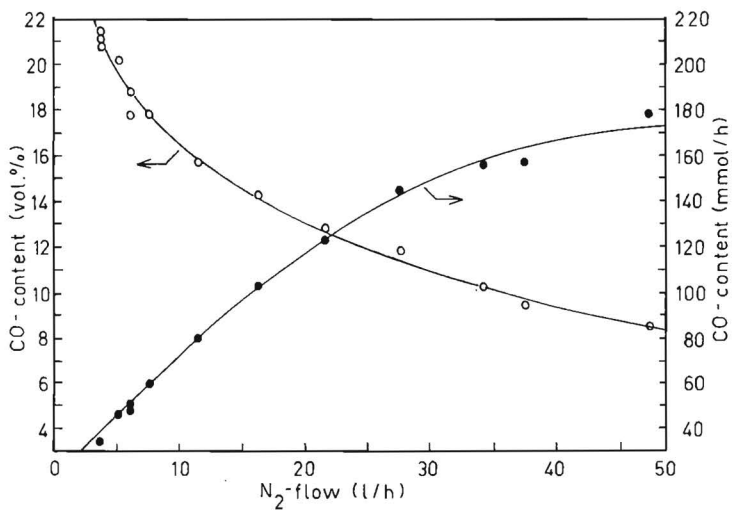
Fig. 5.7. The influence of the nitrogen flow on the CO content in the exhaust
gas stream during carbothermal reduction at 1400 °C, when the CO level
has reached a stationary value. The CO content is given in volume %
and in mmol/h of the exhaust gas stream.

Therefore a higher gas velocity will decrease the critical pellet diameter.

A comparison between figs. 5.4 and 5.6 shows that, in case pore diffusion can be neglected (the curve at 1500 °C in fig. 5.4 and the curve for small pellets in fig. 5.6), a period of constant CO concentration is absent. Apparently this period indicates that pore diffusion is rate controlling.

Fig. 5.5 shows a strong relation between the reaction rate and the flow. At a flow of 24 l/h the conversion after two hours is equal to the conversion after 6 hours at 6 l/h. A disadvantage of a higher flow rate is the formation of more 15R: at 24 l/h, after 2 hours the reaction product contained 80 wt% β'-$Si_3Al_3O_3N_5$ and 17 wt% 15R; at 6 l/h, after 6 hours the product contained 81 wt% β'-$Si_3Al_3O_3N_5$ and 8 wt% 15R. A possible explanation is the higher loss of SiO due to the higher flow rate. A higher SiO loss might promote the formation of the Al-richer 15R phase at the cost of the β'-$Si_3Al_3O_3N_5$.

The influence of the flow is also measured with the following CO monitoring experiment. The CO curves of the experiments with pellets of 2 - 4 mm6at 1400 °C show a period of constant CO content (see fig. 5.4). If during this period the gasflow is varied the CO level will change. In fig. 5.7 the change of the CO level is shown as function of the flow. The dilution by the higher nitrogen flow rate will cause a lowering of the CO level. If the CO flow is plotted in mmol/h instead of in the percentage CO it can be seen that the CO content in fact increases at higher flow rates. Since a higher CO flow rate indicates a higher reaction rate it can be stated that an increase of the nitrogen flow increases the reaction rate. At very high nitrogen flow rates, (> 30 l/h) the influence on the reaction rate becomes very small.

Van Dijen et al. [8] described the influence of flow and pellet size by the Reynolds number eq. (2.15). They stated that for Re < 0.05 mass transfer (film diffusion) must be rate determining and that pore diffusion can be neglected up to a pellet diameter of 2 mm. Under these conditions the reaction rate in a packed bed with a porosity of 40 % is proportional to $d_p^{-1}Re^{1/3} = v_g^{1/3}d_p^{-2/3}$ [8]. For Re > 0.05 the chemical reaction becomes the rate controlling step. This description with Re is not able to explain experiments that show no influence of pellet size. On the other hand the flow dependency of the reaction rate with $v_g^{1/3}$ fits reasonably well with the data from figs. 5.5 and 5.7.

Influence of the composition

The composition of the starting mixture has a large influence on the reaction mechanism and reaction times. The influence of additives on the reaction and
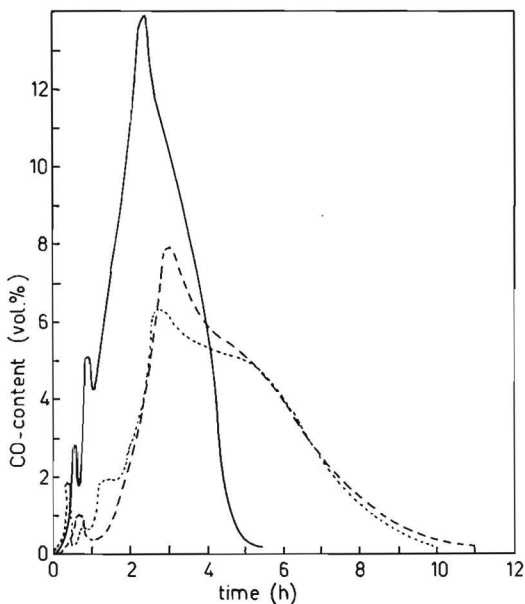
Fig. 5.8. The CO content in volume % of the exhaust gas during carbothermal reduction at 1400 °C in dependence of additions.

(—— = 6 wt% Fe_2O_3, ----- = no addition, ····· = 6 wt% $CaCO_3$).
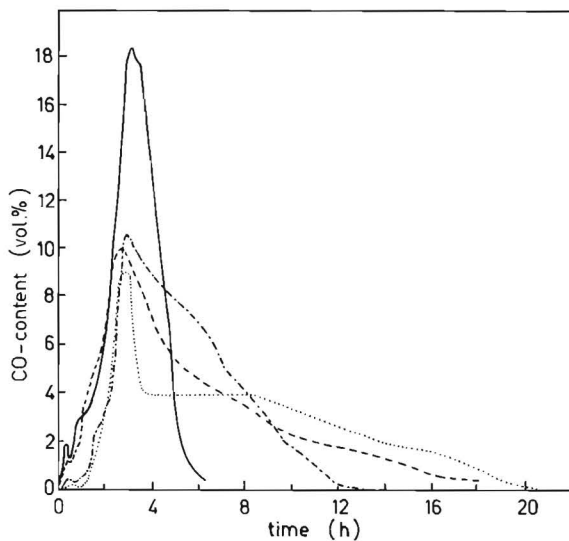
Fig. 5.9. The CO content in volume % of the exhaust gas during carbothermal reduction of different SiO_2/Al_2O_3 sources at 1400 °C (cf. table 5.1).

(—— = P, ----- = NZ, ----- = M, ····· = Al_2O_3/SiO_2)

reaction products of a mixture of kaolin M and carbon was studied by CO monitor experiments. MgO, Fe_2O_3, $CaCO_3$, Y_2O_3 and TiO_2 were used as additives (additive concentration was 1, 2 and 6 wt%). The experiments were carried out using slipcasted tablets at 1400 °C and a nitrogen-flow of 12 l/h. The size and porosity of pellets and tablets are different. Therefore the compositions of the reaction products of both cannot be compared. The reaction products were analysed by XRD and the results are given in table 5.3. As shown in table 5.1 the main natural impurities in kaolin M are Fe_2O_3 (0.33 wt%) and TiO_2 (1.67 wt%). These impurities result in traces Fe_3Si and TiN in all the reaction products (these traces are not mentioned in table 5.3).

TABLE 5.3

The composition of the crystalline reaction products (in wt%) of experiments with different additives.

addition		sialon	Al_2O_3	15R	other			
MgO	1	48	--	--	$MgAl_2O_4$	41	mull.	11
	2	42	--	--		58		
	6	42	--	--		58		
Fe_2O_3	1	44	12	--	Fe_3Si	2	Si_3N_4	42
	2	38	16	--		2		44
	6	48	--	--		3		49
$CaCO_3$	1	76	18	6	--			
	2	83	7	10	--			
	6	73	--	27	--			
Y_2O_3	1	62	26	3	YAG	9		
	2	54	26	1		19		
	6	31	31	--		38		
TiO_2	1	63	--	--	mull.	30	TiN	7
	2	87	10	--		--		3
	6	68	10	--		17		5
none*		72	18	10	--			

sialon = $\beta'\text{-}Si_3Al_3O_3N_5$ mull. = mullite -- = not detected
* cf Table 5.1 for the impurities present in the kaolin M.
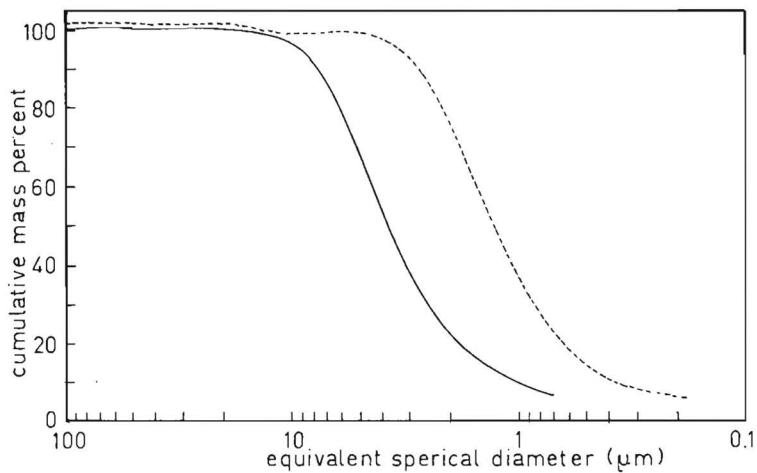
Fig. 5.10. Particle size distribution of sialon powder derived from kaolinite after one (——) and two (---) milling procedures.
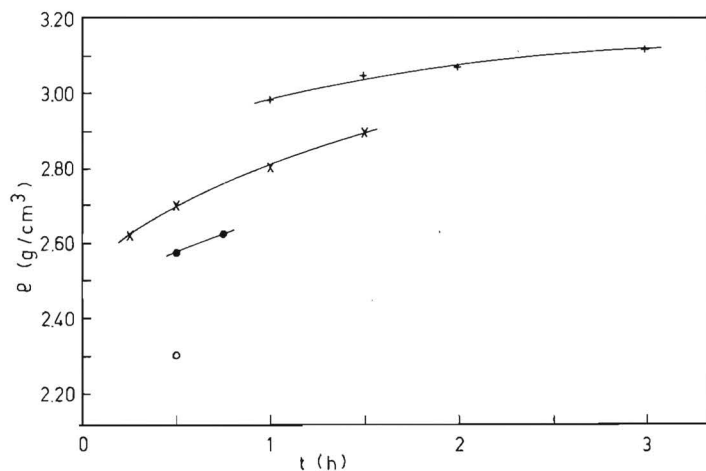
Fig. 5.11. Density as function of the sintering time for sialon powder derived from kaolinite (o: 1600 °C, •: 1700 °C, x: 1750 °C, +: 1800 °C).

Y_2O_3 addition resulted in the formation of yttrium aluminium garnet (YAG) and MgO addition in the formation of spinel $MgAl_2O_4$. $CaCO_3$ and TiO_2 did not influence the amount of β'-$Si_3Al_3O_3N_5$ significantly. An increasing amount of $CaCO_3$ decreased the amount of Al_2O_3 and increased the amount of 15R. This increase of 15R with the calcium concentration is also noticed in the reaction sintering experiments described in section 3.6. Fe_2O_3 promoted the formation of β-Si_3N_4 instead of β'-$Si_3Al_3O_3N_5$. Higgens [9] also reported that Fe_2O_3 lowered the z-value of the produced sialon.

Only the addition of Fe_2O_3 had a strong influence on the reaction rate. The total reaction time was reduced to 6 h while the other mixtures had a reaction time of about 9 h (see fig. 5.8).

The influence of the Al_2O_3/SiO_2 source on the reaction has been investigated. The reaction of three different kaolins and of a mixture of SiO_2 and Al_2O_3 was studied by CO experiments (fig. 5.9). The three clays differ in composition as well as in morphology (see table 5.1). The CO monitorings show a very fast reaction for kaolin P and the slowest reaction for the mechanical mixture of Al_2O_3 and SiO_2. Kaolin M reacted faster than kaolin NZ. The compositions of the reaction products of the four experiments are given in table 5.4.

TABLE 5.4

The composition of the reaction products (in wt%) of experiments with different Al_2O_3/SiO_2 sources.

Al_2O_3/SiO_2 source	β'-$Si_3Al_3O_3N_5$	Al_2O_3	15R	β-Si_3N_4
M kaolin	74	17	9	--
P kaolin	100	--	-	--
NZ kaolin	55	--	9	36
Al_2O_3/SiO_2	60	40	-	--

Explanations for the results with kaolin P are the very high specific surface and the presence of a relatively large amount of Fe_2O_3 (1.8 wt%) and CaO (0.65 wt%). In spite of the high Fe_2O_3 content the reaction product contained β'-$Si_3Al_3O_3N_5$ only and no β-Si_3N_4. The slow reaction of the mixture of SiO_2 and Al_2O_3 will be due to both the relatively bad mixing of the compounds compared to the molecular mixing within the kaolins and to the purity of the minerals. Be-
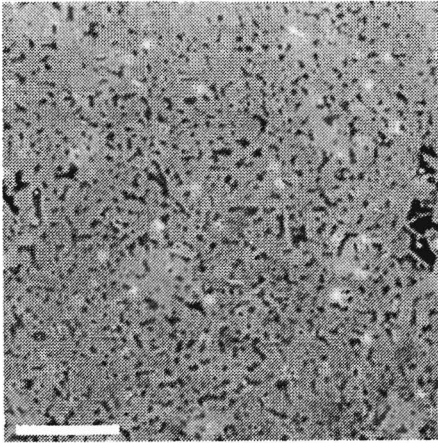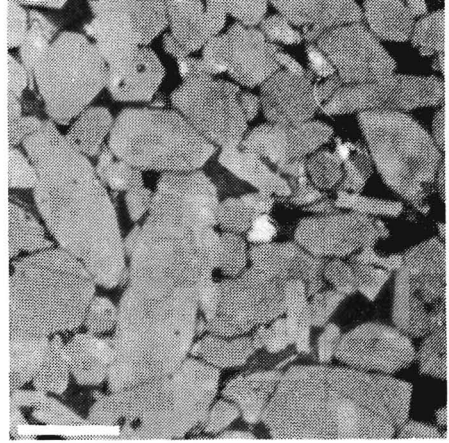
(a) bar = 50 μm   (b) bar = 10 μm

Fig. 5.12. Residual porosity (a) and microstructure (b) of a sample sintered from coarse sialon powder for 3 h at 1800 °C.
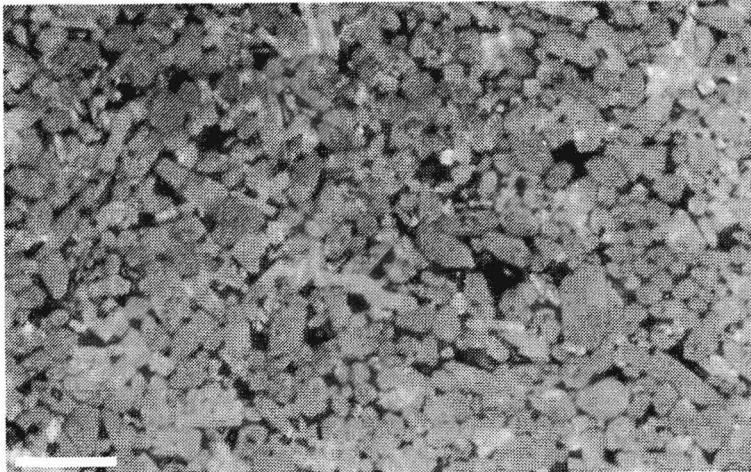
Fig. 5.13. Microstructure of a sample sintered from fine sialon powder for 1 h at 1700 °C (bar = 10 μm).

cause of the absence of impurities no liquid phase will be formed which would accelerate the reaction. The difference between the kaolins NZ and M is possibly due to the purity of the kaolin NZ which caused a somewhat slower reaction. A reason for the formation of β-Si_3N_4 is not found.

5.4 Sintering behaviour of kaolin derived sialon

The sintering experiments were done with two kaolinite derived sialon powders. As described in 5.2 the difference between the powders was an additional milling procedure. The particle size distributions are given in fig. 5.10. As can be seen the distribution function has remained the same while the median agglomerate size decreased by a factor 3 from 3.8 to 1.3 μm.

The first experiments were done with the coarse powder. Using the results in section 3.6 for mixtures with CaO, the conditions for a first sintering experiment were chosen at 1600 °C and 0.5 MPa nitrogen pressure for 0.5 h. This resulted in a density of 2.31 g cm^{-3} ($\rho_{rel} \approx 75$ %). Temperature and time were increased until optimum density resulted. The results of these experiments are given in fig. 5.11. The weight loss of all samples is less than 0.5 wt%. A temperature increase from 1800 °C to 1850 °C resulted in completely molten samples indicating this temperature is too high. A temperature of 1820 °C gave the same results as 1800 °C (see fig. 5.11). The sample sintered for 3 h at 1800 °C still contained some porosity (fig. 5.12). The microstructure (fig. 5.13a) is very coarse, with large needle shaped grains with an aspect ratio of 5 and length up to 20 μm. The Vickers hardness, HV2, of this sample was 13.5 GPa. As a result of these experiments a batch of large tablets (Ø 20 mm) was sintered at 1800 °C for 4 h in order to measure the mechanical properties.

The poor sinterability and unfavourable microstructure gave cause to the extra milling procedure. XRD of this powder gave exactly the same diagram as given in fig. 5.1. No traces of β-Si_3N_4 due to wear of the milling balls were found. A first experiment was done at 1750 °C for 1 h. The tablets were cracked, obviously due to evaporation of gaseous products. This is confirmed by the high weight loss of these samples (7 wt%). The density was nearly 3.0 g cm^{-3} (the large cracks were filled with water during the density measurement) which is still much higher than the similar specimens of the coarse powder. Because of the high weight loss a second experiment was done at 1700 °C and 1 h. This resulted in uncracked samples with a density of 3.10 g cm^{-3}, which is equal to the

density of samples of coarse powder sintered for 3 h at 1800 °C. Increasing the sintering time to 1.5 h did not affect the density or weight loss (0.5 wt%). An increase of temperature to 1720 °C resulted in a somewhat lower density (3.08 g cm^{-3}) and a weight loss of 0.5 wt%.

Fig. 5.13b shows an etched sample sintered for 1 h at 1700 °C. The grain size of the sialon is reduced by about a factor 2 with respect to the sialon produced from the coarse powder. The maximum needle length is 10 μm at an aspect ratio of about 4. Thus the agglomerate size reduction by a factor of 3 strongly increased the sinterability of the powder, resulting in an additional improved microstructure. The Vickers hardness HV2 of this sample was equal to that of the sample sintered from coarse powder: 13.5 GPa. A batch of large tablets for the measurement of mechanical properties was sintered at 1690 °C for 1 h.

The sintered samples contained much less 15R than the unsintered powder (10 % versus 3 %). Probably 15R reacts during the sintering procedure with the SiO_2 in the liquid phase to β'-$Si_3Al_3O_3N_5$.

5.5 Conclusions

Carbothermal production of β'-$Si_3Al_3O_3N_5$ from kaolinite takes place by a complex reaction mechanism. The intermediate reaction products are the same at both reaction temperatures studied, 1400 °C and 1500 °C. Besides the known reaction mechanism of sialon formation from mullite, silicon carbide, carbon and nitrogen [5], a second mechanism is found. This mechanism comprises the decomposition of mullite and carbon into silicon carbide and aluminium oxide whereafter these compounds react with nitrogen into β'-$Si_3Al_3O_3N_5$ and 15R.

An increasing nitrogen flow increases the reaction rate but very large flows result in a high 15R content. The reaction rate can be increased by decreasing the pellet size but only up to a certain critical value. Below the critical pellet diameter the chemical reaction becomes rate determining and a further decrease of the pellet size does not increase the reaction rate.

Addition of $CaCO_3$ promotes the formation of 15R. Addition of Fe_2O_3 increases the reaction rate strongly and promotes the formation of β-Si_3N_4.

The sintering behaviour of sialon derived from kaolinite is strongly dependent on the powder processing after carbothermal production. After thorough milling a high density sialon can be prepared by sintering for 1 h at 1700 °C. The Vickers hardness of this sialon is 13.5 GPa. The grains are needle shaped with a maximum length of 10 μm and an aspect ratio of 4.

References

1. F.K. van Dijen, "The carbothermal production of $Si_3Al_3O_3N_5$ from kaolin, its sintering and its properties", Ph.D. Thesis, Eindhoven University of Technology, 1986.

2. A.M. van Neerven, "Reaction engineering aspects of the carbothermal production of β'-sialon from kaolin", M.Sc. Thesis, Centre for Technical Ceramics, Eindhoven University of Technology (1988).

3. J.G. Lee and I.B. Cutler, "Sinterable sialon powder by reaction of clay with carbon and nitrogen", Am. Ceram. Soc. Bull. 58(1979)869-871.

4. F.K. van Dijen, C.A.M. Siskens and R. Metselaar, "Carbothermal production of β'-sialon", Proc. Int. Conf. Science of Ceramics 12, Saint-Vincent, 1983, ed. P. Vincenzini, Grafiche Galeati, Imola (1984)427-433.

5. I. Higgens and A. Hendry, "Production of β'-sialon by carbothermal reduction", Br. Ceram. Trans. J. 85(1986)161-166.

6. F.K. van Dijen, R. Metselaar and C.A.M. Siskens, "Large scale production of fine non-oxide ceramic powders", Sprechsaal 117(1984)627-629.

7. E.T. Turkdogan, "Physical chemistry of high temperature technology", Academic Press, New York, (1980).

8. F.K. van Dijen, R. Metselaar, C.A.M. Siskens, "Reaction rate limiting steps in carbothermal reduction processes", J. Am. Ceram. Soc. 68(1985)16-19.

9. A.M. van Neerven, F. Blömer, R. Metselaar, "Reaction engineering parameters of the carbothermal production of β'-sialon from kaolin", Euro-ceramics vol. I, eds. G. de With, R.A. Terpstra and R. Metselaar, Elsevier Appl. Sci. London (1989)572-576.

chapter 6

MECHANICAL PROPERTIES OF $Si_3Al_3O_3N_5$

6.1 Introduction

Following the investigations described in the previous chapters, 21 series of sialon tablets were prepared. In 6.2 the process conditions of the series are given. The series are characterized by the measurement of the density, the hardness, the composition, Young's modulus, Poisson's ratio and the fracture toughness. The bi-axial strength is measured with a ball-on-ring set up. This method and the results are described in 6.3. As an introduction to the wear resistance measurements a short review of literature on wear of ceramics is given in 6.4.1. The wear resistance is measured with a pin-on-plate apparatus. A description of the apparatus and the experimental results are given in 6.4.2 and 6.4.3.

6.2 Characterization of the $Si_3Al_3O_3N_5$ materials

The characterization of the 21 sialon materials is given in tables 6.1 and 6.2. The batches 1 to 11 were prepared by reaction sintering mixtures of Si_3N_4, Al_2O_3 and AlN with the indicated additive. Because of swelling problems with large tablets at high CaO contents no batch was prepared with 5 wt% CaO. The batches 12 and 13 are sialons sintered from sialon powder prepared by carbothermal reaction from kaolin (see chapter 5). All these batches were sintered in a gas pressure sintering furnace under conditions given in table 6.1. The green samples consisted of tablets of 7 g with a diameter of 18.5 mm and density of 2.1 g cm^{-3}. The green samples for the batches 12 and 13 had a diameter of 17.5 mm and density of 1.7 g cm^{-3}.

The batches 14 to 21 were prepared by reaction hot-pressing. The samples were tablets of 20 g with a diameter of 29 mm and density of 2.1 g cm^{-3}. The pressure of 21.8 MPa was applied at about 1450 °C. Further conditions are given in table 6.1.

The density of the sintered and hot-pressed samples is given in table 6.1. The calculated relative density is more than 99.5 % for all batches. However, optical microscopy showed a larger porosity. As discussed in previous chapters this difference is due to inaccuracy of the theoretical density. The highest porosity was observed for the 'kaolin' sialons (see fig. 5.12).

The composition of the crystalline phase of the batches is determined by X-ray diffraction (see 3.3). The results are given in table 6.2. The sialons prepared from kaolin derived sialon powder also contained traces of Fe_3Si and TiN.

The larger amount of 15R in batch 12 in comparison to batch 13, is probably due to the long sintering time at high temperature, resulting in decomposition of β'-$Si_3Al_3O_3N_5$. As expected from the results given in chapters 3 and 4, for the CaO doped sialons the amount of 15R increases with increasing CaO content. The hot-pressed samples contained some α-Si_3N_4. The concentration α-Si_3N_4 increases with the additive content.

Young's modulus (E) and Poisson's ratio (ν) were obtained with the pulse-echo method. The longitudinal wave velocity (v_l) and the transverse wave velocity (v_t) were measured at 10 and 5 MHz respectively. With these two values Young's modulus and Poisson's ratio can be calculated according to [1]:

$$\nu = \frac{1}{2} - \frac{v_t^2}{2(v_l^2 - v_t^2)} \tag{6.1}$$

$$E = 2\rho v_t^2(1 + \nu) \tag{6.2}$$

The measurements were performed on ground samples with a surface roughness of 2 μm. The attenuation being small, no corrections were made for internal material damping. The values given in table 6.2 are averages of all the samples within the batch. The average Young's modulus and Poisson's ratio are 226.9 ± 3.5 GPa and 0.298 ± 0.04 respectively. Batch 18 is not included in these averages because of its different composition (see table 6.2). Young's modulus and Poisson's ratio of hot-pressed Al_2O_3 are 400 GPa and $\nu = 0.24$ [2] respectively and for hot-pressed Si_3N_4 300 GPa and 0.26 (data from a commercially available Si_3N_4 from Gimex). Thus higher Young's modulus and Poisson's ratio of batch 18 are caused by the presence of Al_2O_3 and Si_3N_4. The values for E and ν obtained are in good agreement with those of Wills et al. [3]. They reported, for a sialon with a z-value of two, 234 GPa for E and 0.29 for ν.

Both properties are hardly influenced by the production method or the concentration and kind of additive. They seem to decrease slightly with increasing amount of additive though this effect is not significant. The Young's modulus of the sialons derived from kaolin is lower than that of the reaction sintered or reaction hot-pressed sialons. This may be caused by the higher concentration impurities or the somewhat higher porosity of the 'kaolin' sialons.

Out of one sample of each batch four specimens were prepared for fracture toughness measurements. These specimens are $1 \times 3 \times 15$ mm with a notch of approximately 0.45 mm in their centre (SENB specimens). Knoop indentations (20 N)

were made on both sides of the specimen at the root of the notch for crack in-
itiation. The fracture toughness can be calculated by [4]:

$$K_{Ic} = \frac{3\,P\,L}{B\,W^{3/2}}\ f\!\left(\frac{a}{W}\right)\tag{6.3}$$

where $f\!\left(\dfrac{a}{W}\right)$ is a compliance function:

$$f\!\left(\frac{a}{W}\right) = 1.93\left(\frac{a}{W}\right)^{\frac{1}{2}} - 3.07\left(\frac{a}{W}\right)^{\frac{3}{2}} + 14.53\left(\frac{a}{W}\right)^{\frac{5}{2}} - 25.11\left(\frac{a}{W}\right)^{\frac{7}{2}} + 25.80\left(\frac{a}{W}\right)^{\frac{9}{2}}\tag{6.4}$$

with L the support distance, B the width and W the height of the specimen. The
length of the notch is denoted by a. The experiments were done in a nitrogen
atmosphere at a relative humidity of 1 % (dew point -35 °C). The notch depth a
was measured after the Knoop indentations were made. The relative notch depth
(a/W) varied from 0.16 to 0.26. The average value was 0.20.

The results of the K_{Ic} measurements are given in table 6.2. The sample stan-
dard deviation in the measurements of one batch of four specimens is about 10%.
The average K_{Ic} for CeO_2 doped sialons is 3.5 and for CaO doped sialons
2.7 MPa m$^{1/2}$. The fracture toughness of reaction sintered sialons is similar to
that of hot-pressed sialons with comparable composition. K_{Ic} of hot-pressed
sialon without additive is equal to that of the CeO_2 doped specimens. A compari-
son of batch 1 with 2, 4 with 5 and 6 with 7, indicates that an increase of the
additive content results in a decrease of K_{Ic}. For the hot-pressed batches this
effect cannot be observed because every batch is hot-pressed under different
conditions. For the reaction sintered batches with CeO_2, a higher sintering tem-
perature seems to result in a lower K_{Ic} (compare batches 1 and 2 with 4 and 5).
This is not observed for CaO doped sialons (batch 6 and 8). For the 'kaolin'
sialons, K_{Ic} is highest for the batch with the higher sintering temperature and
longer sintering time. The addition of small amounts of TiO_2, SiO_2 and Fe_2O_3
does not influence the fracture toughness. The fractures are mainly trans-
granular (fig. 6.1).

Fracture toughness data for sialons, given in literature [3,5-7], were ob-
tained by the indentation technique. Wills et al. [3] reported for a reaction
sintered sialon with z = 2, a K_{Ic} of 2.2 MPa m$^{1/2}$. The fracture toughness of a
sialon with z = 3 was 1.9 MPa m$^{1/2}$ [5]. This increased to 2.2 MPa m$^{1/2}$ after a
heat treatment. Ekström et al. [6] studied the K_{Ic} as function of the z-value
for sialons prepared by hot-isostatic-pressing. They found that K_{Ic} decreased

with increasing z and measured a fracture toughness of 3 MPa m$^{1/2}$ for β'-Si$_3$Al$_3$O$_3$N$_5$. Thus the measured K_{Ic} values of 3.5 and 2.7 MPa m$^{1/2}$ for CeO$_2$ and CaO doped sialons respectively are good in comparison with these data. The average K_{Ic} for 'kaolin' sialon 2.8 MPa m$^{1/2}$ is also reported by Lee et al. [7].

Hardness data from previous chapters are:
- reaction sintered sialon with CeO$_2$: 16.4 GPa
- reaction sintered sialon with CaO: 13.5 GPa
- hot-pressed sialon with CeO$_2$: 16.9 GPa
- hot-pressed sialon with CaO: 15.0 GPa
- kaolin derived sialon: 13.5 GPa

The concentration and process conditions did not influence the hardness significantly. The hardness of the batches of sialons is given in table 6.2. The average hardness of all batches is 15.2 ± 0.7. The only batch with a significantly higher hardness is batch 18. This batch was hot-pressed with 3 wt% CeO$_2$ for only 0.08 h resulting in incomplete conversion. The differences between the data of table 6.2 and results from hardness measurements in previous chapters can be caused by environmental conditions.

Czernuszka and Page [8] reported that hardness measurements on ceramics are affected by indentation load, temperature and relative humidity. All experiments were done at 2 N and the changes in temperature will have been too small to affect the hardness measurements. Variations in the relative humidity may have influenced the measurements. In previous chapters series of samples with one kind of additive were measured. The measurements were done over a long range of time, thus changes in the relative humidity of the air can be expected. The measurements represented in table 6.2 were done within a few days. The indentation diagonal is about 15 μm with a read-off error of 0.3 μm. This error results in a deviation in the hardness of 0.7 GPa. Thus it can be concluded that within the accuracy of the measurement the hardness is not influenced by the kind and concentration of additive nor by the process conditions.

Some hardness data given in literature are: 15 GPa for hot-isostatic-pressed β'-Si$_3$Al$_3$O$_3$N$_5$ [6] and 16.7 and 17.3 GPa for a reaction sintered β'-Si$_3$Al$_3$O$_3$N$_5$ with and without heat treatment [5]. Lee et al. [7] reported a hardness of 13.3 GPa for a 'kaolin' sialon. In view of the variation in hardness data, noted at the beginning of this section, these data are in agreement with the data obtained in this study.

The microstructure of the different sialons has already been described in chapters 3, 4 and 5. All reaction sintered and reaction hot-pressed samples

TABLE 6.1

Process conditions and resulting density (ρ) for the sialon batches with the indicated additive. Given are the sintering temperature and time during both sintering steps (T_1, T_2 and t_1, t_2) for the (reaction) sintered batches 1 - 13. The N_2-pressure is 0.5 MPa at the first and 10 MPa at the second step. The hot-pressing temperature and time are given for the hot-pressed batches 14 - 21.

no.	additive (wt%)	T_1 (°C)	t_1 (h)	T_2 (°C)	t_2 (h)	ρ (g/cm³)
1	1.0 CeO_2	1600	0.5	1650	0.5	3.091
2	3.0 CeO_2	1600	0.5	1650	0.5	3.137
3	5.0 CeO_2	1600	0.5	1650	0.5	3.168
4	1.0 CeO_2	1650	0.5	1700	0.3	3.096
5	3.0 CeO_2	1650	0.5	1700	0.3	3.132
6	1.0 CaO	1550	0.5	1600	0.5	3.085
7	3.0 CaO	1550	0.5	1600	0.5	3.098
8	1.0 CaO	1600	0.5	1650	0.5	3.083
9	1 CaO, 0.5 SiO_2	1600	0.5	1650	0.5	3.077
10	1 CaO, 0.5 TiO_2	1600	0.5	1650	0.5	3.085
11	1 CaO, 0.5 Fe_2O_3	1600	0.5	1650	0.5	3.081
12	kaolin (coarse)*	1800	4.0			3.113
13	kaolin (fine)*	1690	1.0			3.100
14	—	1800	0.75			3.077
15	0.5 CeO_2	1700	0.75			3.092
16	1.0 CeO_2	1650	0.75			3.101
17	3.0 CeO_2	1600	0.75			3.130
18	3.0 CeO_2	1600	0.08			3.208
19	0.5 CaO	1675	0.75			3.080
20	1.0 CaO	1650	0.75			3.081
21	3.0 CaO	1625	0.75			3.082

* Starting material is kaolin derived sialon powder (see 5.4)

TABLE 6.2

Hardness (HV2), Young's modulus (E), Poisson's ratio (ν), fracture toughness (K_{Ic}) and composition of the sialon materials prepared under the conditions given in table 6.1.

no.	HV2 (GPa)	E (GPa)	ν (-)	K_{Ic} (MPa m$^{1/2}$)	composition (wt%)* 1	2	3	4	5	6
1	15.1	229.0	0.300	4.06	98	2				
2	15.3	229.8	0.298	3.63	95	5				
3	15.3	228.5	0.296	3.20	93	7				
4	14.9	230.0	0.300	3.70	97	3				
5	14.5	230.4	0.298	2.80	96	4				
6	15.2	229.7	0.297	2.81	96	4				
7	14.2	227.5	0.300	2.60	86	14				
8	14.7	229.2	0.297	2.79	97	3				
9	14.7	228.1	0.297	2.68	97	3				
10	15.5	228.4	0.297	2.79	97	3				
11	15.5	227.2	0.296	2.89	94	6				
12	14.0	220.7	0.292	3.07	90	9+				
13	14.9	218.3	0.299	2.51	96	3+				
14	15.7	226.3	0.302	3.51	98	1		1		
15	15.3	228.3	0.302	3.53	96		2	2		
16	15.7	228.3	0.300	3.52	95		3	2		
17	15.3	225.8	0.298	3.94	89		8	3		
18	17.3	248.5	0.285	3.26	62	23			10	5
19	15.3	227.2	0.300	2.60	96		3	1		
20	15.3	225.2	0.297	2.46	92	2	4	2		
21	14.5	219.6	0.285	2.72	80	7	11	2		

* 1 = β'-$Si_3Al_3O_3N_5$ 4 = β-Si_3N_4

  2 = 15R   5 = Al_2O_3
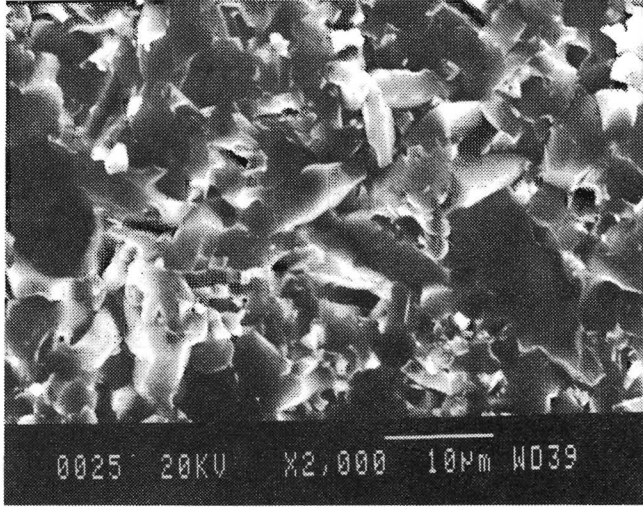
  3 = α-Si_3N_4 6 = AlN

+ both 'kaolin' sialons contained traces of TiN and Fe_3Si

(a)
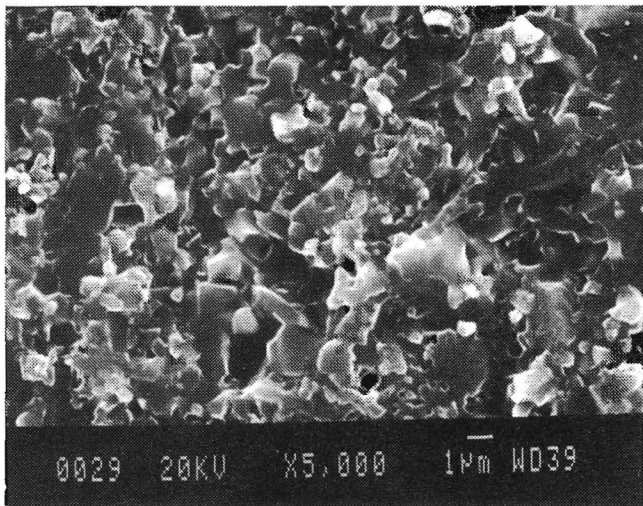
(b)

Fig. 6.1. Fracture surfaces of two K_{Ic} specimens: (a) batch 1, reaction sintered with 1 wt% CeO_2 and (b) batch 17, hot-pressed with 3 wt% CeO_2.

contain large clusters of 15R phase. The fact that the regions of 15R are of similar size for all specimens indicates that the presence of these clusters is caused by insufficient powder processing. The grain size in reaction sintered sialons is larger than that in hot-pressed sialons and depends on the exact processing conditions. Longer sintering times and/or higher sintering temperatures result in coarsening of the structure (figs. 3.3, 3.5). The grains of reaction sintered specimens are needle shaped with an average aspect ratio of 4. The maximum needle length for CaO doped sialons was 5 - 10 μm and for CeO_2 doped sialons 10 - 30 μm. The maximum grain size of the hot-pressed specimens is 2 μm, these grains are nearly equi-axed. The fracture surfaces in fig. 6.1 also show the large difference in grain size between the reaction sintered and the hot-pressed sialons. CeO_2 doped reaction sintered specimens have a very broad grain size distribution. Space between large needles is filled with small needles resulting in a bi-modal grain size distribution.

6.3 Strength measurements

6.3.1 Experimental details

The strength of the sialons was determined by a ball-on-ring test. According to literature [9,10], for ceramics bi-axial strength measurement should be preferred over beam tests commonly used. In three- and four-point bending tests there is always a chance of measuring edge effects. Reviews of several bi-axial strength testing methods are given by Shetty et al. [11] and de With et al. [10]. Both concluded that the ball-on-ring test is the best testing method.

In the ball-on-ring test a disk specimen is supported on a ring and centrally loaded with a ball. To minimize frictional stress a circular ball-bearing with freely moving balls is used instead of a continuous ring support. Generally the stress distribution for the ball-on-ring test in the loaded central area is approximated by a region of uniform surface pressure with radius b. Kirstein et al. [12] developed a special application of Bassali's [13] solution for bending of thin elastic plates supported at several points. For a uniform concentric load, the maximum radial and tangential stresses at the center are equal and given by:

$$\sigma_{bi} = \frac{3P(1 + v)}{4\pi d^2} \left[1 + 2\ln \frac{a_s}{b} + \frac{(1 - v)}{(1 + v)} \left[1 - \frac{b^2}{2a_s^2} \right] \frac{a_s^2}{R_d^2} \right] \qquad (6.4)$$

where P is the load, d the thickness of the disk, a_s the radius of the circle of support points, R_d the radius of the disk, and b the radius of the region of uniform loading at the center. Analysis of the stress at the centre area of the disk [10] showed that b can be safely approximated by one-third of the thickness d. Further the influence of the size of the loading ball appeared to be negligible.

The strength was measured on nine samples for each batch listed in table 6.1. The samples of the (reaction) sintered batches had a radius of about 9 mm, thickness of 1 mm and were tested with a radius a_s of 6 mm. The samples of the hot-pressed batches had a radius of approximately 16 mm, thickness of 1 mm and were tested with a radius a_s of 10 mm. The strain rate for the hot-pressed samples was $5.8 \cdot 10^{-4}$ s^{-1} and for the (reaction) sintered samples $4.7 \cdot 10^{-4}$ s^{-1} resulting in a crosshead speed of 108 and 84 mm/h respectively. The measurements were performed at ambient temperature in nitrogen at a dew point of -35 °C (relative humidity 1 %).

6.3.2 Results and discussion

The results of the strength measurements are summarized in table 6.3. The strength for (reaction) sintered specimens is comparable to the strength of hot-pressed specimens with similar composition. The average strength of all samples with CaO, 405 MPa, is lower than that of samples with CeO_2, 462 MPa.

The strength of batch 8, with 1 wt% CaO, is relatively high: 490 MPa. Apparently the higher sintering temperature in comparison to batch 6 results in an increase of the strength. Probably the samples of batch 8 contain less microporosity though the densities of these samples are not higher than those from batch 6. The high strength of batch 8 indicates that the average lower (room temperature) strength for the CaO doped sialons is not due to the presence of CaO itself. Addition of impurities lowers the strength: the strength of batches 9-11 sintered under similar conditions as batch 8 have a lower strength than batch 8.

Generally the variation of the additive content from 0.5 to 5 wt% does not influence the strength significantly. Only from a comparison of batch 6 and 7,

sintered at similar conditions, it might be concluded that an increasing amount of CaO decreases the strength.

The strength of batches 4 and 5 is somewhat higher than that of batches 1 and 2. This also indicates that a higher sintering temperature increases the strength. In view of the much coarser structure of the batches 4 and 5 (see fig. 3.3) this is unexpected. Possible explanations are a homogenization of the structure or a decrease of the microporosity at higher sintering temperatures. However, analysis could not confirm this.

TABLE 6.3

Bi-axial strength of the 21 sialons specified in table 6.1. Given are the average strength of nine samples (σ_{bi}) calculated by eq. (6.4) and the (sample) standard deviation ($\Delta\sigma_{bi}$).

no.	σ_{bi} (MPa)	$\Delta\sigma_{bi}$ (MPa)	no.	σ_{bi} (MPa)	$\Delta\sigma_{bi}$ (MPa)
1	455	35	11	441	45
2	467	58	12	378	16
3	438	37	13	452	50
4	485	38	14	347	45
5	480	26	15	469	52
6	385	39	16	460	51
7	356	41	17	443	62
8	490	28	18	389	68
9	428	35	19	346	40
10	442	47	20	374	37
			21	383	36

The strength of the batches 13 and 14, sintered from sialon powder derived from kaolin, is 378 MPa and 452 MPa respectively. Thus the strength of the sialon prepared from the fine sialon powder with the smaller grain size is much higher.

The strength of batch 18, 3 wt% CeO_2 hot-pressed for 0.08 h at 1600 °C, is relatively low: 389 ± 68 MPa. This is probably due to the presence of micro-cracks (see fig. 6.2). The presence of these cracks can be explained as follows: at the application of the pressure during the hot-pressing procedure cracks are
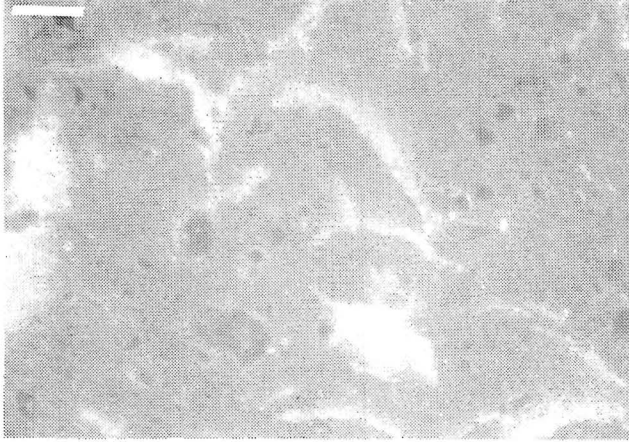
(bar = 10 μm)

Fig. 6.2. Microcracks in a hot-pressed material (batch 18) visible in polarized light.
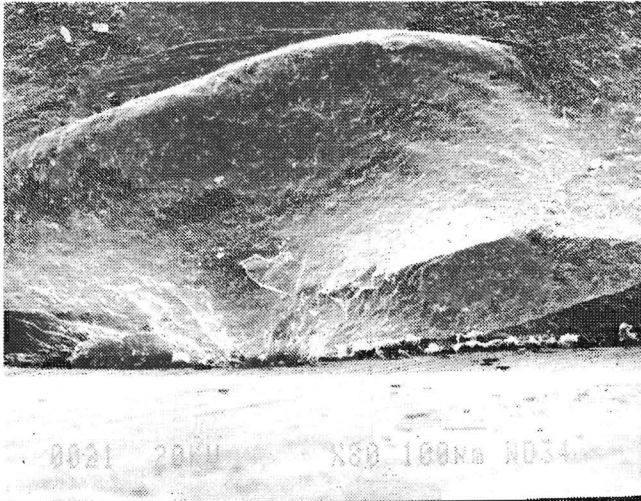

Fig. 6.3. Crack origin in a hot-pressed sample. The crack originates from a defect introduced by the grinding procedure.

introduced in the samples. If the hot-pressing time is long enough these cracks are healed. Because of the short hot-pressing time of batch 18, (some of) the cracks were still present.

Microscopic analysis of the fracture surfaces showed that the cracks were not introduced by large microstructural defects. The fractures were mainly trans-granular. It is likely that the strength is strongly determined by the surface finish of the specimens. McKinney and Herbert [14] showed that the fracture stress and surface finish are related for low porosity ceramics. A relation between the grinding procedure and the strength is confirmed by the following observation. Most specimens were broken in 3 or more wedges. However, a part of the hot-pressed specimens was broken in two pieces. The onset of the crack was in all these specimens parallel to the grinding direction. Fig. 6.3 shows the crack origin introduced by the grinding procedure in such sample.

Kishi et al. [15] suggested a heat treatment in air to reduce the influence of surface machining flaws. Therefore a few spare specimens of hot-pressed batches were heat treated in air for 2 hours at 1100 °C. The bi-axial strength of these specimens was 453, 640, 456, 565 and 616 MPa for samples of batch 14, 18, 19, 20 and 21 respectively. The strength of these five samples is signifi-cantly higher than the average strength of the corresponding batches (see table 6.3). To study the influence of surface oxides and other effects caused by the heat treatment, like the removal of residual stresses, more samples should be tested after different heat treatments.

The variation of the strength within one batch can be analyzed by the Weibull statistics [16]. The Weibull equation describes the probability of failure, P_f, as a function of the fracture stress, σ_{bi} [16]:

$$P_f = 1 - \exp\left[-\left(\frac{\sigma_{bi} - \sigma_u}{\sigma_n}\right)^{m_w}\right] \tag{6.5}$$

where σ_u is a lower level of stress at which P_f falls to zero and σ_n is a norma-lizing factor. The exponent m_w is the Weibull modulus which describes the width of the distribution. The higher the Weibull modulus, the narrower the strength distribution. To determine a reliable value for the Weibull modulus it is necessary to have at least 20 or preferably 30 or more test points. Although only 9 samples of each batch were available the Weibull moduli were estimated. There are several methods to determine the Weibull parameters [17]. Because of the limited number of samples, here the linear least squares analysis combined with a weight function and the following failure probability was used [17]:

$$P_{fi} = \frac{i - 0.5}{n} \qquad\qquad (6.6)$$

where P_{fi} is the fracture stress of the ith ranked specimen and n the total number of specimens. To obtain reliable safety factors, σ_u should be set to zero.

The average Weibull modulus for (reaction) sintered batches is 14 ± 5 and for hot-pressed batches 9 ± 2. This lower modulus for the hot-pressed batches may be caused by the possible presence of cracks introduced by the application of the pressure.

To compare the bi-axial strength data obtained with uni-axial strength data presented in the literature, both methods should be related to each other. Dortmans and de With [18] compared three different models to predict bi-axial from uni-axial strength data. The predictions for the mean strength by the three models do not differ substantially. For a Weibull modulus of 10 and a failure probability of 50 %, the three point bending strength (for specimens of $50 \times 4.5 \times 3.5$ mm) appeared to be about 75 % of the bi-axial strength [18].

Mitomo et al. [19] reported a strength of 370 MPa for reaction sintered β'-$Si_3Al_3O_3N_5$. This value was obtained by a three point bending test. The average bi-axial strength of the reaction sintered β'-$Si_3Al_3O_3N_5$ (batches 1 to 5) with CeO_2 is 465 ± 19 MPa, from which a three point bending strength of 350 MPa is calculated. Thus within the accuracy of the data the strength of the CeO_2 doped sialons is equal to the strength data of Mitomo [19]. The calculated three point bending strength of batch 8, with 1 wt% CaO, is 370 MPa. The strength of the other CaO doped sialons is lower than the strength obtained by Mitomo: 310 MPa (calculated three point bending strength).

For two hot-pressed sialons with $z = 2$ and slightly different compositions, three point bending strengths of 430 and 470 MPa were reported [20]. The calculated three point bending strengths of hot-pressed sialon without additive, with CaO and with CeO_2 are 260, 290 and 360 MPa respectively. Batch 18 is not included in the average for CeO_2 doped sialons because of the different composition. Two reasons can be given for the lower strength observed. Firstly, the strength decreases with increasing z value: Tani et al. [21] reported a three point bending strength decreasing from 490 to 370 MPa for z increasing from 1 to 4. Secondly, as mentioned before it is possible that because of the hot-pressing procedure used, cracks are introduced in the samples.

Kishi et al. [15] prepared two sialons with $z = 0.5$: one using the common mixture of Si_3N_4 and Al_2O_3 and one using a spray dried mixture of

Si_3N_4 and aluminium-isopropoxide solution. Three point bending strength of these (hot-pressed) sialons were 484 and 1480 MPa respectively. However, these values are measured after a heat treatment which, as shown earlier in this section, can increase the strength with about a factor 1.5. Taking this into account, the strength for the conventional powder processed sialon is rather low in comparison with a sialon with z =1 of Tani et al. [21] while the sialon prepared from the spray dried mixture is about twice as strong. This can be explained by the homogeneous structure of this sialon and shows the large improvement of properties that can be obtained by optimum powder processing.

The effect of additives on the three point bending strength of hot-pressed β'-$Si_{6-z}Al_zO_zN_{8-z}$ with z = 1 has been studied by Nakamura et al. [22]. The strengths for sialons without, with 5 wt% CeO_2 and with 5 wt% TiO_2 were 465, 855 and 580 MPa respectively [22]. Though the addition of CeO_2 does increase the strength, this is not as substantial as reported by Nakamura et al. According to Nakamura addition of TiO_2 increases the strength. For reaction sintered specimen, batch 7, the opposite is observed.

The highest strengths for sialons sintered from sialon powder derived from kaolinite are observed by Lee et al. [7]: 250 MPa for a sialon without additive and 310 MPa for a sialon with YAG. Both values represent three point bending strengths. The calculated three point bending strength for the sialon batches of kaolin are 285 MPa for the coarse powder and 340 MPa for sialon sintered from the fine powder. Thus the strength obtained for the kaolin derived sialons is very high. The strength of batch 13 (the fine sialon powder) is comparable to that of reaction sintered sialons.

6.4 Wear resistance measurements

6.4.1 Introduction

A definition of wear is "the progressive loss of material from the surface of a solid body due to mechanical action, i.e. the contact and relative motion against a solid, liquid or gaseous counterbody" (DIN 50320 [23]). Friction is the resistance to motion and arises from interactions of solids at the real area of contact. Both friction and wear are not intrinsic material properties but are characteristics of the engineering system (tribosystem). As a consequence the results from different tests can hardly be compared. Differences in testing

Fig. 6.4. Pin-on-plate apparatus (Central Workshop Technical University
Eindhoven). A photo of the apparatus and a scheme of the
data acquisition system are shown.

apparatus and testing conditions result in different wear behaviour. Examples of testing apparatus for laboratory testing are rotating pin-on-disc, reciprocating pin-on-disc, ring-and-block and annulus-on-annulus. Conditions that can influence the measurements are the humidity of the atmosphere, normal load, velocity, testing temperature, total testing time, surface roughness, lubrication, composition and shape of the counterbody.

According to DIN 50320 [23], wear processes can be classified by 4 wear mechanisms: adhesion, abrasion, surface fatigue and tribo-chemical reaction. Based on these wear mechanisms several models to describe volume wear or wear rate have been developed [24-28].In models for sliding wear the wear is proportional with the sliding distance and the normal load. Only in the model described by Kato [25] wear is proportional with $P^{9/8}$. In most models the wear is related to material constants like hardness, Young's modulus, Poisson's ratio, shear modulus and fracture toughness.

Some experiments on the sliding wear of silicon nitride and sialons are described in [29-34]. Normal load in the experiments varies from 3 to 1600 N, velocity from 0.04 to 9 m/s and sliding distance from 1 - $15 \cdot 10^4$ m. Most experiments were performed in air and resulted in high friction coefficients f_c, between 0.5 and 1. Kapsa [30] studied the influence of relative humidity R.H., and found f_c = 0.1 at 60 % R.H. and f_c = 0.04 at 10 % R.H. using a diamond pin against silicon nitride. Woydt et al. [29] noticed an increasing wear rate at increasing temperature and a high wear/low wear transition with increasing velocities at temperatures above 400 °C. This transition could be explained by a change in the tribo-chemical reaction.

At room temperature material removal is mainly caused by: 1) surface polishing and 2) the generation and propagation of cracks, leading to formation of loose wear particles [31-34]. Surface polishing occurs especially at low loads and low velocities.

Conway et al. [34] studied the influence of the velocity and normal load on the wear rate of sialon/cast iron sliding pairs. They found a decreasing wear rate at increasing velocity. The increase of weight loss as function of the sliding distance was stronger at increasing load and velocity. The friction coefficient decreased during the first 100 m to 0.10 - 0.13 which is very low in comparison to other experiments in air [29,31,32]. A decrease of the friction coefficient at the onset of the experiments has also been reported by Kapsa [30]. The decrease was stronger if a rough diamond pin was used instead of a smooth diamond pin. This indicates that the decrease of f_c at the beginning is
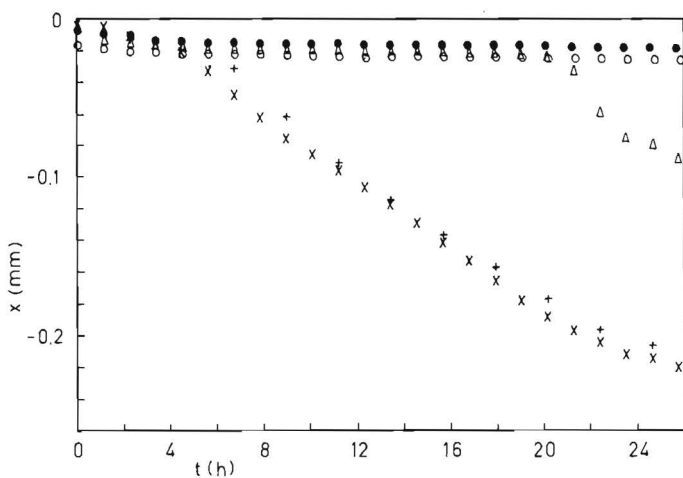
(a)
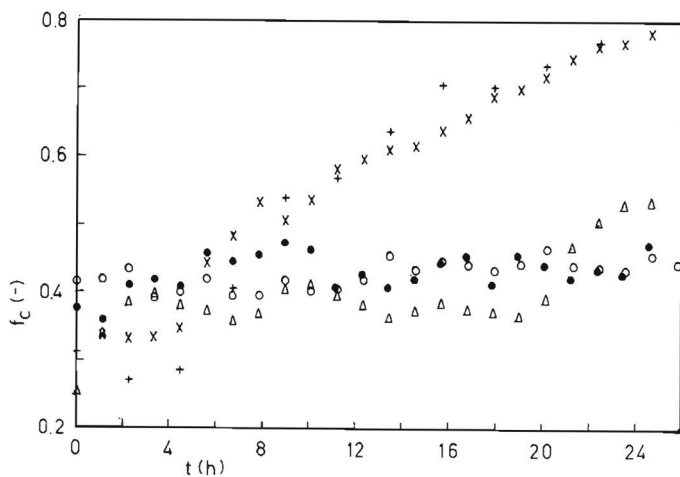
(b)

Fig. 6.5. Wear (a) and friction coefficient (b) as function of time for reaction
sintered material with 1 wt% CaO (2 Hz, 8 N).

due to a polishing effect.

As mentioned in the beginning of this section the differences in process conditions make it impossible to compare results from different testing apparatus. Agreement exists only with respect to some qualitative outlines like the influence of load and sliding distance and the general wear mechanism at room temperature.

6.4.2 Experimental details

Friction and wear measurements described in this chapter were performed with the pin-on-plate apparatus (built by the Central Workshop of the Technical University Eindhoven) shown in fig. 6.4. In this set-up a pin reciprocates on a disk. The tracklength of the pin can be chosen 10, 20 or 30 mm. The frequency of the pin is variable from 0 to 16, 8 or 5 Hz for a track length of 10, 20 and 30 mm respectively. The normal force is applied by dead weight loading. With the available weights the maximum force is 8 N. The apparatus can be used under controlled atmosphere. The maximum specimen size is a disk with a radius of 25 mm. The minimum specimen size is restricted by the tracklength of 10 mm. The specimen is clipped on top of a furnace. The maximum temperature for the experiments is 800 °C.

To prevent influence of changes in the relative humidity of the air in the laboratory, the experiments were done under a nitrogen flow. The experiments were started at a dew point of -20 °C (R.H. 4.4 %). During the experiment the dew point decreased further to -40 °C (R.H. 0.6 %). The flow rate was 420 l/h.

The pin was in fact a 'ball-holder' for balls with a radius of 2 mm. In preliminary experiments steel pins with a diameter of 5 mm and top radius of 4 mm were used. All experiments were done at room temperature and a tracklength of 10 mm.

The sum of the depth of the weartrack and the wear of the pin was measured by an extensometer (Sangamo DG1). The friction force was measured with a force transducer. With a computerized data acquisition system the displacement and force were simultaneously sampled periodically under external triggering control. After each external trigger pulse 2560 measurements were done with an internal frequency. The values of the displacement signal were averaged. Since the pin reciprocates over the sample the force signal will approximate a block wave. In order to calculate the friction coefficient the auto-powerspectrum of

127
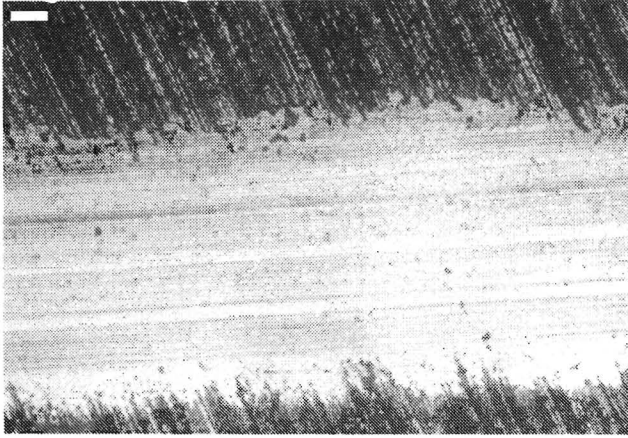
(a)
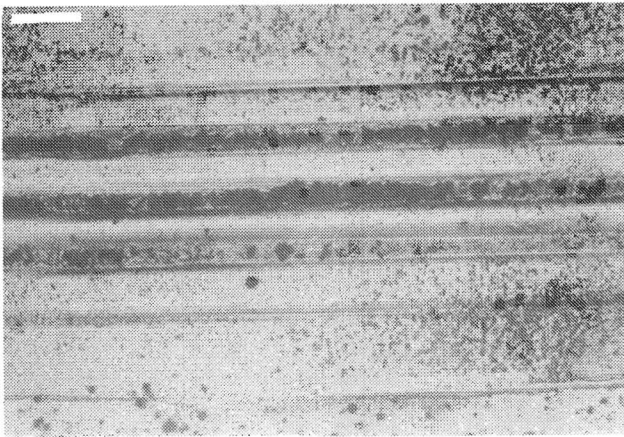
(b)

Fig. 6.6. Wear tracks of the experiments of fig. 6.5. Visible are a polished wear track (a) and a wear track with grooves parallel to the wear direction and areas with abrasive wear (b). (bar = 100 μm)

the force signal was calculated with the fast fourier transformation (FFT) [35]. The FFT was averaged over 5 time-records of 512 points, taken consecutively from the 2560 data points sampled.

The total energy was approximated by integrating the first, third and fifth order harmonic of the power density spectrum. The friction coefficient f_c was calculated from this value according to:

$$f_c = 1.309 \frac{(P_1 + P_3 + P_5)^{1/2}}{F_n} \tag{6.7}$$

where P_i is the power of the ith harmonic and F_n the static normal force. Thus after each external trigger pulse two values were obtained: the average wear depth and the friction coefficient.

The choice of the internal frequency was based on the pin frequency. For pin frequencies ≤ 2 Hz the internal frequency was 25 Hz and for pin frequencies between 2 and 4 Hz the internal frequency was 50 Hz. Because of the short time-interval needed to obtain the 2560 samples (maximum $2560/25 = 102$ seconds) in comparison with the time-interval between two external pulses, the average wear depth and friction coefficient thus obtained may be seen as instantaneous values.

6.4.3 Results and discussion

After some preliminary experiments to choose the pin material, two series of experiments were done. The first series was performed under varying conditions on reaction sintered β'-$Si_3Al_3O_3N_5$ with 1 wt% CaO. The purpose was to study the influence of the experimental conditions on the wear behaviour and to determine optimum conditions for the second series of experiments. The second series, per-formed under these 'standard' conditions, was meant to investigate the (differ-ences in the) wear behaviour of several β'-sialons from table 6.1.

Three different pin materials were tested. The testing conditions for these experiments were: 4 N load, pin frequency of 4 Hz, 72 h and air. First material was steel (Stavax) because a steel/ceramic couple is likely to be used in prac-tice. However, as could have been expected, in this system only the pin showed wear damage whereas the track on the disc was only slightly polished. It was therefore not possible to study the wear behaviour of the ceramic material in

(a)

0007 20KV X1,000 10μm WD38
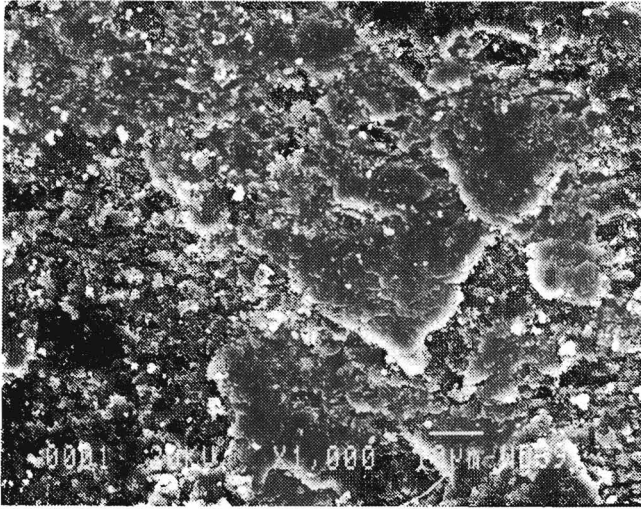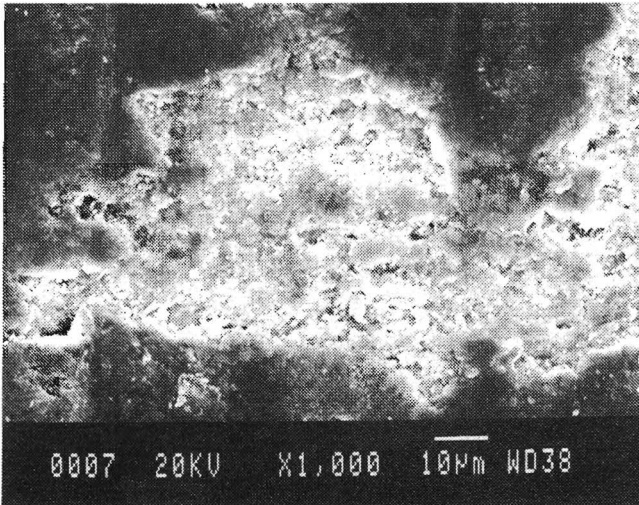
(b)

Fig. 6.7. A wear track of one of the experiments of fig. 6.5 in the stage of abrasive wear (a) and the onset of abrasive wear at the end of the wear track (b) (SEM).

this system. As an alternative two ceramic counter materials were tested: SiC and ZrO_2. Both materials were polished balls with a radius of 2 mm. After 72 h the SiC ball did not result in wear of the disc. Like in the case of the steel pin, the track was only slightly polished whereas the ball was clearly worn. The Y_2O_3 stabilized ZrO_2 did cause wear of the disc and was therefore chosen as counter material in the experiments.

To study the reproducibility of the wear measurements, five experiments were done in nitrogen for 26 h at 2 Hz and 8 N (see fig. 6.5). The wear curves can be devided into three parts: 1) an initial decrease of x, which will be caused by an initial flattening of the ZrO_2 ball, 2) a part with a very low wear rate and 3) a part with a high wear rate. Though the wear behaviour during the second stage (low wear rate) and third stage (high wear rate) itself is quite reproducible, the transition between the second and third part occurs stochastically (see fig. 6.5). Microscopic analysis showed that the low wear rate can be correlated to polishing of the surface (fig. 6.6a). Small debris particles, trapped between the ball and the pin, caused tracks parallel to the wear direction (fig. 6.6b). Grains were pulled from the bottom of these tracks resulting in abrasive wear. Next to this process, fatigue wear was observed. On the 'polished' areas, fatigue cracks were formed perpendicular to the wear direction (fig. 6.11a). Grains were pulled from the cracks resulting in abrasive wear (fig. 6.6b). Finally abrasive wear became the only wear mechanism (fig. 6.7a).

The friction coefficient of these measurements is given in fig. 6.5b. In that part of the wear curve where polishing is the main wear process, the friction coefficient is constant and about 0.4. Abrasive wear causes an increase in the surface roughness which results in an increasing friction coefficient. Although the transition from polishing to abrasive wear seems to occur stochastically the wear rate and increase of f_c during the stage of abrasive wear are reproducible.

To ensure reproducible results, the conditions had to be chosen such that the friction coefficient was stable during the entire experiment. Therefore some experiments were done at 4 N, 2 Hz and 4 N, 1 Hz (fig. 6.8). Under the last conditions a good reproducibility was obtained. All further experiments were done in nitrogen atmosphere at 4 N and 1 Hz.

Generally in literature, it is assumed that the wear is proportional to the frequency, or that the wear as function of the total number of cycles is independent of the frequency. However, at increasing frequency the acceleration of the pin at both ends of the track will be increased resulting in a higher wear rate. Microscopic analysis showed that, especially at high pin frequencies, the
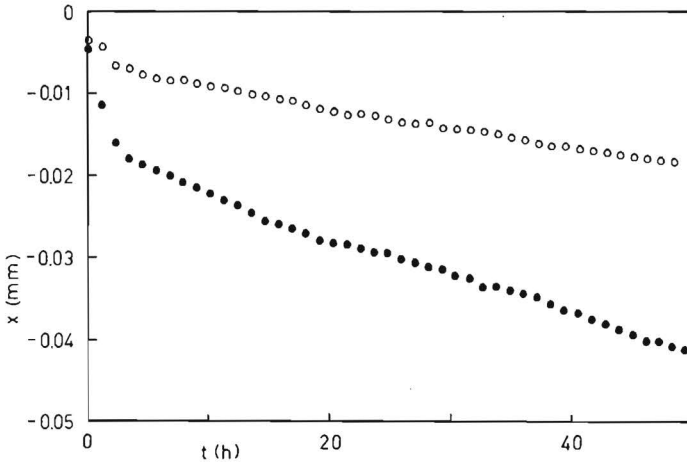
(a)
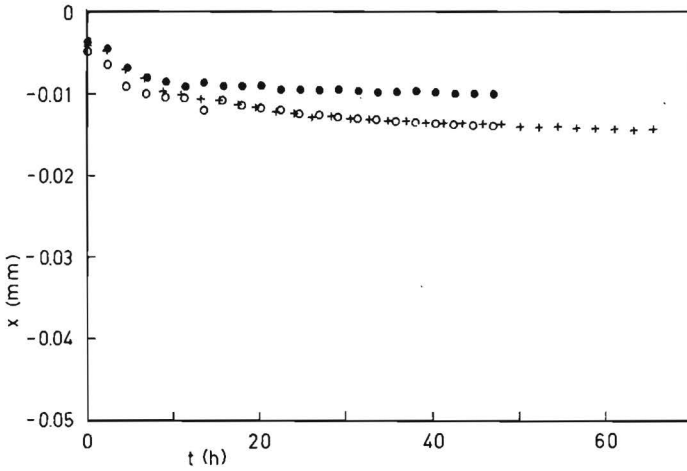
(b)

Fig. 6.8. Wear experiments on reaction sintered sialon with 1 wt% CaO at 2 Hz, 4 N (a) and 1 Hz, 4 N (b).

(a)

(b)

Fig. 6.9. Wear during wear experiments on batches 12 (a) and 21 (b).

133

(a)

(b)

Fig. 6.10. Wear tracks of batch 21 and 11 (bar = 10 μm).

wear at the ends of the track was more severe than in the middle. Abrasive wear often started at the ends of the wear track (fig. 6.7b).

In the second series of experiments the following batches were tested: 2, 11 (reaction sintered), 12 and 13 (kaolin source), 14, 17, 18 and 21 (hot-pressed). The composition, process conditions and some properties of the batches are given in the tables 6.1 to 6.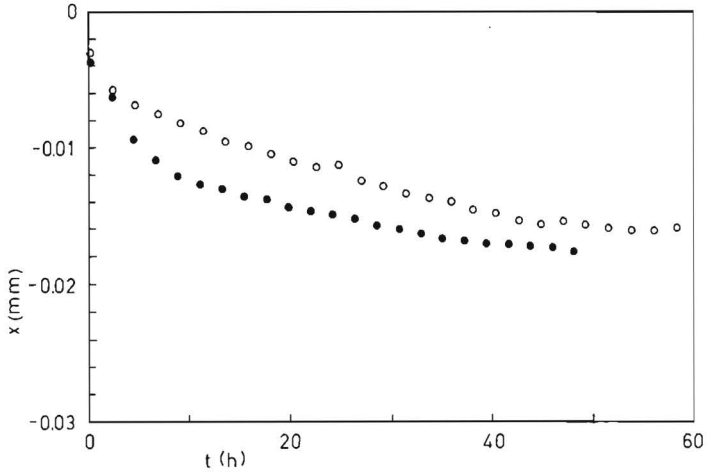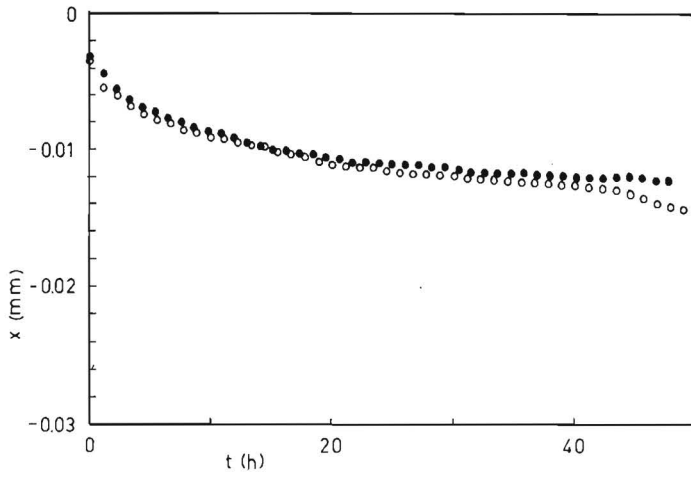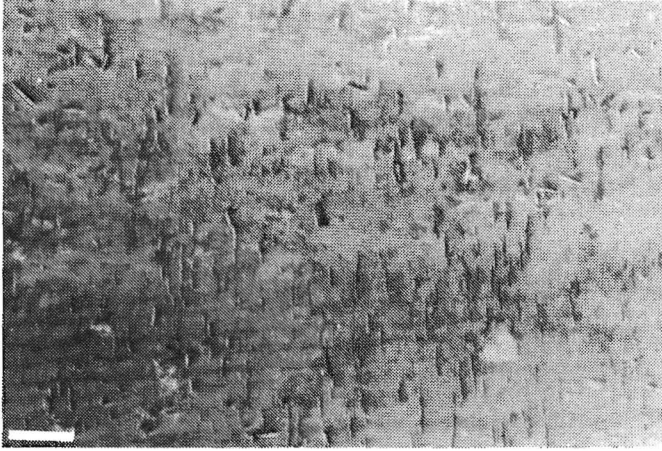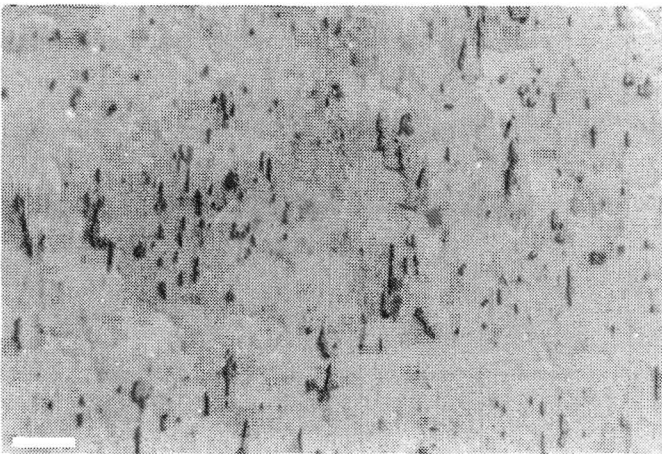3. All the experiments lasted 48 h and were done in duplicate. The samples were ground and had a surface roughness of 0.2 μm. The wear direction was perpendicular to the grinding direction.

The reproducibility varied from reasonable to very good (see fig. 6.9). In all cases the wear depth was less than 0.03 mm. The friction coefficient was constant at a value between 0.4 and 0.5. There was no relation between the wear rate and the value of f_c. Although the wear curves and friction coefficient showed no significant differences between the batches tested, microscopic analysis showed differences in wear behaviour.

Figs. 6.10 and 6.11 illustrate some of the wear tracks. It appears that the grooves, parallel to the wear direction, are not always present in both experiments of one material. Due to the polishing effect, a part of the microstructure becomes visible. Clusters of 15R phase are visible in the tracks on reaction sintered and reaction hot-pressed specimens (fig. 6.10b). The wear rate of the 15R phase seems to be lower than that of the matrix. This might be caused by the somewhat higher density of these regions. The number of fatigue cracks is larger in materials with a small grain size. In materials with large grain sizes the intergranular phase is removed and the grains can be seen. This effect can be observed in the reaction sintered batch with 3 wt% CeO_2 (batch 2) and both the kaolin derived sialons (fig. 6.11a,b). In the coarse sialon prepared from kaolin (batch 12) no fatigue cracks are observed.

6.5 Conclusions

The production method and process conditions have no influence on the hardness, Young's modulus and Poisson's ratio of β'-$Si_3Al_3O_3N_5$. The microstructure of the reaction sintered and reaction hot-pressed materials is very inhomogeneous due to insufficient powder processing.

The fracture toughness as well as the bi-axial strength are influenced by the additives and process conditions. Generally the properties of the CaO doped sialons are worse than those of the CeO_2 doped materials. However, under certain

(a)
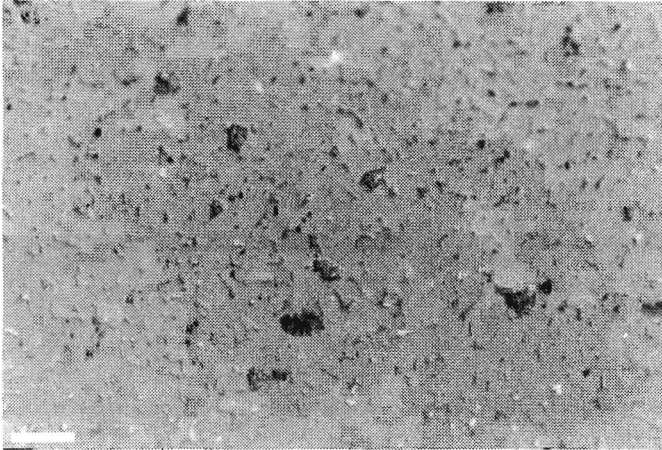
(b)

Fig. 6.11 Wear track of a coarse (a) and fine (b) kaolin derived sialon
(bar = 10 μm).

process conditions for reaction sintered sialon with 1 wt% CaO, it was possible to obtain a strength similar to that of CeO_2 doped sialon. The properties of reaction sintered material were similar to those of hot-pressed materials with comparable composition.

Sialon, sintered of sialon powder derived from kaolin, had a strength and fracture toughness comparable to those of the reaction sintered or reaction hot-pressed sialon with CaO. Thus the impurities in the kaolin did not decrease the room temperature properties measured. This is confirmed by the fact that addition of small amounts of SiO_2, TiO_2 or Fe_2O_3 did not influence the properties of the reaction sintered sialon significantly.

The relation between K_{Ic} and σ_{bi}, and the grain size is not unambiguous. For the kaolin derived sialon the K_{Ic} increased and the σ_{bi} decreased with increasing grain size. For CeO_2 doped reaction sintered sialon the opposite was observed.

Reproducible wear measurements were only obtained at low pin frequency and low normal force: such that the experiments comprised only the stage in which surface polishing is the main wear mechanism. The friction coefficient of ZrO_2/sialon was 0.4 - 0.5 during surface polishing. The friction coefficient increased when abrasive wear became the dominant wear mechanism. The transition between these two stages occurred stochastically. The wear rate and friction coefficient were the same for all sialons tested. At large grain sizes the intergranular phase was removed during wear and less fatigue cracks were formed.

137

References

1. H.F. Pollard, "Sound waves in solids", ed. Pion Limited, London 1977.

2. R. Morrell, "Handbook of properties of technical & engineering ceramics, Part 2 data reviews section: High-Alumina ceramics", ed. HMSO, London 1987.

3. R.R. Wills, R.W. Stewart and J.M. Wimmer, "Effect of composition and X-phase on the intrinsic properties of reation-sintered sialon", Ceram. Bull. 56 (1977)194-200.

4. W.F. Brown and J.E. Srawley, "Plain strain crack toughness testing of high strength materials", ASTM-STP-410, ed. ASTM Philadelphia 1967.

5. M.B. Trigg and E. Tani, "Effect of fabrication routes and heat treatments on the microstructure of silicon nitride based materials", Ceramic Developments, ed. C.C. Sorrell and B.Ben-Nissan, Mater. Sci. Forum 34-36(1988)593-597.

6. T. Ekström and P. Olsson, "β-Sialon ceramics prepared at 1700 °C by hot isostatic pressing", J. Am. Ceram. Soc. 72(1989)1722-1724.

7. H.L. Lee, H.J. Lim, S. Kim and H.B. Lee, "Thermomechanical properties of β-sialon synthesized from kaolin", J. Am. Ceram. Soc. 72(1989)1458-1461.

8. J.T. Czernuszka and T.F. Page, "A problem in assessing the wear behaviour of ceramics: load, temperature and environmental sensitivity of indentation hardness", Ceramic surfaces and surface treatments, ed. R. Morrell and M.G. Nicholson, The British Ceramic Society, Stoke on Trent, (1984)145-156.

9. M.N. Giovan and G. Sines, "Biaxial and uniaxial data for statistical comparisons of a ceramic's strength", J. Am. Ceram. Soc. 62(1979)510-515.

10. G. de With and H.H.M. Wagemans, "Ball-on-ring test revisited", J. Am. Ceram. Soc. 72(1989)1538-1541.

11. D.K. Shetty, A.R. Rosenfield, P. McGuire, G.K. Bandal and W.H. Duckworth, "Biaxial flexure tests for ceramics", Am. Ceram. Soc. Bull. 59(1980)1193-1197.

12. A.F. Kirstein and R.M. Woolley, "Symmetrical bending of thin circular elastic plates of equally spaced point supports", J. Tes. Natl. Bur. Stand. 71(1967)C1-C10.

13. W.A. Bassali, "The transverse flexure of thin elastic plates supported at several points", Proc. Cambridge Philos. Soc. 53(1957)728-743.

14. K.R. McKinney and C.M. Herbert, "Effect of surface finish on structural ceramic failure", J. Am. Ceram. Soc. 53(1970)513-516.

15. K. Kishi, S. Umebayashi and E. Tani, "Influence of microstructure on strength and fracture toughness of β-sialon", J. Mater. Sci. 25(1990)2780-2784.

16. W.E.C. Creyke, I.E.J. Sainsbury and R. Morrel, "Design with non-ductile materials", ed. Appl. Sci. Publishers, London 1982.

17. B. Bergman, "How to estimate Weibull parameters", Engineering with ceramics 2, eds. R. Freer, S. Newsam and G. Syers, The Institute of Ceramics, Stoke on Trent, (1987)175-185.

18. L.J.M.G. Dortmans and G. de With, "Weakest-link failure predictions for ceramics using finite element post-processing", accepted for J. Eur. Ceram. Soc.

19. M. Mitomo, N. Kuramoto, Y. Inomata and M. Tsutsumi, "The strength of reaction sintered β-sialon", Yogyo-Kyokai-Shi 88(1980)489-496.

20. M. Mitomo, Y. Hasegawa, Y. Bando, A. Watanabe and H. Suzuki, "The strength of hot-pressed β-sialon", Yogyo-Kyokai-Shi 88(1980)298-303.

21. E. Tani, S. Umebayashi, K. Okuzono, K. Kishi and K. Kobayashi, "Effect of composition on mechanical properties of β-Sialon", Yogyo-Kyokai-Shi 93(1985)370-375.

22. H. Nakamura, S. Umebayashi, K. Kishi, E. Tani and K. Kobayashi, "The effects of additives on bending strength of hot-pressed β-sialon with z = 1", Yogyo-Kyokai-Shi 93(1985)175-181.

23. DIN 50320, "Verschleiss - Begriffe, Analyse von Verschleissvorgängen, Gliederung des Verschleissgebietes", Beuth Verlag, Berlin 1979.

24. J.T. Burwell, "Survey of possible wear mechanisms", Wear 1(1957/58)119-141.

25. K. Kato, "Tribology of ceramics", Wear 136(1990)117-133.

26. D.C. Cranmer, "Cermic tribology - needs and opportunities", Tribology Trans. 31(1988)164-173.

27. J.F. Braza, H.S. Cheng and M.E. Fine, "Silicon nitride wear mechanisms: rolling and sliding contact", Tribology Trans. 32(1989)439-446.

28. M.A. Moore and F.S. King, "Abrasive wear of brittle solids", Wear of materials 1979, ed. K.D. Ludema, W.A. Glaeser, S.K. Rhee, New York, (1979)275-285.

29. M. Woydt and A. Skopp, "Influence of ambient temperature and sliding velocity under unlubricated sliding conditions on friction and wear of Si_3N_4 up to 1000 ^oC", cfi/Ber. 66(1989)416-432.

30. P. Kapsa and Y. Enomoto, "Sliding damage on hot-pressed and sintered silicon nitride caused by a diamond tip under controlled humidity", Wear 127(1988) 65-83.

31. V. Aronov and T. Mesyef,"Wear in ceramic/ceramic and ceramic/metal reciprocating sliding contact, part 1", J. Tribology 108(1986)16-21.

32. M.G. Gee, "Some observations of ceramic-metal sliding wear", Engineering with ceramics 2, ed. R. Freer, S. Newsam and G. Syers, The Institute of Ceramics, Stoke on Trent, (1987)141-153.

33. S.A. Horton, J. Denape, D. Broussaud, D. Dowson, F.L. Riley and N. Wallbridge, "The wear behaviour of sialon and silicon carbide ceramics in sliding contact", Proc. Int. Conf. Non-Oxide Tech. Eng. Ceram. 1985, ed. S. Hampshire, Elsevier Appl. Sci., London (1986)281-298.

34. J.C. Conway, R.N. Pangborn, P.H. Cohen and D.A. Love, "Dry sliding wear behavior of an Si-Al-O-N ceramic", Wear 126(1988)79-90.

35. D.E. Newland, "Random vibrations and spectral analysis", ed. Longman, London 1975.

chapter 7

CONCLUSIONS AND RECOMMENDATIONS

Conclusions

High density β'-$Si_3Al_3O_3N_5$ can be produced by **reaction sintering** of mixtures of Si_3N_4, Al_2O_3 and AlN with only small amounts (1 - 5 wt%) of CeO_2 or CaO addition. The reaction sintering temperatures in a two-step gas pressure sintering procedure vary from 1500 to 1600 °C in the first step and from 1550 to 1700 °C in the second step. Samples with more than 3 wt% CaO are hard to sinter because the tendency to swell limits the maximum sintering temperature. The swelling increases with increasing additive content, sintering temperature and sample size and is due to evaporation of liquid phase.

Samples without additive can only be densified by **hot-pressing**. To obtain high density, the pressure has to be applied at about 1450 °C: the onset of the reaction to β'-$Si_3Al_3O_3N_5$. Apparently the reaction enhances the densification. The addition of CaO or CeO_2 decreases the hot-pressing temperature from 1800 °C for mixtures without additive to 1600 °C for mixtures with 3 wt% CeO_2.

Besides the known reaction mechanism for sialon formation from mullite, SiC, carbon and nitrogen, a second reaction mechanism for the **carbothermal production of β'-$Si_3Al_3O_3N_5$** has been found. This mechanism comprises the decomposition of mullite and carbon into SiC and Al_2O_3 whereafter these compounds react with nitrogen to β'-$Si_3Al_3O_3N_5$ and 15R.

A study of the influence of the pellet diameter on the reaction rate resulted in the determination of a **critical pellet diameter**. The reaction rate can be increased by decreasing the pellet diameter but only up to a certain critical value which depends on the temperature. Below this critical pellet diameter pore diffusion in the pellet is not rate determining anymore thus further decrease of the diameter does not increase the reaction rate. With the introduction of this critical pellet diameter apparent contradicting data, concerning the influence of the pellet diameter on the reaction, can be understood.

After thorough milling the sialon prepared by carbothermal reaction from kaolin can be sintered to high density in 1 hour at 1690 °C.

The differences in the **room temperature properties** of the sialons produced along different routes are small. Poisson's ratio, Young's modulus and the hardness (HV2) of the sialons are 0.30, 227 GPa and 15 GPa respectively. The average fracture toughness is 3.0 MPa m$^{1/2}$. The bi-axial strength varies from 346 to 490 MPa and seems to be influenced mainly by the process conditions and not by the type or content of additive.

The grain size decreases and the amount of intergranular phase increases with increasing additive content. The microstructure of the reaction sintered and

reaction hot-pressed materials is inhomogeneous: large clusters of 15R ($\varnothing$ 10 μm) are visible in all samples due to insufficient powder processing. Nevertheless the strength and K_{Ic} are good in comparison with literature values. The properties of the 'kaolin' sialons are comparable to those of the reaction sintered or hot-pressed sialons and very good when compared with literature. Apparently the impurities in the kaolin do not influence the room temperature properties measured. This agrees with the fact that small amounts of SiO_2, TiO_2 and Fe_2O_3 do not influence the properties of reaction sintered sialon significantly.

The **wear behaviour** of sialon against ZrO_2 can be divided in two stages. Firstly, a period of constant friction coefficient (0.4 - 0.5) and low wear rate in which surface polishing is the main wear mechanism. In a second stage, fatigue cracks are formed perpendicular to the wear direction and abrasive wear begins, resulting in an increasing friction coefficient and substantially larger wear rate. The transition between these stages is not well defined. The wear rate and friction coefficient of all sialons tested are the same. The wear resistance of the 'kaolin' sialons is as good as that of the reaction sintered and hot-pressed sialons.

Recommendations

The properties of the reaction sintered and reaction hot-pressed sialons can be improved by optimization of the powder processing. As has been shown for the 'kaolin' sialons, thorough milling can improve the sintering behaviour considerably. Another possibility is the use of other starting materials.

The use of tablets as starting material for hot-pressing can lead to microcracking. It is therefore recommended to use loose powder as starting material. Possibilities to protect the die from sticking of the sample are: 1) the use of a foil as lining of the die and 2) the use of a die consisting of two parts, such that in case of sticking only the inner part of the die has to be replaced.

The influence of differences in the amount and composition of the intergranular phase on the properties will be larger at high temperatures. For high temperature applications, testing of the sialons at elevated temperatures is necessary.

The transition from the first wear stage (surface polishing) to the second stage (abrasive wear) seems to be stochastic. Since the life-time of ceramic parts will be correlated to the onset of abrasive wear, this transition should be studied more thoroughly. For example, the relation between the transition and the process parameters (pin frequency and load) and the influence of lubrication on this transition should be examined.

143

SUMMARY

The purpose of the investigations described in this thesis, was to optimize different production routes for β'-$Si_3Al_3O_3N_5$ and to study the influence of the production process parameters and additives on the properties of the product. The three production methods used were: reaction sintering in a gas pressure furnace, reaction hot-pressing and sintering of sialon powder derived from kaolin. CaO and CeO_2 were used as sintering additives. An advantage of the kaolin process is the low cost of the raw materials. A disadvantage is the impurity of the materials. SiO_2, TiO_2 and Fe_2O_3 are common impurities of kaolin. The influence of 0.5 wt% of these oxides in reaction sintered sialon with 1 wt% CaO was studied.

The starting material for reaction sintering and reaction hot-pressing was a mixture of Si_3N_4, Al_2O_3 and AlN. The sinterability of tablets from this mixture without sintering additives was poor (maximum relative density 82 %). It is shown that the powder processing influences this sinterability. Thus further optimization of the powder processing is recommended.

For tablets with CaO and CeO_2 addition, a two-step-sintering process was optimized. A two-step sintering consists of a sintering at T_1 and 0.5 MPa N_2 pressure to close the open porosity. In the next step, pressure and temperature are increased to 10 MPa and T_2, respectively. Under these conditions sintering is continued until full density. Optimum conditions for the first sintering step for the CeO_2 doped material were 0.5 h and 1600 °C. For the second sintering step two different sets of conditions were determined: 0.5 h at 1650 °C and 0.3 h at 1700 °C. Samples with CaO addition showed a strong tendency to swell which limited the maximum sintering temperature. The tendency to swell increased with the CaO content and sample size and was probably caused by the evaporation of liquid phase. Sintering conditions for samples with 3 wt% CaO were 0.5 h at 1500 °C followed by 0.5 h at 1550 °C. For material with 1 wt% CaO the sintering temperatures could be increased with 50 or 100 °C.

Tablets without additive could be hot-pressed at 1800 °C, 0.75 h and 21.8 MPa. To obtain high density, it was necessary to apply the pressure at about 1450 °C. The hot-pressing temperature was reduced by the addition of CaO and CeO_2. The hot-pressing temperatures for 0.5, 1.0 and 3.0 wt% CaO were 1675, 1650 and 1625 °C and for 0.5, 1.0 and 3.0 wt% CeO_2 1700, 1650 and 1600 °C respectively. The hot-pressing time was 0.75 h.

The composition of the materials was β'-$Si_3Al_3O_3N_5$ with 2 - 14 wt% 15R. Hot-

pressed samples also contained up to 11 wt% α-Si_3N_4. Part of the 15R was present as clusters with a diameter of approximately 10 μm, independent of the production route. This was probably caused by insufficient milling and/or mixing of the powder mixture. The grains in reaction sintered material were needle shaped with an aspect ratio of about 4. The grain size increased with increasing sintering temperature and time and decreased with increasing additive content. The maximum needle length for CaO doped material was 5 - 10 μm and for CeO_2 doped material 10 - 30 μm. The grain size distribution was strongly bi-modal: space between large needles was filled with small grains. The grains in hot-pressed materials were equi-axed. The grain size was much smaller: maximum 2 μm.

β'-$Si_3Al_3O_3N_5$ can be prepared also from kaolin by carbothermal reaction. Main parameters in this process are: temperature, time, nitrogen flow and the pellet diameter. The reaction rate increased with increasing temperature and flow rate. A decreasing pellet diameter increased the reaction rate only up to a certain critical value. Below this diameter, dependent on the reaction temperature, pore diffusion in the pellet is not rate determining. With the introduction of this critical pellet diameter the apparent contradicting data concerning the influence of the pellet diameter can be understood.

An addition to the reaction mechanism was found: the formation of β'-$Si_3Al_3O_3N_5$ and 15R from SiC, Al_2O_3 and N_2. The sinterability of the sialon powder was strongly influenced by the powder processing. An additional milling procedure reduced the sintering temperature from 1800 °C to 1690 °C and the sintering time from 4 to 1 h. As a consequence the maximum grain size was reduced from 20 μm to 10 μm at an aspect ratio of 4 à 5.

The hardness (HV2) of all sialons was 15.2 ± 0.7 GPa. The relative density was ≥ 98 %. Young's modulus and Poisson's ratio were 226.9 ± 3.5 GPa and 0.298 ± 0.04 respectively.

The maximum fracture toughness (K_{Ic}) was 4.1 MPa m$^{1/2}$, measured for reaction sintered specimens with 1 wt% CeO_2. For CaO doped sialons, K_{Ic} was generally lower than for CeO_2 doped materials. The fracture toughness seemed to decrease with increasing additive content, probably due to the increasing amount of intergranular phase. This effect was not observed for hot-pressed materials. This is due to the fact that all hot-pressed batches were prepared under different conditions and K_{Ic} is dependent on the process conditions.

Strength measurements were performed with a ball-on-ring set up. The strength σ_{bi}, varied from 346 to 490 MPa m^{-2}, strongly dependent on the process condi-

tions. The relation between K_{Ic} or σ_{bi} and the grain size is ambiguous. For the kaolin derived sialons the strength decreased and the K_{Ic} increased with increasing grain size. For reaction sintered sialon doped with CeO_2 the opposite was observed. No explanation, e.g. strong change in aspect ratio, could be found.

Some wear measurements were done in a pin-on-plate set up, with a ZrO_2 pin. The observed wear mechanisms were: surface polishing, abrasive wear and fatigue wear. During the period in which polishing is the main wear mechanism, the friction coefficient f_c was constant at a value between 0.4 and 0.5. Abrasive wear was caused by debris trapped between the pin and plate. Fatigue cracks were formed perpendicular to the wear direction and resulted finally in abrasive wear. Due to abrasive wear f_c and the wear rate were increased. Although the low wear and high wear regions are quite reproducible, the transition between the stages occurred stochastically. The wear rate was similar for all sialons tested, within the accuracy of the measurement. Nevertheless microscopic analysis showed marked differences in the wear scar of several sialons.

In general the differences in room temperature properties were small. The properties of kaolin derived sialons were very good in comparison with literature values and comparable to those of the reaction sintered and hot-pressed materials. Thus the impurities of the kaolin did not influence the room temperature properties significantly. This is confirmed by the fact that the addition of 0.5 wt% SiO_2, TiO_2 or Fe_2O_3 had no significant influence on the properties of the sialon. Although the properties of the reaction sintered and hot-pressed sialons were good, the inhomogeneous microstructure suggests that the properties might be improved by further optimization of the powder processing. More marked differences can be expected in high temperature properties like high temperature strength or creep.

SAMENVATTING

Het doel van het onderzoek beschreven in dit proefschrift, was het optimaliseren van verschillende productieroutes voor het bereiden van β'-$Si_3Al_3O_3N_5$ en het bestuderen van de invloed van de productieroute en van additieven op de eigenschappen van het product. De drie onderzochte productiemethoden zijn: reactie-sinteren in een hoge druk sinteroven, reactie-heetpersen en het sinteren van sialonpoeder, bereid via carbothermische reactie uit kaolien. CaO en CeO_2 zijn gebruikt als sinterhulpmiddel. Het voordeel van het kaolien proces is de lage prijs, een nadeel is de onzuiverheid van de grondstoffen. SiO_2, TiO_2 en Fe_2O_3 zijn veel voorkomende verontreinigingen in kaolien. Daarom is de invloed van 0,5 gew% van deze oxiden op reactiegesinterde sialon met 1 gew% CaO onderzocht.

Het uitgangsmateriaal voor reactie-sinteren en reactie-heetpersen is een mengsel van α-Si_3N_4, Al_2O_3 en AlN. De sinterbaarheid van tabletten van dit mengsel zonder sinterhulpmiddel was slecht (maximale relatieve dichtheid 82 %). Er is aangetoond dat de sinterbaarheid vergroot kan worden door het verbeteren van de poedervoorbereiding, zodat een verdere optimalisering van de poedervoorbereiding aan te bevelen is.

Voor tabletten met CaO en CeO_2 als sinterhulpmiddel is een twee-staps sinterproces geoptimaliseerd. Een dergelijk proces bestaat uit een sinterstap op een temperatuur T_1 en stikstofdruk van 0,5 MPa waarbij gesinterd wordt tot gesloten porositeit. Daarna wordt de druk verhoogd tot 10 MPa en de temperatuur tot T_2. Onder deze condities wordt verder gesinterd tot volledige dichtheid. De optimale conditie voor de eerste sinterstap van materiaal met CeO_2 is 0,5 u op 1600 °C. Voor de tweede sinterstap zijn twee sets parameters bepaald: 0,5 u op 1650 °C of 0,3 u op 1700 °C.

Tabletten met CaO vertoonden een sterke neiging tot zwellen, waardoor de maximale sintertemperatuur werd beperkt. Deze neiging tot zwellen nam toe met het CaO gehalte, de sintertemperatuur en de preparaatafmetingen en werd vermoedelijk veroorzaakt door het verdampen van vloeibare fase. Sintercondities voor tabletten met 3 gew% CaO zijn 0,5 u op 1500 °C gevolgd door 0,5 u op 1550 °C. De sintertemperaturen voor monsters met 1 gew% CaO zijn 50 tot 100 °C hoger.

Preparaten zonder sinterhulpmiddel waren wel goed heet te persen, onder de volgende condities: 0,75 u, 1800 °C en 21,8 MPa. Voor het verkrijgen van volledige dichtheid was het noodzakelijk de druk aan te brengen bij een temperatuur van ca. 1450 °C. Het toevoegen van CaO en CeO_2 verlaagde de heetperstemperatuur

aanzienlijk: 0,5, 1,0 en 3,0 gew% CaO resulteerde in een heetperstemperatuur van 1675, 1650 en 1625 °C, en 0,5, 1,0 en 3,0 gew% CeO_2 in 1700, 1650 en 1600 °C. In alle gevallen is een heetperstijd van 0,75 u toegepast.

De kristallijne fase bestaat uit β'-$Si_3Al_3O_3N_5$ met 2 tot 14 gew% 15R. De heetgeperste tabletten bevatten tevens tot 11 gew% α-Si_3N_4. Een deel van het 15R was aanwezig in clusters van ca. 10 μm, onafhankelijk van de productiemethode. Dit is waarschijnlijk het gevolg van onvoldoende menging en/of maling van het poedermengsel. De korrels in de reactiegesinterde preparaten zijn naaldvormig met een lengte : breedte verhouding van ca. 4. De korrelgrootte neemt toe met de sintertemperatuur en -tijd en neemt af met de hoeveelheid sinterhulpmiddel. De maximale naaldlengte in monsters met CaO is 5 - 10 μm en in monsters met CeO_2 10 - 30 μm, afhankelijk van de proces- condities. De korrelgrootteverdeling is sterk bi-modaal: de ruimte tussen grote kristallen is opgevuld met kleine kristallen. De korrels in heetgeperste preparaten zijn equi-axiaal met een maximale diameter van 2 μm.

β'-$Si_3Al_3O_3N_5$ kan ook gemaakt worden via carbothermische reactie uit kaolien. Belangrijke parameters in dit proces zijn de temperatuur, tijd, N_2 gassnelheid en de pelletdiameter. Het verhogen van de temperatuur en gassnelheid versnelt de reactie. Uit dit onderzoek is gebleken dat het verkleinen van de pelletdiameter slechts tot een bepaalde (temperatuursafhankelijke) waarde de reactie versnelt. Beneden deze kritische pelletdiameter is poriediffusie in de pellet niet meer snelheidsbepalend. Met de introductie van een kritische pelletdiameter kunnen ogenschijnlijk tegenstrijdige data betreffende de invloed van de pelletdiameter verklaard worden.

Naast het bekende reactiemechanisme, waarbij β'-$Si_3Al_3O_3N_5$ wordt gevormd uit SiC, mulliet, C en N_2, is een tweede reactiemechanisme aangetoond. Dit mechanisme betreft de vorming van β'-$Si_3Al_3O_3N_5$ en 15R uit SiC, Al_2O_3 en N_2. De sinterbaarheid van sialonpoeder is sterk afhankelijk van de poedervoorbereiding: een extra maalprocedure bracht de sintertemperatuur terug van 1800 °C naar 1690 °C en de sintertijd van 4 u naar 1 u. Dit had tot gevolg dat de maximale korrelgrootte afnam van 20 μm tot 10 μm bij een lengte : breedte verhouding van 4 à 5.

De relatieve dichtheid van de sialon materialen is ≥ 98 %. De hardheid is 15,2 ± 0,7 GPa. Young's modulus en Poisson's constante zijn respectievelijk 226,9 ± 3,5 GPa en 0,298 ± 0,04.

De hoogste breukweerstand K_{Ic}, 4,1 MPa m$^{1/2}$ is gemeten voor een reactiegesinterd sialon met 1 gew% CeO_2. Voor sialons met CaO toevoeging is de K_{Ic}

gemiddeld lager dan voor sialons met CeO_2 toevoeging. De breukweerstand neemt af met toenemend additiefgehalte, vermoedelijk door de toenemende hoeveelheid intergranulaire fase. Dit is niet waargenomen bij heetgeperste series. Dit kan verklaard worden uit het feit dat deze series onder verschillende condities geproduceerd zijn en K_{Ic} afhankelijk is van de procescondities.

De sterktemetingen zijn uitgevoerd met een ball-on-ring test. De sterkte varieert van 346 tot 490 MPa m^{-2} en is sterk afhankelijk van de procescondities. De relatie tussen K_{Ic} en σ_{bi} enerzijds en de korrelgrootte anderzijds is niet eenduidig. Voor de 'kaolien' sialons neemt K_{Ic} toe en σ_{bi} af met toenemende korrelgrootte. Voor reactiegesinterde sialons met CeO_2 toevoeging geldt het omgekeerde. Een oorzaak, b.v. een sterk veranderde lengte : breedte verhouding van de kristallen, is hiervoor niet gevonden.

Een aantal slijtagemetingen is uitgevoerd met een pin-on-plate met een ZrO_2 pintop. De optredende slijtagemechanismen zijn: polijsten, abrasieve slijtage en vermoeiingsslijtage. In het gebied waar polijsten het voornaamste mechanisme is, is de wrijvingscoëfficiënt f_c constant en heeft een waarde tussen 0,4 en 0,5. Abrasieve slijtage wordt veroorzaakt door debris tussen de pin en plate. Loodrecht op de slijtrichting ontstaan vermoeiingsscheurtjes die uiteindelijk ook leiden tot abrasieve slijtage. Tengevolge van abrasieve slijtage neemt de oppervlakteruwheid toe. In dit gebied neemt f_c toe en is de slijtagesnelheid aanmerkelijk hoger. Hoewel de meting zowel het gebied met lage als met hoge slijtagesnelheid goed reproduceerbaar is, is de overgang tussen beide gebieden stochastisch bepaald. Binnen de nauwkeurigheid van de meting zijn geen verschillen in f_c en de slijtagesnelheid tussen de geteste sialons gevonden. Microscopisch onderzoek liet wel een aantal verschillen zien in de gevormde slijtagesporen.

In het algemeen zijn de gevonden verschillen in de kamertemperatuureigenschappen beperkt. De eigenschappen van 'kaolien' sialon zijn goed in vergelijking met literatuurwaarden en vergelijkbaar met die van reactiegesinterd of heetgeperst sialon. De verontreinigingen in de kaolien hebben dus geen invloed op de kamertemperatuur-eigenschappen. Dit wordt bevestigd door het feit dat het toevoegen van 0,5 gew% SiO_2, TiO_2 of Fe_2O_3 geen invloed had op de eigenschappen van reactiegesinterd sialon. Hoewel de eigenschappen van de reactiegesinterde en heetgeperste sialons goed zijn, geeft de inhomogene microstructuur aan dat deze waarschijnlijk verbeterd kunnen worden door een verdere optimalisatie van de poedervoorbereiding. Verder is het te verwachten dat de verschillen tussen de materialen duidelijker worden wanneer hoge temperatuur-eigenschappen, zoals bijvoorbeeld hoge temperatuur-sterkte of kruip, gemeten worden.

NAWOORD

Op deze plaats wil ik eenieder die heeft bijgedragen aan het tot stand komen van dit proefschrift hartelijk bedanken.

De praktische steun van een aantal personen wil ik niet onvermeld laten. Carin Scholte heeft binnen het IOP project een bijdrage geleverd aan het onderzoek naar de carbothermische produktie van sialon. Leon Poels verrichtte in het kader van zijn afstuderen onderzoek aan het heetpersgedrag van sialon en de pin-on-plate opstelling. Marco Hendrix installeerde het data acquisitie systeem voor de pin-on-plate. Jacquelien van den Boogaart wil ik bedanken voor de spontane hulp en opbouwende kritiek bij het maken van dit proefschrift.

CURRICULUM VITAE

Ik ben geboren op 20 maart 1962 te Amsterdam. Na het eindexamen Gymnasium-β aan de Van der Waalsscholengemeenschap te Amsterdam, in 1980, ben ik begonnen aan de studie voor metaalkundig ingenieur aan de Technische Hogeschool te Delft. Mijn afstudeerwerk met als onderwerp "Structurele relaxatie aan metallische glazen", werd uitgevoerd binnen de vakgroep Fysisch Chemische Metaalkunde onder leiding van prof. dr. ir. A. van den Beukel en in juni 1986 afgesloten.

Van oktober 1986 tot oktober 1990 heb ik binnen het Centrum voor Technische Keramiek (CTK) te Eindhoven gewerkt aan het project "Produktie en eigenschappen van oxynitriden".

Esther Kokmeijer.

STELLINGEN

Het feit dat in het overgangsgebied van c/a = 3 de breukweerstand berekend uitgaande van median cracks en palmquist cracks eenzelfde waarde oplevert is geen bewijs dat het hele gebied met één van beide vergelijkingen beschreven kan worden.

P. Miranzo and J.S. Moya, Ceram. Int. 10(1984)147-152

Hoewel experimenteel blijkt dat poriediffusie bij 1400 $^{\circ}$C te verwaarlozen is voor pelletdiameters beneden 1 mm, maken de complexiteit van het reactie-mechanisme en de deeltjesgrootte distributie van kaolien het onmogelijk in dit gebied een Thiele modulus ≤ 0.3 te bepalen uit conversie-tijd curven bij ver-schillende pelletdiameters.

A.M. van Neerven, F. Blömer and R. Metselaar, Euro-ceramics vol. 1,
Elsevier, London (1989)572-576
Dit proefschrift hoofdstuk 2

Naast onderzoek naar recyclingsmogelijkheden van afvalstromen is het minstens zo belangrijk het slijtageonderzoek te bevorderen teneinde de levensduur van produkten te verlengen.

H.P. Jost, Wear 136(1990)1-17

Zonder het gebruik van markers in het systeem Si-SiC/NiCrAl superalloy kan geen uitspraak gedaan worden over de diffunderende elementen.

M.R. Jackson and R.L. Mehan, Ceram. Eng. Sci. Proc. vol 7-8 2(1981)
787-797
R.C.J. Schiepers, F.J.J. van Loo, G. de With, J. Am. Ceram. Soc. 71(1988)
C284-C287

Gezien de problemen bij de produktie van technische keramiek met reproduceerbare mechanische eigenschappen kan het nut van de ontwikkeling van data bases voor deze eigenschappen op dit moment betwijfeld worden.

R.K. Govila, J. Am. Ceram. Soc., 73(1990)1744-1751
Workshop on Ceramics High Temperature materials Data Bank, Petten (NL),
May 1990

Het persgedrag van poederagglomeraten kan niet door middel van analyse van slechts één persing beschreven worden.

R.L.K. Matsumoto, J. Am. Ceram. Soc. 73(1990)465-468

Een zwart gat is in wezen een anti-gat.

De vraag in hoeverre het traditionele rollenpatroon is aangeboren dan wel aangeleerd, is niet alleen, zoals G. Koremans stelt, niet te beantwoorden maar bovendien niet relevant in de discussie of er meer mogelijkheden moeten komen om van dit patroon af te kunnen wijken.

G. Koremans, Intermediair 12 mei 1989

Het doodzwijgen van doden doet afbreuk aan de waarde die die personen aan het leven hebben toegevoegd.

EG-gesubsidieerde contractresearch leidt in toenemende mate tot ongesubsidieerde contactresearch.

Brite Manual 1990

Grootscheeps hergebruik van afval door recycling is alleen mogelijk indien louter esthetische normen worden aangepast.